Control for Transient Response of Turbocharged Engines

Dariusz Cieslar

Gonville and Caius College

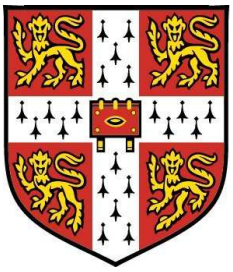

Department of Engineering

University of Cambridge

A thesis submitted for the degree of

Doctor of Philosophy

March 2013

Acknowledgements

First and foremost, I would like to thank Professor Keith Glover and Professor Nick Collings not only for giving me the opportunity to conduct my research under their guidance, but also for creating a stimulating and exciting environment to study. From the perspective of the project described in this thesis, I would like to appreciate their readiness for support and consultations. Considering more general experience, I value witnessing their respect for an intellectual effort, a critical approach to arguments and a passion for a proportionate, clear and accurate expression of thoughts.

I direct special thanks to two excellent colleagues: Dr Alex Darlington and Dr Paul Dickinson. Alex has made invaluable contributions at early stages of the project helping to specify its direction and to develop experimental facilities. Paul has always been willing to discuss and critically assess my ideas. In difficult moments I could rely on his expertise and support.

I would like to acknowledge the funding of Engineering and Physical Sciences Research Council (EPSRC) under the Programme Grant: Control for Energy and Sustainability managed by Professor Malcolm Smith of the University of Cambridge and Professor Richard Vinter of Imperial College London. I would like to express my gratitude to all collaborators from industry, especially to Rob Helle-Lorentzen, Andy Scarisbrick, Dr Stelios Karagiorgis, Dr Jon Dixon, and Dr Geoff Capon from Ford's Dunton Technical Centre, and Peter Fussey and Dr Tony Truscott from Ricardo UK, for many fruitful meetings.

The development and maintenance of the experimental test rig would not be possible without the skills and commitment of John Harvey and Michael Underwood from Hopkinson Laboratory.

Finally, I would like to express my gratitude to my dear wife, Agata, and my family for their support and patience.

As required by the University Statute, I hereby declare that this dissertation is the result of my own work and includes nothing which is the outcome of work done in collaboration except where specifically indicated in the text.

This dissertation contains no more than 65,000 words and 150 figures.

Abstract

The concepts of engine downsizing and down-speeding offer reductions in CO_2 emissions from passenger cars. These reductions are achieved by reducing pumping and friction losses at part-load operation. Conventionally, rated torque and power for downsized units are recovered by means of turbocharging. The transient response of such engines is, however, affected by the static and dynamic characteristics of the turbo-machinery. Recent advances in engine simulation and control tools have been employed for the purpose of the research reported in this thesis to identify and verify possible air-path enhancements.

A systematic method for evaluating various turbocharger assistance concepts is proposed and discussed in this thesis. To ensure a fair comparison of selected candidate systems, an easily reconfigurable controller providing a close-to-optimal operation, while satisfying physical limits, is formulated. This controller is based on the Model Predictive Control framework and uses a linearised mean value model to optimise the predicted behaviour of the engine. Initially, the controller was applied to a 1D simulation model of a conventional light-duty Diesel engine, for which the desired closed-loop features were verified.

This procedure was subsequently applied to various air-path enhancement systems. In this thesis, a turbocharger electric assistance and various concepts based on compressed gas injection were considered. The capability of these systems to improve engine response during 3^{rd} gear tip-in manoeuvre was quantified. This investigation was also complemented with a parametric study of how effectively each of the considered methods used its available resources. As a result, injecting compressed gas into the exhaust manifold was identified as an effective method, which to date has attracted limited attention from engine research community.

The effectiveness of the exhaust manifold assistance was experimentally verified on a light-duty Diesel engine. The sensitivity of the improvements to compressed gas supply parameters was also investigated. This led to the development of the BREES system: a low component count, compressed gas based system for

reducing turbo-lag. It was shown that during braking manoeuvres a tank can be charged to the level sufficient for a subsequent boost assistance event. Such a functionality was implemented with a very limited set of additional components and only minor changes to the standard engine control.

Keywords: Downsizing, CO_2 Emissions, Diesel Engine, Air-path, Turbocharger, Transient Response, Boost Assistance, Mean-Value Models, 1D Simulation Models, Model Predictive Control, Optimal Control, Experimental Engine Study

Contents

List of Figures

List of Tables

Nomenclature

Roman Symbols

A	area / system matrix
B	input matrix
C	output matrix
c	coefficient
D	diameter
d	system disturbance
F	force
f	function
g	gravity
J	inertia
k	step
L	length / distance / radius
M	molecular mass
m	mass
N	rotational speed

N_c	control horizon
N_p	prediction horizon
n	number
P	power
p	pressure
Q	heat
R	specific gas constant for dry air
Re	real part of a complex number
r	ratio / initial condition function
S	speed factor
s	constraint function
T	torque / final time
T_s	sample time
t	time
U	internal energy
u	system input
V	volume
w	mass flow
$\bar{w}$	mass flow in mg/stroke
X	concentration by volume
x	system state
Y	concentration by mass

y	system output

Greek Symbols

η	efficiency / coefficient
γ	ratio of specific heats for dry air
λ	air-fuel equivalence ratio / eigenvalue
Φ	optimisation cost function
ρ	density
τ	time constant
θ	temperature

Subscripts

a	pre-compressor
act	actual
ad	air drag
air	air
amb	ambient
B	brake / shaft
b	post-compressor
brk	braking
c	fuel conversion / post-turbine volume / continuous
cf	Chen-Flynn
cmp	compressor
$conv$	conventional

$cool$	cooler
ct	cycle time
cyl	cylinders
d	displacement
e	engine / engine block
F	friction
f	fuel
$fact$	factor
fd	final drive
FME	friction mean effective
fr	frontal
g	gear
I	indicated
i	index / intake
ic	intercooler
is	isentropic
L	linearised
max	maximum
or	orifice
P	pumping
ref	reference
res	motion resistance

rev	reversible
rr	rolling radius / rolling resistance
ss	steady-state
$stiff$	stiffness
$stoich$	stoichiometric
t	turbocharger
trb	turbine
V	vehicle
v	volumetric
wh	wheels
x	exhaust

Other Symbols

$CO_{2,spec}$	specific CO_2 emissions (g/km)
c_p	specific heat at constant pressure
c_v	specific heat at constant volume

Acronyms

$ACEA$	European Automobile Manufacturers' Association
AFR	Air-to-Fuel Ratio
BDF	Backward Differential Formula
$bmep$	brake mean effective pressure
$BREES$	BRaking Exhaust Energy Storage
BSR	Blade Speed Ratio

CAD	Crank Angle Degree
CAF	Cycle-Average Filter
CAN	Controller Area Network
CCP	CAN Calibration Protocol
CF	Carbon Fraction
CFD	Computational Fluid Dynamics
CI	Compression Ignition
DOC	Diesel Oxidation Catalyst
DTF	Discrete Time Filter
ECU	Electronic Control Unit
EGR	Exhaust Gas Recirculation
EPA	Environmental Protection Agency
$ERFC$	Emphasis on Reducing Fuel Consumption
EV	Electric Vehicle
HEV	Hybrid Electric Vehicle
ICE	Internal Combustion Engine
LHV	Lower Heating Value
LLS	Linear Least Squares
LPV	Linear Parameter Varying
MAF	Mass Air Flow
MAP	Manifold Absolute Pressure
$MIMO$	Multi-Input Multi-Output

MPC	Model Predictive Control
MPG	Miles per Gallon
$MVEM$	Mean Value Engine Model
NA	Naturally Aspirated
$NARX$	Non-linear autoregressive exogenous model
$NEDC$	New European Drive Cycle
$NMPC$	Non-linear MPC
NVH	Noise, vibration, harshness
OCP	Optimal Control Problem
PCO_2	Performance-CO_2 Emissions Index
PID	Proportional-Integral-Derivative
PM	Particulate Matter
$PSFI$	Performance-Size-Fuel Economy Index
QP	Quadratic Programming
RPM	Revolutions per Minute
$RT-MPC$	Real-Time Model Predictive Control
SI	Spark Ignition
$SISO$	Single-Input Single-Output
SQP	Sequential Quadratic Programming
TEA	Turbocharger Electric Assistance
TWC	Three-Way Catalyst
$UEGO$	Universal Exhaust Gas Oxygen

VGT	Variable Geometry Turbine
WOT	Wide Open Throttle

Chapter 1

Introduction

1.1 Reduction of CO_2 emissions as a new objective for technology development

For several decades automotive research and development has been focused on meeting ever-more stringent emissions regulations. Such legislation virtually mandated the introduction of customised electronic engine management systems as well as sophisticated exhaust gas aftertreatment. As a result very significant reductions of emissions have been achieved. These processes continue and new caps on pollutants are being progressively introduced, especially with respect to Diesel engines.

A similar legislative route has already been undertaken to tackle CO_2 emissions. Addressing this issue requires, however, a very different approach as capturing carbon dioxide from exhaust gases is not a feasible solution [Sullivan and Sivak, 2012]. Emissions of CO_2 are closely coupled with fuel consumption and belong to the vehicle's, rather than the engine's exclusive, features. Therefore, the range of plausible technologies is broad. Among the many approaches that have been considered, the most popular include alternative powertrains (e.g. electric, hybrid electric, alternative fuels), reducing engine losses (e.g. downsizing, downspeeding, reducing pumping losses by pressure charging) and advanced combustion systems.

A regulation setting targets in the EU for the near future was passed by the

European Parliament in May 2009 [EU] (for a detailed description please refer to the original document). According to this regulation, manufacturers have to ensure that the average specific CO_2 emissions of a certain percentage of their cars registered within the EU in a given year does not exceed a legislated level. The first limit to be phased in is 130 g/km, which will be applicable to the average of the entire fleet of a given manufacturer by 2015. The second target is 95 g/km in 2020. Excess emissions premiums have been progressively applied since 2012. In 2019 they will reach €95 for each excess gram per kilometre times the total number of registered cars produced by a given manufacturer. These severe penalties reflect the magnitude of expected investments required to develop technologies to meet the legislated targets.

1.2 Recent progress in engine technology

Analysing automotive technology and emissions trends over past several decades leads to a moderate optimism about what to expect over the next few years. Due to the lack of complete long-term data for Europe, the data for the United States published by the US Environmental Protection Agency [EPA, 2012] are used as a starting point. The evolution of the key characteristics of passenger cars since 1975 is shown in Figure 1.1a. During the first five years CO_2 emissions and engine power were reducing. This was caused by high fuel prices and the introduction of the Corporate Average Fuel Economy (CAFE) standards [MacKenzie, 2009]. The following 25 years were characterised by marginal variations in CO_2 emissions, a relatively rapid increase in engine power, a significant increase in vehicle mass and an appreciable increase in vehicle size. It should be emphasised that a certain portion of the increment in vehicle power was necessary to compensate for the increased mass. In turn, about a third of the average vehicle mass increment since 1980 was caused by an enhanced safety and emissions reduction equipment [Zoepf, 2011]. The EPA data for the last few years indicate that a new phase began after 2005, when engine power and weight stopped increasing and CO_2 emissions started to drop.

The EPA data were also analysed in [An and DeCicco, 2007], where the Performance-Size-Fuel Economy Index (PSFI) based on the ratio of maximum

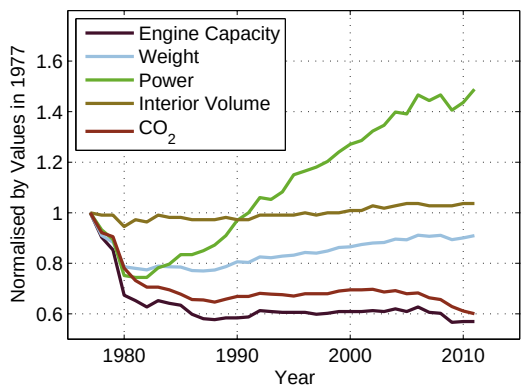

(a) Evolution of vehicle parameters

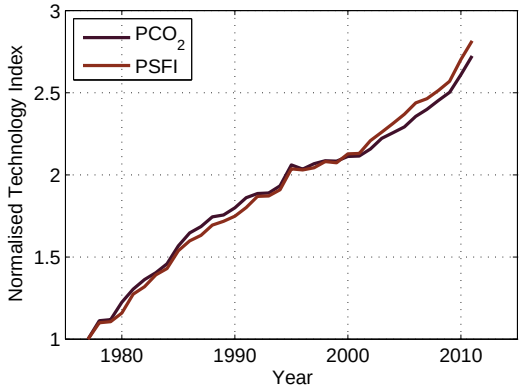

(b) Evolution of PSFI and PCO_2 in the US

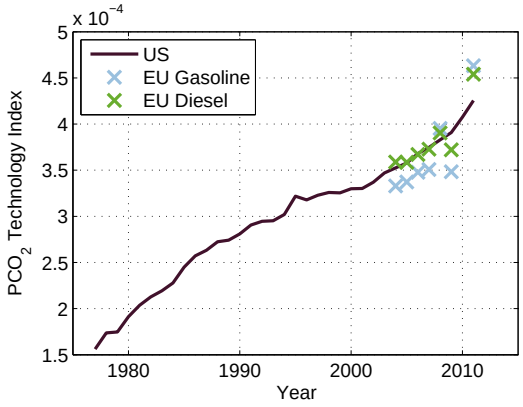

(c) Evolution of PCO_2 in Europe

Figure 1.1: Historical trends is vehicle features.

engine power P_{max} to vehicle mass m_V, the interior volume V_V and the fuel economy expressed in miles per gallon (MPG) was introduced:

$$PSFI = \frac{P_{max}}{m_V} V_V MPG \tag{1.1}$$

and almost a linear progress in this index over the years was observed (see Figure 1.1b). It is thus concluded that for the last 40 years passenger car technology has undergone a steady development. This uniform trend in the PSFI emphasises the fact that a particular balance between various factors of vehicle characteristics depends on design decisions. To quantify the trade-off between performance and fuel economy the ERFC (Emphasis on Reducing Fuel Consumption) parameter was introduced in [Cheah et al., 2009]. This metric compares the fuel economy

improvement realised in a given year versus the possible one under the scenario of maintaining all the other vehicle parameters constant. The ERFC was calculated for EPA data in [MacKenzie, 2009] and three phases were identified. The index was falling in 1980s from values above 100% to 0 in early 1990s and remained around this level for about 10 years. Over the last years of analysed data (up to 2008) the index started to rise again, up to about 40% in 2008. The ERFC index is a useful metric to quantify the priorities of technology improvement.

To analyse the European fleet in a similar manner, a non-standard index - PCO_2 - is now proposed. The definition includes specific CO_2 emissions ($CO_{2,spec}$) instead of the fuel economy used in the PSFI. Due to the lack of vehicle size data, it is defined as follows:

$$PCO_2 = \frac{P_{max}}{m_V} \frac{1}{CO_{2,spec}} \tag{1.2}$$

This metric is more appropriate for the European market than the PSFI index because of the popularity of Diesel engines in the EU. The PSFI neglects the difference in the densities and calorific values of Diesel and gasoline fuels. The comparison of the normalised values of both indices for the US data is shown in Figure 1.1b. The trends are very similar, but the PCO_2 is less linear as it neglects the change in vehicle size. Using this metric the European data since 2004 [EEA, 2012] can be compared with the US records as shown in Figure 1.1c. For the first four years the EU data correlate well with the US data, but the last three years are less conclusive. Therefore, additional data for engine size and power from the European Automobile Manufacturers' Association (ACEA) are also considered and shown in Figure 1.2 [ACEA, 2012]. With this addition similarities in the US and European trends are more apparent. A noticeable drop in the average engine power recorded in 2009 for both European gasoline and Diesel engines (see Figure 1.2b) explains the drop in the PCO_2 index for that year. Moreover, a significant reduction in the average gasoline engine capacity and CO_2 emissions of gasoline engines converging to the levels of Diesel engines could be explained by an increased popularity of smaller units.

Average CO_2 emissions of new passenger cars registered in the UK in a given year are published yearly by the Department for Transport as shown in Figure 1.3a [DfT, 2012a]. Two phases can be distinguished with the rate of reduction

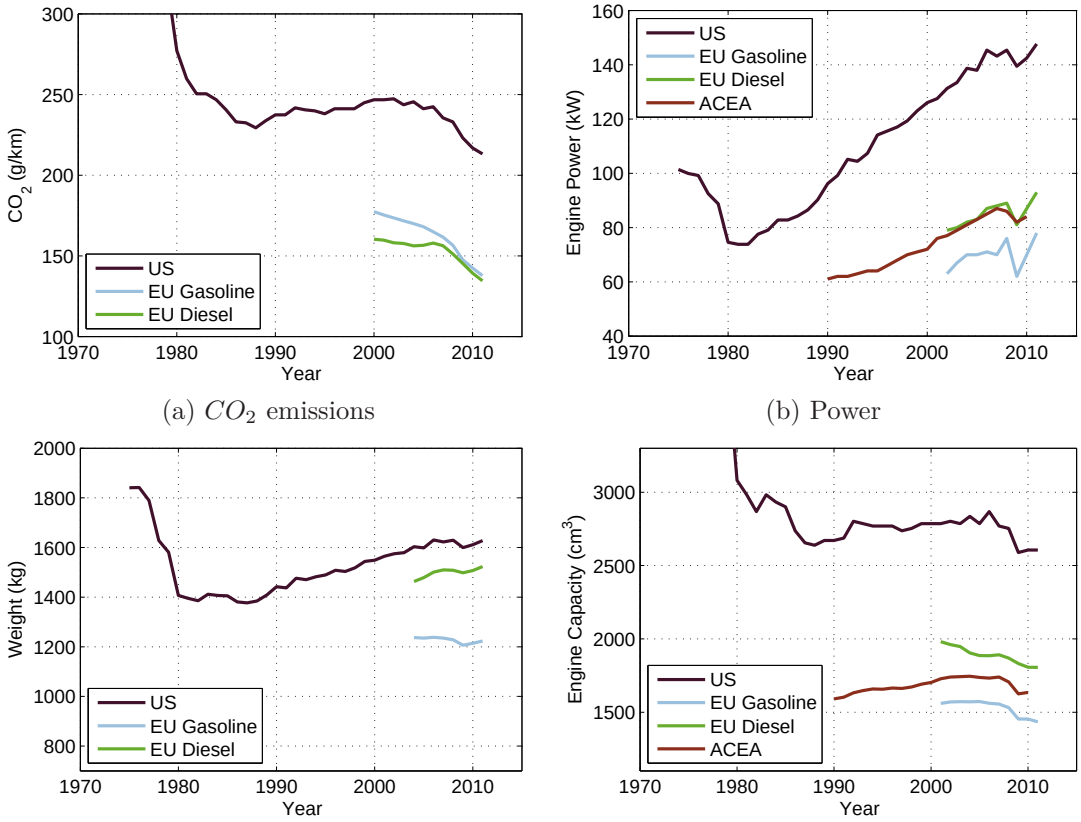

(a) CO_2 emissions

(b) Power

(c) Weight

(d) Engine capacity

Figure 1.2: Comparison of vehicle parameters in the US and the EU.

increasing significantly in 2008. A year on year improvement calculated from these data together with a constant yearly improvement required from current levels to meet the legislated EU targets are shown in Figure 1.3b. This indicates that the 2015 target should be achieved with only modest improvements. The 2020 target requires maintaining the reduction at the challenging level of 4.8 g/km per year.

A detailed study of the European market trends including the prediction of future fleet mix can be found in [Bhatt, 2010]. Various scenarios were considered with the optimistic one assuming the ERFC at the level of 75%. The resulting prediction of year to year reductions was at the level of 4 g/km, which indicates how significant progress is currently required.

Continuing the high level analysis, one can identify a number of factors that

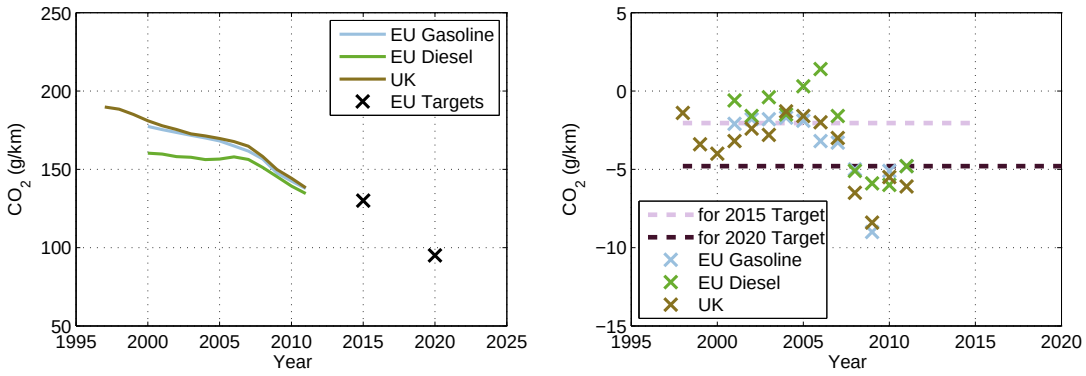

(a) CO_2 emissions

(b) Year on year improvement

Figure 1.3: Trends in CO_2 emissions for the EU and the UK.

may make meeting the CO_2 targets more difficult. These include the introduction of new emission regulations and the introduction of a new drive cycle for the assessment of CO_2 emissions. On the other hand the European regulation currently incentivises vehicles emitting less than 50 g/km, in effect electric vehicles or hybrids with a significant battery size.

Furthermore, it is necessary to emphasise that the reduction of CO_2 emissions can be achieved with the current technology, but at the cost of compromised vehicle driveability, performance and/or size. This scenario would lead to a deterioration in the growth of the PCO_2 index. The actual challenge is to maintain or accelerate the long-term trend in the PCO_2, but with more emphasis on the fuel economy factor. The vehicles offered on the market have to meet the legislated targets and still be attractive for customers, because only the registered ones will be assessed against the EU targets. It is, therefore, valuable to review the factors considered by car buyers during the selection of a next vehicle. The results of the survey conducted by the GfK Automotive for the Low Carbon Vehicle Partnership (2000 respondents) [Dixon and Hill, 2009] and the data from the Department for Transport for 2010 (730 respondents) and 2011 (803 respondents) [DfT, 2012b] are shown in Figure 1.4. The most critical parameters are: price, fuel consumption/CO_2 emissions, vehicle size and reliability. Technologies offering benefits in CO_2 reduction have to be assessed with appreciation of all these criteria.

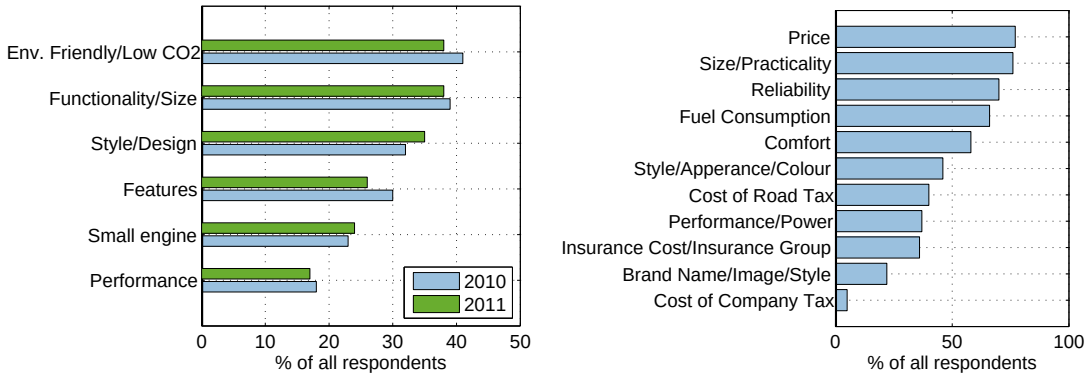

(a) Source: Department for Transport (b) Source: GfK Automotive for LowCVP

Figure 1.4: Factors considered by customers when buying a next car.

1.3 Candidate powertrain configurations

Selection of the most suitable powertrains for future vehicles is currently a highly debated topic. The complexity of this question and associated social, economic and technological uncertainties often lead to the consideration of various scenarios for the future powertrain mix [Bhatt, 2010], [Thiel et al., 2010], [Offer et al., 2010], [Densing et al., 2012], [Pasaoglu et al., 2012]. In many of these studies internal combustion engine (ICE) based solutions are expected to remain the dominant or one of the major propulsion systems in the short and mid-term horizon [MacLean and Lave, 2003] [Bhatt, 2010],[Densing et al., 2012], [Pasaoglu et al., 2012], [NRC, 2011]. Diesel and gasoline fuels benefit from high specific energy at the levels above 40 MJ/kg and high energy density of about 35 MJ/l which makes them well-suited for transport purposes. Internal combustion engines are well-established technologically and benefit from broad social acceptance and a well developed infrastructure. Simultaneously they still undergo constant development, which can be deduced from the evolution of the PCO_2 index presented earlier. Future challenges include reducing emissions at affordable costs, low running costs and limited crude oil resources.

Electric (EV) and hybrid electric vehicles (HEV) are often considered as the most promising alternatives. Wider acceptance of pure electric vehicles requires a change in the attitude of potential owners to a limited range, significantly longer times required for recovering this range (e.g. kilometres of range per

minute of charging could be a suitable metric) and investments in the charging infrastructure, but EVs offer zero tank-to-wheel emissions. Well-to-tank CO_2 emissions vary geographically due to local energy generation infrastructures and in some areas pure electric vehicles may actually have a negative overall impact. In spite of recent developments, both EV and HEV powertrains still suffer from shortcomings in current battery technology, which include cost and a relatively low energy density [Guzzella and Sciarretta, 2005], [NAIGT, 2009].

Due to expectations of an increasing Diesel engine aftertreatment cost and increased Diesel fuel prices, gasoline is often regarded as a primary fuel for future light-duty applications. A number of technologies for improving the fuel economy of spark ignition (SI) and compression ignition (CI) engines are currently being introduced to the market and further advances are envisaged [Ricardo Inc., 2008], [Reitz, 2013]. These improvements are estimated to deliver CO_2 emissions reductions comparable to full hybrid vehicles, but at a more affordable cost [Rueger, 2009], [Thiel et al., 2010], [Shahed and Bauer, 2009]. Key concepts include direct fuel injection, low temperature combustion, aggressive engine downsizing and turbocharging, flexible valve actuation, Stop/Start systems and improvements in transmissions [FURORE], [Ricardo Inc., 2008].

It is expected that the EU 2015 targets can be met with conventional powertrain technologies, whereas to meet the 2020 targets hybrid functionalities will have to be adopted. Such a concept was verified for a European C-class vehicle as a part of the HyBoost project sponsored by the UK Technology Strategy Board [King et al., 2012]. The demonstrator vehicle was shown to achieve the performance of a baseline naturally aspirated (NA) 2.0 litre gasoline engine, but with specific CO_2 emissions reduced from 169 g/km to 94.9 g/km (assessed over the New European Drive Cycle (NEDC)). The main reduction was realised by replacing the original NA engine with a downsized 1.0 litre 3-cylinder turbocharged unit, which was found to give a reduction of 49 g/km. A gearbox with higher gear ratios cut another 5 g/km. Synergies between the concepts of ICE downsizing and mild hybrid functionalities were demonstrated utilising an ultra-capacitor system, i.e. short-term electrical energy storage. In comparison to standard batteries, ultra-capacitors are characterised by significantly higher specific power density and lower energy density. In the HyBoost concept the electric motor/generator

was mounted on the front-end accessory drive. This enabled energy recuperation during tip-out and braking periods, Stop/Start functionality and engine torque assistance. These functionalities reduced the CO_2 emissions by further 14.2 g/km. In summary, the HyBoost project demonstrated that reducing CO_2 emissions by engine downsizing is indeed effective.

1.4 Engine downsizing and turbocharging

In order to exploit the potential of emissions reduction offered by Three-Way Catalysts (TWC), air-to-fuel ratio (AFR) in gasoline engines is controlled to the stoichiometric value. The composition of the exhaust gas is then such that NO can be reduced to N_2 and O_2, and CO and unburned hydrocarbons (HC) can be oxidised to CO_2 and H_2O [Heywood, 1988].

It is convenient to introduce the parameter λ relating the actual AFR to the stoichiometric AFR:

$$\lambda = \frac{AFR}{AFR_{stoich}} \tag{1.3}$$

Gasoline engines have always used a throttle for load control. The spark will only ignite the mixture if the local air-to-fuel ratio is approximately stoichiometric. Therefore, before the advent of catalytic after-treatment, engines would typically operate in the range $0.8 \leq \lambda \leq 1.2$. The TWC solution forces the use of $\lambda \cong 1$, except at very high torque demands. The requirement of maintaining λ close to 1 means that the level of injected fuel, and thus load, is determined by the magnitude of the intake flow.

A throttle adjusts the pressure in the intake manifold, which affects the quantity of air entering the combustion chamber during the intake phase. At part-load conditions this has a negative effect on fuel economy, as the engine has to perform work to suck the air into the chamber. This effect is visualised in Figure 1.5, where examples of p-V diagrams generated in Ricardo WAVE for the wide open throttle (WOT) and part-load conditions of a generic SI engine are shown.

Pressure charging is the concept of increasing the intake manifold pressure (boost pressure) to levels above ambient conditions. This allows one to burn more fuel in the engine. To achieve a certain power requirement, engines of

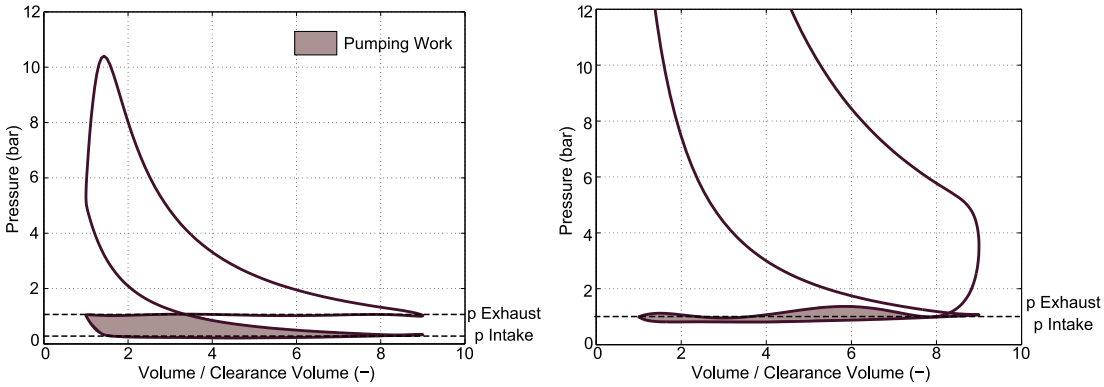

(a) Pumping at part load (b) Pumping at WOT

Figure 1.5: Pumping losses in a NA engine.

smaller swept volumes can thus be used. Such units are then less-throttled at part-loads, what leads to reduced pumping losses. This, together with reduced friction losses that roughly scale with engine swept volume [Ricardo Inc., 2008], are the main mechanisms behind higher fuel efficiencies of downsized engines. The level of acceptable engine swept capacity reduction depends on the capability of the pressure charging system and the limits of the combustion system.

Regarding engine performance, it is desirable for a downsized engine to match as far as possible the characteristics of a baseline unit. Brake mean effective pressure (*bmep*) is a performance measure that relates the rated brake torque T_{rated} to the displacement volume V_d of an engine [Heywood, 1988]:

$$bmep = \frac{T_{rated} 4\pi}{V_d} \tag{1.4}$$

bmep is a useful way of comparing engines - it can be thought of as a measure of how effectively the engine swept volume is utilised. Arguing by example, figures representative for a typical European family car are used. The peak engine torque of 220 Nm and a displacement volume of 2.0 litres is equivalent to a *bmep* value of about 13.5 bar - see Figure 1.6. This value is consistent with typical current NA engines [Ricardo Inc., 2008]. An engine with 40% reduction in swept volume ($V_d = 1.2$ litre) and a similar level of *bmep* would deliver the torque of 132 Nm. In order to restore the initial torque level the *bmep* has to be increased to 23 bar, which can be achieved by pressure charging. Industrial research groups focusing

on aggressive engine downsizing have established their *bmep* targets at the level of 30-35 bar [Fraser et al., 2009].

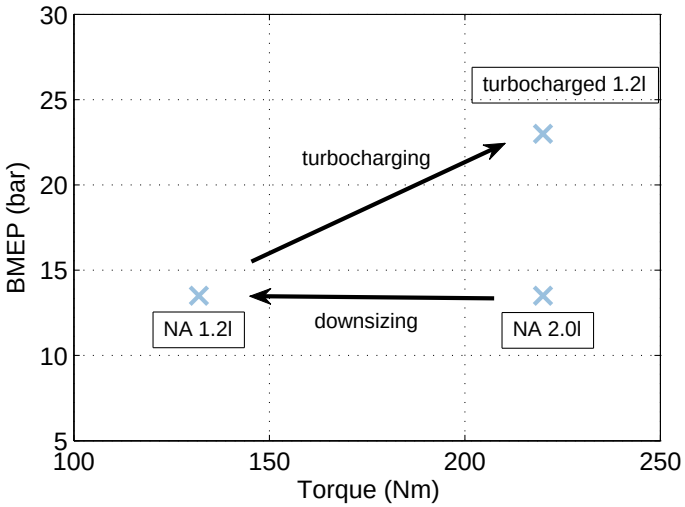

Figure 1.6: Torque restoration for a downsized engine.

The most popular implementation of pressure charging is realised using a turbocharger. It is a device consisting of a turbine and a compressor attached to a single shaft. The turbine converts some of the energy available in the in-cylinder gas (of high pressure and temperature) just as the exhaust valve opens to power that in turn drives the compressor. The compressor then generates an increased pressure in the intake manifold. Such a mechanism is very effective and for many years single stage turbocharging has been widely used in Diesel engines. A central problem concerning an ICE and a turbocharger is that an engine has to operate over a very wide range of air flows, while the turbochargers only deliver significant boost at somewhere near their maximum speed - thus the selection of an appropriate turbocharger for a given engine is a compromise.

The limitations of turbo-machinery performance mean that at low engine speeds generating high boost pressures is challenging. This difficulty is primarily caused by the surge line of the compressor and the inertia of the entire turbocharger. The surge line of a given compressor is usually defined as pressure ratios that for given turbocharger mass flows result in flow instabilities. In an engine equipped with a single turbocharger, the surge line of the compressor can

be directly translated to the static limit of the maximum low speed steady-state torque - see Figure 1.7 (from [Shahed and Bauer, 2009]).

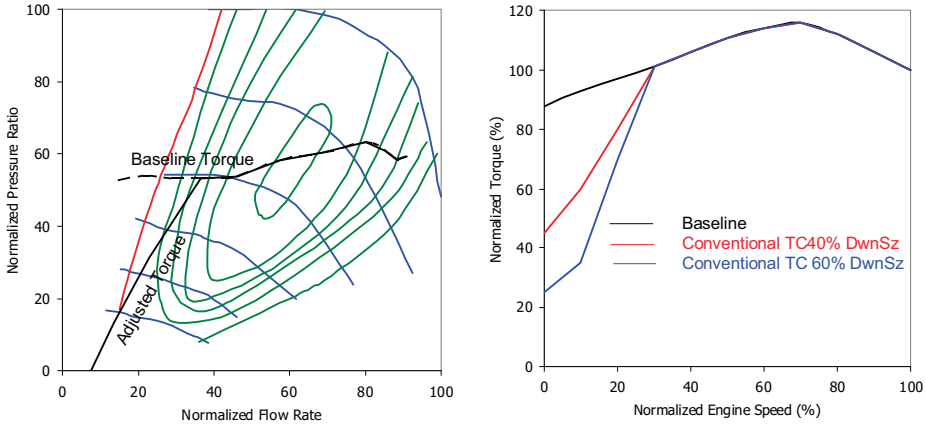

(a) Generic compressor map

(b) Effect on engine torque

Figure 1.7: Compressor surge line limiting the low speed steady-state torque.

The second limitation is caused by the transient response of the turbocharger. The rate of turbocharger acceleration is affected by its inertia, which introduces the slowest dynamic mode in the engine's air-path. This effect is called turbo-lag and is most pronounced during accelerations from low engine speeds.

The benefits and challenges introduced by engine downsizing and turbocharging are conceptually visualised in Figure 1.8. A smaller engine swept volume and pressure charging lead to reduced pumping losses. This results in a better match between the high efficiency island and the usual driving range. The dynamic range of a corresponding NA engine (i.e. maximum torque and power) can be recovered by means of turbocharging, but, as already noted, delivering low speed torque is challenging.

A thorough review of various methods for improving transient response for Diesel engine can be found in [Rakopoulos, 2009]. Conventional approaches to combat the problem of delivering low speed torque include two stage turbocharging, variable geometry turbines (VGT) and supercharging. Two stage turbocharging and VGTs add significant expense to the engine's air system and VGTs for SI engines are very expensive due to the high exhaust temperatures. Mechanical supercharging is very effective at increasing the low end torque but suffers from

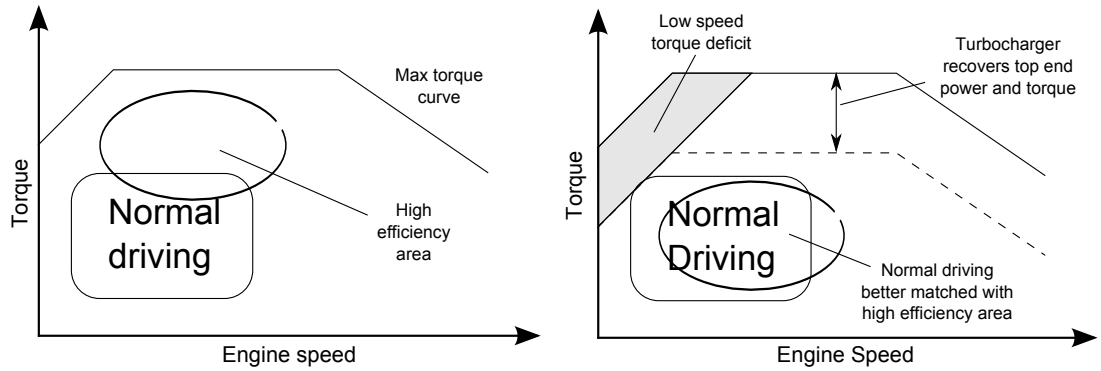

(a) NA engine map (b) Downsized engine map

Figure 1.8: Illustration of advantages and challenges for engine downsizing.

the trade-off between performance, fuel economy and cost effectiveness [George et al., 2004], [Lecointe and Monnier, 2003]. A separate category of systems addressing this problem includes the concepts benefiting from an additional energy storage: electric superchargers, turbocharger electric assistance and pneumatic assistance systems. Certain improvements can be also achieved by adjusting the fuel injection and valve actuation strategies during transients. Late fuel injection results in increased pressure and temperature of the exhaust gas, thus the turbocharger can be accelerated faster. Late injection, however, compromises the combustion efficiency. Early exhaust valve opening acts in a similar fashion, but, in Diesel engines, in addition to compromising efficiency leads to increased soot emissions. Late intake valve opening during transients reduces the valve overlap, thus mitigating the problem of the gas flow from the pressurised exhaust manifold to the intake manifold, where pressure is below the steady-state level [Rakopoulos, 2009].

In the two stage configuration a smaller turbocharger, characterised by a relatively low inertia, is designed for operation at lower mass flows. This way significantly higher intake manifold pressures are achieved for lower engine speeds. The bigger turbocharger operates at higher mass flows and is capable of delivering boost pressures required to restore the rated power. A simulation-based optimisation of two stage turbocharging for a CI engine was considered in [Saulnier and Guilain, 2004]. The authors concluded that a satisfactory steady-state performance can be relatively easily achieved, but delivering improved transient re-

sponse is challenging.

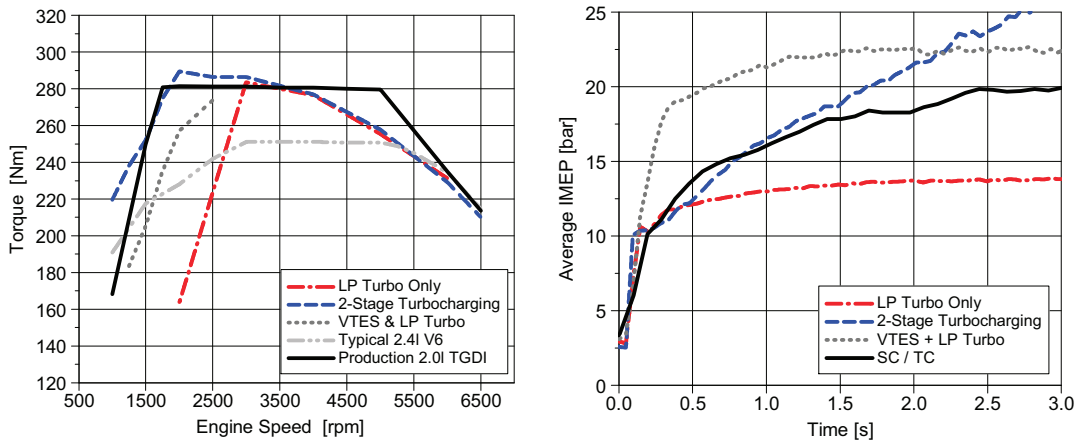

(a) Steady-state results

(b) Transient performance

Figure 1.9: Various charging systems tested on a downsized engine prototype.

Experimental results for various pressure charging systems tested on a prototype downsized 1.2l engine were presented in [Fraser et al., 2009]. The following air-path architectures were implemented: a single low pressure turbocharger (LP Turbo Only), two turbochargers arranged in series and an electric charger in series with a turbocharger (VTES + LP Turbo). The resulting full-load steady-state torques (see Figure 1.9a) were compared with a production 2.0l turbocharged gasoline direct injection engine (TGDI). It was confirmed that the single stage turbocharger was able to meet the torque requirements for medium and high engine speeds, but the torque deficit at low speeds was very significant. The second turbocharger at the high pressure stage mitigated this effect and the overall system had better characteristics than those of the 2.0l TGDI engine. In comparison to the air-path with a single turbocharger, the configuration with the electric charger resulted in a significant improvement of the torque curve, but was unable to match the characteristics of the baseline unit.

The assessment of transient response was performed applying a full-load demand at a fixed engine speed of 1250 RPM and recording the values of indicated mean effective pressure (see Figure 1.9b). The response of a different engine equipped with a supercharger in series with a turbocharger (SC/TC) was treated as a benchmark, because such a system was already in mass production. It

appeared that the configuration with an electric charger offered the best performance. The turbo-lag effect remained significant in the case of two turbochargers in series. In this way, the trade-off between the steady-state characteristics and the transient performance of various air-path systems was highlighted.

Turbocharger assistance can be implemented using an electric motor integrated with the turbocharger shaft or by means of compressed air injection. The turbocharger electric assistance (TEA) systems were considered in simulations and evaluated experimentally in a number of recent publications reporting significant benefits in transient response [Balis et al., 2003], [Katrasnik et al., 2005], [Ibaraki et al., 2006]. Additionally, under suitable circumstances, the electric motor can be operated as a generator. This implements a turbo-compounding functionality and contributes to the overall fuel consumption figures.

Adding an electrically driven compressor at the low pressure stage was also investigated in [Yamashita et al., 2010], [Tavcar et al., 2011], George et al. [2004]. A similar system was used in the HyBoost project [King et al., 2012] and was shown to improve both the low speed steady-state characteristics and the transient response. The configuration with an electric charger can outperform the TEA concept, because it increases the pressure upstream of the main compressor. As a consequence, the surge line of the latter is not limiting the overall operation.

Injecting compressed air to improve the operation of internal combustion engines has been considered in numerous publications. Injection into the intake manifold of a marine Diesel engine was shown to improve the load acceptance in [Papalambrou and Kyrtatos, 2009]. In spite of controlling the injection with an advanced control system, issues related to preventing compressor surge were reported. A supercharger air hybrid concept was described in [Ma and Ma, 2010]. The authors proposed to use a supercharger during braking to charge a low pressure air tank. The collected air was then available for intake manifold injection to improve the transient response of a downsized engine. Other related concepts proposed to use the engine block as a pump to charge a compressed air tank during braking [Herrera, 1998],[Kang et al., 2008], [Lee et al., 2010]. During acceleration, the compressed air was released to the cylinders and the engine operated as an air-driven motor. Various arrangements were considered with the tank connected

to the exhaust manifold [Kang et al., 2008] or the intake manifold [Lee et al., 2010]. These concepts assumed active or even fully variable valvetrains to facilitate all the required engine operating modes, but some promising fuel economy benefits were reported.

The possibility of improving the transient response by secondary air injection into the exhaust manifold was mentioned in [Watson and Janota, 1982]. This idea was not investigated in detail, because this observation was only considered as a useful side effect of injecting the air for oxidising CO and HC, when running a gasoline engine with rich mixture at the WOT conditions.

Each boost assist concept suffers from the requirement of an energy generation and storage. In the case of mechanical and electric concepts the energy could be harvested by regenerative braking (or external charging for the electric assist). Otherwise the power required has had to be generated by burning fuel in the engine, i.e. at a modest efficiency ($\approx 20\%$). This clearly leads to CO_2 penalties. Nevertheless, it was shown in [Katrasnik et al., 2005] that improving the transient response of an engine by utilising the stored electric power to accelerate the turbocharger is more fuel efficient than providing an additional torque directly to the crankshaft. Similar concerns apply to air-path systems with compressed air assist. The air, however, can be pressurised during braking using engine work, which would otherwise be wasted.

The concept of a hybrid pneumatic engine equipped with an additional cylinder valve allowing for compressed air storage and injection was described in [Donitz et al., 2009]. In the proposed implementation an active valvetrain was not needed, only the additional compressed air valve required more flexible control. This concept allowed for significant flexibility in engine operating modes, which in turn led to significant fuel consumption benefits and the mitigation of turbo-lag.

There exist a lot of commonalities between pressure charging applied to CI and SI engines. Therefore, potential improvements in transient response would be beneficial for both variants. The main differences include [Guzzella and Amstutz, 1998]:

1. exhaust gas temperature - in the case of SI engines, exhaust temperatures are much higher, and despite their advantages widespread adoption of vari-

able geometry turbochargers has not occurred due to the requirement of more expensive materials - in [Hancock et al., 2008] a VGT primarily designed for CI engines was applied to a downsized SI engine, but required a cooling system for the exhaust manifold, EGR cooling and overfuelling for component protection

2. the engine load in the case of CI engines is primarily controlled by the amount of injected fuel, whereas in SI engines the load is primarily controlled by the quantity of air and fuel

3. gasoline engine can and do suffer from auto-ignition ("knock") of a part of the charge, which sets limits to the operational envelope; also the phenomenon of "mega-knock" has recently been reported, which is related to pre-ignition [Heywood, 1988]

1.5 Summary

Passenger vehicle technology has recently undergone a major change in its development objectives - meeting CO_2 emissions targets has become as necessary as meeting toxic emissions targets. This new direction focuses more significantly on the attributes of complete vehicles, therefore there is a wide range of solutions being considered. In spite of a recent period of constant average fleet fuel economy figures, engine technology has been progressing at a stable pace for the last 40 years. However, the benefits of new improvements were mainly utilised to increase engine power, vehicle safety and passenger convenience. It is envisaged that the ICE based technology can progress further, but to meet the legislated targets the emphasis should be placed on CO_2 emissions reduction. This is acceptable by customers, because CO_2 emissions are directly related to fuel economy that is one of the major factors considered before buying a next car. Other important factors include vehicle practicality/size, reliability and cost. For these reasons, ICE technology, as opposed to alternative powertrains, is likely to remain the dominant propulsion system in vehicle fleets for several decades.

One of the widely accepted concepts for improving fuel economy in gasoline engines is engine downsizing and down-speeding. Diesel engines can also benefit

from increased levels of pressure charging. Selection of an appropriate air-path configuration is vital and a number of competing technologies are available. They differ by steady-state and transient characteristics, control flexibility, impact on fuel economy and an associated cost.

1.6 Objectives of this study

This study investigates the turbocharging technology with a particular focus on control for transient engine operation. The investigation was based on a Diesel engine due to the availability of suitable equipment, the interest of industrial collaborators and the consistency with current trends in industrial research and development.

Introduction of a turbocharger to the engine air-path results in the addition of a very slow mode to its dynamics. High pressures in the intake manifold can be generated once the compressor is spinning at a sufficiently high speed, whilst the acceleration rate is strongly affected by the inertia of the turbocharger. In standard configurations, the turbocharger is accelerated by the energy extracted from the exhaust gas. Such processes can take up to several seconds and a slow transient torque response of the engine, a phenomenon called turbo-lag, may be perceived by the driver. Mitigating this effect by a low cost technology could improve the driveability of downsized engines and/or allow for more aggressive downsizing, thus leading to better fuel economy figures.

The main objectives of this research included:

1. Designing a family of controllers for downsized/turbocharged engines, which can be easily adapted to various air-path architectures and achieve their close-to-optimal transient performance in laboratory conditions

2. Extensive testing of the transient response of a turbocharged engine with both standard and newly designed control strategies in a limited range of operating conditions

3. Investigation of the fundamental limitations and trade-offs in control of the air-path of turbocharged engines

4. Investigation of the relative merits of the air-path architectures considered

As an example of the enhancement of air-path operation, compressed air assistance was considered. Such a concept can be implemented in a number of ways. Both the most effective physical arrangement and the control of the modified system were investigated.

Chapter 2

Methods and tools

2.1 Introduction

This thesis is primarily concerned with improving the closed-loop performance of turbocharged engines with a particular focus on transient manoeuvres. In this chapter, the methods and tools used to achieve the objectives of this investigation are introduced.

A brief summary of a conventional Diesel air-path control structure is described in 2.1.1. Some advantages and limitations of this established approach are discussed. This leads to the formulation of the scope of this work in 2.1.2.

Specifically for this project an engine test cell was prepared, a new engine was installed and instrumented. The experimental setup together with the reference manoeuvre is described in section 2.2. Section 2.3 contains a description of the development and calibration of a 1D engine and gas dynamics simulation model. Finally, a mean value engine model (MVEM) formulation used in this work together with steady-state and transient calibration procedures are introduced in 2.4.

2.1.1 Conventional Diesel engine air-path control

A conventional light-duty Diesel engine equipped with a VGT/EGR air-path and a common rail direct fuel injection system (see the layout in Figure 2.1) is the basis of this investigation. A simplified diagram of a typical production

style controller structure for such an engine is shown in Figure 2.2 (based on [Bosch, 2011] and [Guzzella and Amstutz, 1998]). There are several important features of this hierarchical arrangement. The strategy is separated at a high level into the fuelling and the air-path control. This is primarily caused by the fact that Diesel engines can operate at a wide range of air-to-fuel ratios. The load control is realised by adjusting the fuelling quantity, whereas the air-path is responsible for delivering the intake gas composition allowing combustion of the fuel under favourable conditions, i.e. such that driver torque demand are met with acceptable tail pipe emissions, noise, vibration and harshness. Moreover, the bandwidth of the fuelling system is much higher than that of the air-path system.

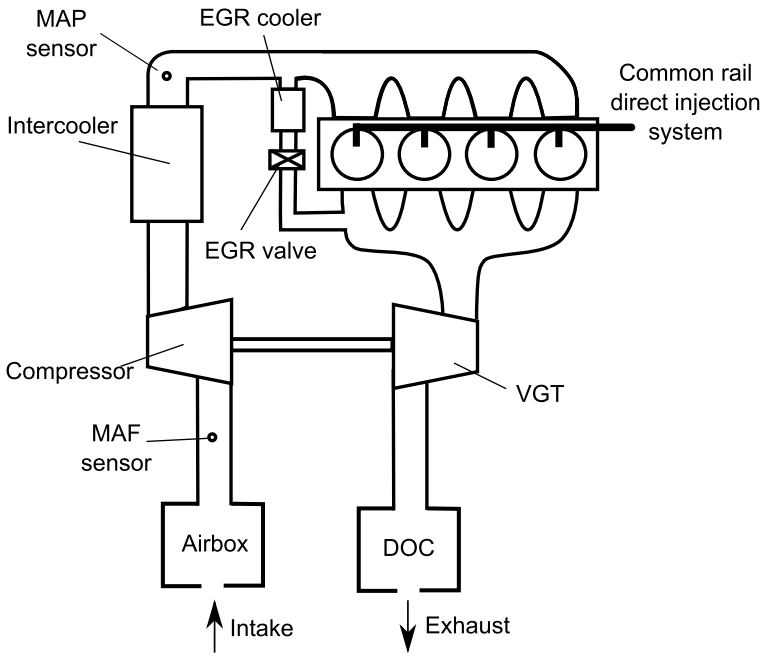

Figure 2.1: Conventional Diesel VGT/EGR air-path.

Common-rail direct injection systems allow for significant flexibility in fuelling strategies with control variables including rail pressure, number of injections per stroke, injection timings and quantities. Set-points for the fuelling system are determined at the controller calibration stage. Each of these signals affects a number of outputs of interest: NOx emissions, particulate matter (PM) emissions and brake specific fuel consumption. Finding the optimal values for the set-points

is a difficult task, because of these complex trade-offs and interactions [Guzzella and Onder, 2004].

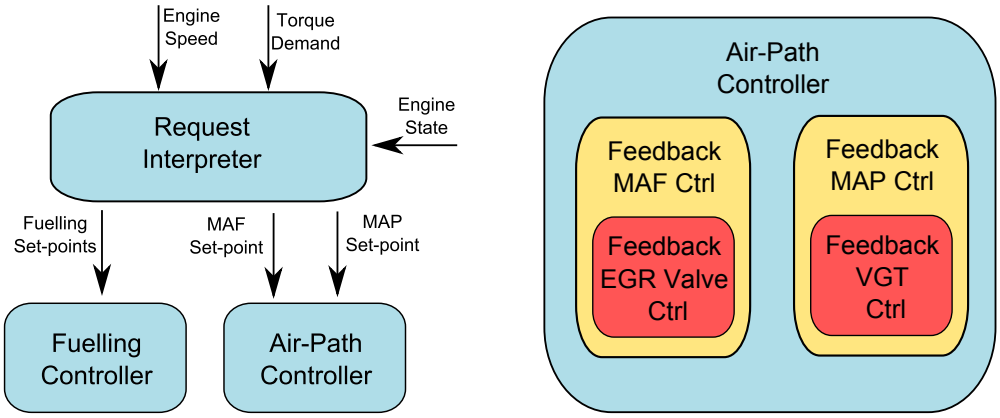

(a) General structure

(b) Hierarchy in air-path controller

Figure 2.2: Simplified diagram of a conventional Diesel engine controller.

The emissions control authority offered by adjusting the fuelling parameters is limited because the levels of toxic emissions (NOx and PM in particular) and smoke are sensitive to in-cylinder gas composition and quantity. The air-path system is used to ensure desirable charge properties. In a conventional setup, the controller treats the air-path as two single-input single-output (SISO) systems. The EGR valve is used to track the desired mass air flow (MAF) and the VGT is modulated to meet the desired intake manifold pressure. [1]

In traditional approaches steady-state set-points for MAF and MAP are determined experimentally. For a grid of operating points (defined by speed and load) the desired values are selected to ensure an acceptable trade-off in performance and emissions. Priorities considered during this selection are often dependent on operating point itself and some correction factors for measured disturbances are included. This steady-state calibration can be interpreted as the highest level of such a control arrangement. The feedback controllers for MAF and MAP define the next level of control. This way the set-points for EGR valve position and VGT rack position are determined. In production style strategies gain-scheduled Proportional-Integral-Derivative (PID) controllers complemented

[1] the notion of intake manifold pressure will be used interchangeably with boost pressure and manifold absolute pressure (MAP)

with feed-forward terms are used. Tracking of the EGR valve and of the VGT rack position set-points is ensured by low level PID controllers. The most common types of actuators are electric and pneumatic. These two variants differ with regard to associated cost, control complexity and bandwidth [Bosch, 2011], [Mehmood et al., 2011].

It is necessary to mention that the air-path and the fuelling control are not fully separated. The minimum AFR in Diesel engines is limited by the smoke limit and is set above the stoichiometric value, often with a certain margin. When the air-path is not able to deliver a sufficient air flow, fuel injection is reduced to avoid exceeding the smoke limit. It is the fuelling controller that is responsible for respecting this limit, because this subsystem is characterised by a much higher bandwidth. Further interactions between the air-path and the fuelling systems are caused by the influence of in-cylinder gas properties on the combustion process [Guzzella and Onder, 2004].

Splitting the air-path control into two SISO channels with PID controllers has a number of well-known drawbacks including compromised performance due to neglecting interactions between the channels and extensive calibration effort. Various approaches have been investigated to address these deficiencies including $\mathcal{H}_\infty$, Model Predictive Control (MPC), sliding mode control, etc (see [Guzzella and Amstutz, 1998]). PID controllers are still the current industrial standard because they fit very well in the well-established technology development processes and require a modest computational power. They allow for splitting the control task into the strategy and the calibration phases. A further division of the control task into smaller subproblems (e.g. correction factors) allows for modularity, thus it is easier to manage. The controllers are scheduled based on engine speed and load. When a problem is reported in a particular operating region, a controller can be recalibrated locally with a limited impact on the global behaviour. Other reasons behind the dominant position of PID-based controllers in current production engine control units (ECU) are code transferability, extendibility and testability [Christen and Busch, 2012].

2.1.2 Scope of investigation and approach

The design of a transient controller for the air-path system, which can be interpreted as the second of the control levels introduced in the previous section, was the main focus of the work described in this thesis. Set-points for MAP and MAF from the original engine calibration were not modified, unless it was useful to simplify the analysis.

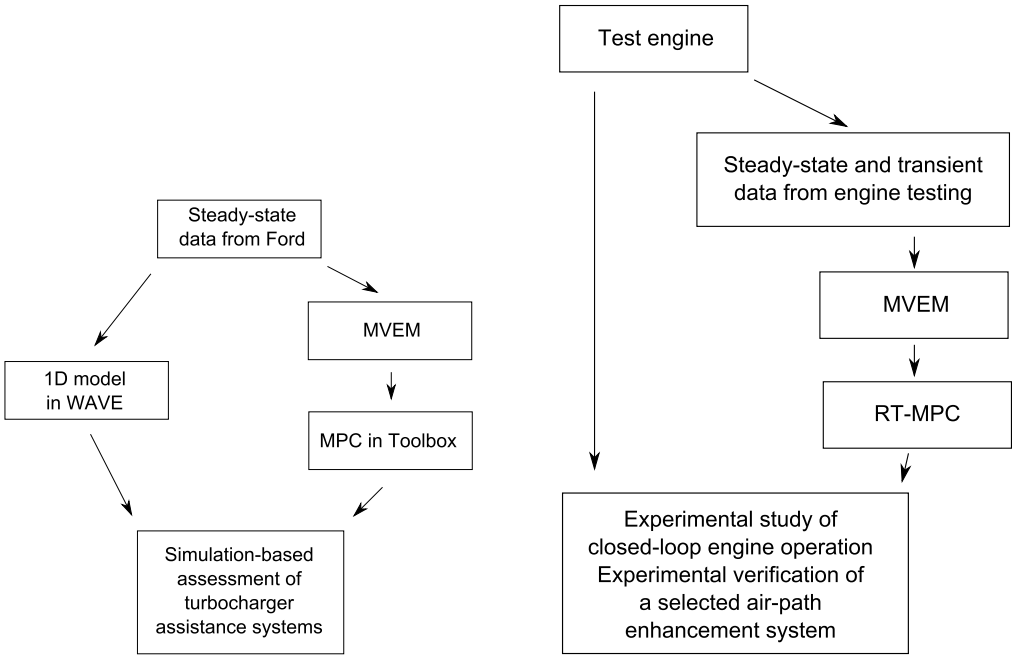

(a) Simulation-based investigation (b) Experimental investigation

Figure 2.3: Models and their calibration for simulation-based and experimental investigations.

The advantages of the investigated control approach were demonstrated in simulations. These features included:

1. flexibility and adaptability to all the considered air-path configurations
2. close-to-optimal closed loop performance

The formulated controller was also able to explicitly address constraints, thus enabling the evaluation of the influence of various limits on the air-path performance.

For this part of work, a 1D engine simulation model was used as an engine simulator and Model Predictive Control (MPC) was implemented using the functions from the Model Predictive Control Toolbox in MATLAB. The 1D model and the MVEM were calibrated based on steady-state engine data supplied by Ford Motor Co.(see Figure 2.3a). The actuators were assumed to be ideal.

The analysis and verification of air-path enhancement concepts, including the prediction of the engine's transient response, were also conducted using the 1D engine simulation model. The most interesting air-path configuration identified through these simulations involved compressed air injection into the exhaust manifold. This concept was then verified experimentally. The influence of assistance system parameters on the overall performance was also examined.

Application of the investigated controller to the actual engine required a Real-Time implementation of MPC (RT-MPC), see Figure 2.3b. It was shown that the low level control of actuators had in fact a considerable influence on the achievable overall operation. Some other practical challenges were also encountered and approaches for their mitigation were proposed. These difficulties included non-negligible actuator dynamics and the determination of state and state derivatives during on-line execution.

In summary, the methods used to achieve the objectives described on page 18 and relevant tools are shown in Table 2.1.

In the following sections the experimental setup, MVEM and 1D simulation model are introduced.

2.2 Experimental setup

2.2.1 Engine

The experimental setup was based on an engine supplied by Ford Motor Co. It was a production passenger car 2.0 litre Diesel unit with the layout shown in Figure 2.1. The specifications of the engine can be found in Table 2.2. The VGT was actuated pneumatically with a position based feedback control. The EGR valve had an electric actuator.

The engine was installed in the test cell with a standard air-box on the inlet

Objective	Question	Method	Tools
Controller	Flexibility and Performance	Simulations	MVEM 1D Model MPC
Trade-offs in Engine Control	Fundamental Limitations	Simulations	1D Model MPC
	Practical Challenges	Experiments	Engine RT-MPC
Relative Merits of Considered Systems	Assessment of Candidates	Simulations	1D Model MPC
	Verification	Experiments	Engine RT-MPC

Table 2.1: Methods and tools used to meet the objectives.

Name	Ford/PSA DW10C
Fuel	Diesel
displacement	1997 cc
no. cylinders	4 in line
no. valves	16
max. power	120 kW (163 bhp)
max. torque	340 Nm
turbocharger	variable geometry
other	compliant with EURO 5 emission standards
	common rail

Table 2.2: Engine specifications.

side. The original exhaust components were mounted up to a Diesel Oxidation Catalyst (DOC). The outlet of the DOC was connected to an exhaust extraction.

The engine was equipped with a set of standard sensors: hot wire mass air flow meter, intake manifold temperature and pressure transducers, and UEGO sensor located downstream of the turbine, but before the DOC.

2.2.2 Test cell and instrumentation

The engine test cell was equipped with a transient AC dynamometer (rated power of 125 kW), which provided the engine load. The dynamometer was controlled in the speed mode and its controller was retuned to ensure a bandwidth sufficient for transient response testing. The engine was connected with the dynamometer via a pneumatically actuated clutch. Shaft torque and speed were measured by a dedicated transducer. Ambient conditions: pressure, temperature and humidity were measured, but not controlled.

The engine was instrumented with a set of strain gauge pressure transducers and K-type 1.5mm diameter thermocouples. A turbocharger speed sensor was mounted in the compressor housing. The operation of this digital sensor was based on pulse induction and the discrimination of eddy currents caused by compressor blades passing in the vicinity of the solenoid sensor. Fuel flow was measured using an AVL 733 Dynamic Fuel Meter and exhaust emissions were measured with a HORIBA EXSA 1500. To cross check the steady-state measurements, a fast CO_2 analyser Cambustion NDIR500 was also connected to the exhaust manifold. See Fig. 2.4 for the layout of additional engine instrumentation.

2.2.3 Control rapid prototyping and data acquisition

The engine was supplied with a development ECU, which was programmed with a close-to-production strategy and calibration. Furthermore, the strategy was configured to be compatible with an ATI rapid prototyping system.

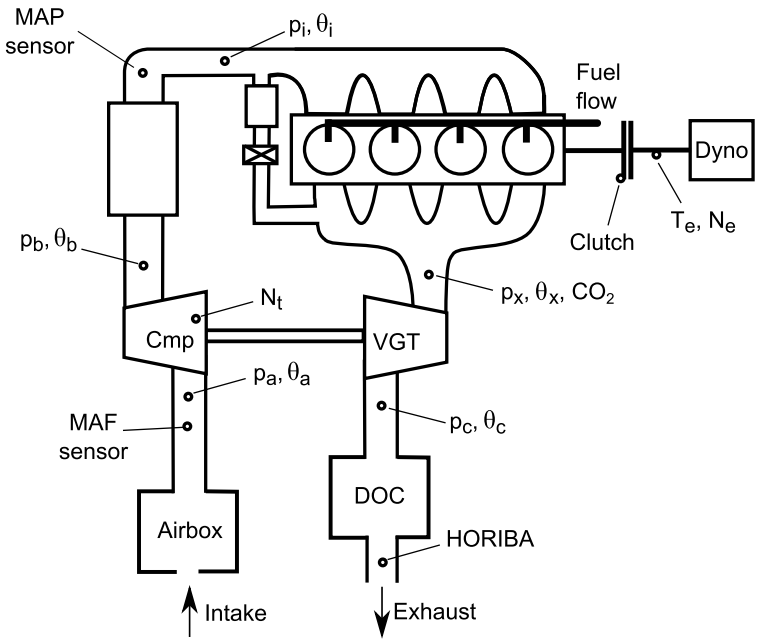

Figure 2.4: Engine with additional instrumentation.

ATI rapid prototyping tools

The ATI Vision software can be used as a calibration tool allowing for supervising and recording the ECU signals and variables. The standard version of the software was also sufficient to calibrate the ECU constants and look-up tables. The communication between the ECU and a PC running the ATI Vision software was realised using CAN Calibration Protocol (CCP).

During the control strategy development and validation process the ability to override any of the ECU variables is very useful. This is possible with the ATI NoHooks tool. Whenever the ECU attempts to access the variable of interest, it is redirected to the memory location with a customised value of this variable (located in spare RAM or ROM regions). In the next step, the it jumps back to the original code [Accurate Technologies, 2013].

ATI OnTarget tool extends the ATI NoHooks functionality. It implements the concept of internal by-passing or 'on-target' prototyping. The same mechanism as in the case of NoHooks is used. This time, however, more complex functions with a range of input signals can be designed and then calibrated on-line.

Executing the new code in the ECU has certain advantages and limitations.

Firstly, there is no need for any external hardware or microprocessor, thus this solution is cost effective. Another attractive feature is that any communication delays and associated issues are avoided. A limited computational power of ECUs is the main reason for considering other options. Model predictive controllers tend to be computationally expensive (in the case of implicit solving) or require significant memory capacity (in the case of explicit setup). With internal bypassing, the prototype code is implemented in the spare ECU memory space, thus the complexity of the code and the number of variables that the new code can use are limited. In the setup developed for this project another limitation imposed on rapid prototyping by executing the code on the ECU was that only the standard sensors and actuators could be used.

The ATI NoHooks and OnTarget tools require the description file (A2L file) and the memory image (Hex file) for the strategy to be modified. Moreover, the information about spare memory regions and methods of disabling checksums is needed. The latter can be usually obtained from an ECU supplier. In the case of this project, all the necessary information and configurations were provided by Ford Motor Co.

dSPACE rapid prototyping system

A modular dSPACE system is another rapid control prototyping environment. Because of the particular requirements of this project, it was used for controlling the test cell and the implementation of the prototype air-path controller. The system was build around a powerful ds1006 processor board (provided by Ricardo UK), which supports model-based development. The board was characterised by much higher specifications than those of the ECU microcontroller (see Table 2.3). The dSPACE setup also featured analogue and digital I/O cards, and a CAN card.

The engine and the test cell were instrumented with a set of additional sensors, the readings of which were all acquired by the dSPACE system. This allowed for implementing an automated supervisory control ensuring a safe operation of the entire test facility.

Experimental testing of the engine was also based on the dSPACE system.

System	ECU	dSPACE ds1006
Processor Name	Freescale MPC5554	AMD Opteron
Processor Speed	132 MHz	2.2 GHz
Available Memory	132 kB	128 MB

Table 2.3: Comparison of rapid prototyping options.

The analogue interface of the dynamometer controller was used to pass a speed reference. The engine load control was realised removing the accelerator pedal and using a dSPACE digital output to generate a suitable PWM signal. To facilitate the air-path control, it was required to be able to modify the internal ECU signals. This was implemented in the form of external bypassing using the RTI Bypass Blockset for MATLAB. The communication between the dSPACE system and the ECU was based on the CCP protocol. To realise such a setup, the A2L file in the ASAM AML (see [ASAM]) compliant format is required for the ECU control strategy. For this reason the original ATI Vision compatible A2L file had to be modified. The fix included importing the AML library of dSPACE and removing non-AML-compliant definitions from the original file.

With this setup, the MPC controller had the access to the additional engine sensors, internal ECU signals, the VGT actuator and the compressed air injection valve (see Figure 2.5).

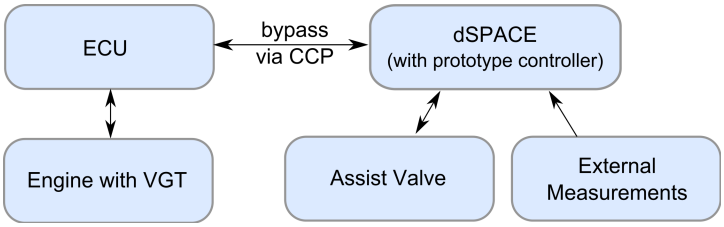

Figure 2.5: Realisation of Real-Time MPC air-path control system.

To ensure the repeatability of the experiments conducted, scripts in Python language were written. This way an automated process for testing any speed/load scenarios was achieved.

2.2.4 Steady-state testing

Steady-state testing is a useful starting point for experimental work, because it verifies the quality of the experimental setup and allows for cross-checking of the available measurements. The steady-state testing results will also be used in the first step of model calibration process.

During the tests the EGR valve was fully closed, because this study is focused on significant engine transients. Fuelling and boost pressure were controlled according to the standard ECU strategy. The dynamometer was responsible for maintaining the desired engine speed, whilst the accelerator pedal input was modulated by the dSPACE system to achieve a desired level of engine torque. Engine speed and fuelling in milligrams per stroke were used to define the engine operating point. The engine was tested in a speed range from idle up to 3000 RPM and in the fuelling range from motoring to full-load as shown in Figure 2.6a.

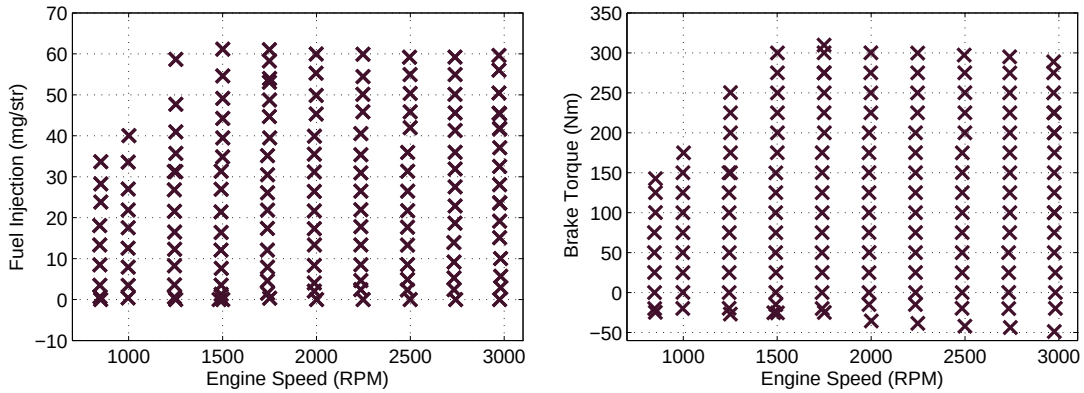

(a) Fuel injection (b) Brake torque

Figure 2.6: Steady-state testing - operating points.

When referring to the engine operation, the definition of steady-state is not obvious, because of a wide range of time constants involved. The slowest air-path dynamics mode is the one associated with the inertia of the turbocharger. The corresponding time constant varies slightly due to system non-linearity, but after several seconds the air-path is considered to have settled. However, much slower heat transfer dynamics affects the turbine side. During significant steps the temperature measured in the exhaust manifold changes for several minutes.

The necessity of waiting for so long is questionable, when one considers the fact that the entire full-load acceleration manoeuvre lasts for less than 10 seconds. In the steady-state measurements considered here the system was allowed to settle for 150 seconds, after which time a recording of 10 seconds was performed.

The measured signals were checked for their plausibility and the time average values over the entire recording were analysed. It is necessary to comment on the accuracy of measuring the gas temperature. In fact, rather than the gas temperature, "the temperature indicated by the sensor is a very accurate measurement of the equilibrium temperature a properly calibrated sensor has reached while exposed to the gas and its surroundings" [Daniels, 1968]. The complex interaction of a thermocouple with its surroundings includes:

1. Radiative heat transfer between a sensor and its surroundings; the temperature of manifold and pipework walls is usually significantly lower than the temperature of the gas - this effect leads to offsets between the thermocouple reading and the actual temperature of gas, magnitudes of the offsets are strongly related to the size of the thermocouple [Ricardo Software, 2011] and vanish for a sensor of infinitely small diameter

2. Convective-conductive heat transfer between a thermocouple and the gas; this is the key phenomenon allowing for measuring the gas temperature; there are considerable dynamics involved [Kar et al., 2004]

3. Conductive heat transfer from a thermocouple to its support

Measuring the gas in the exhaust manifold is particularly challenging. On one hand the thermocouple has to be robust enough to withstand the harsh environment: temperatures above 1000 K and very high velocities. This can be achieved by using thermocouples of bigger diameters - 1.5 mm sensors are often used in testing (for production, sensors with a much larger diameter are used). On the other hand, the exhaust manifold is the volume where the radiation effects are the most significant. The exhaust gas temperature measurement error at steady-state may be as much as several tens of degrees [Ricardo Software, 2011]. Even if the gas temperature is measured "correctly", there is still a problem of temperature/velocity variation across the duct.

The analysis of steady-state data was performed to identify fast and reliable measurements/estimates for air and fuel flow. The drawback of the AVL Fuel Flow meter lies in its low bandwidth. This makes this instrument unsuitable for fast transient manoeuvres. The ECU provides an estimate of the fuel flow based on the fuelling demand. The accuracy of this estimate relies on a knowledge of the characteristics of injectors. Correction factors exist in the ECU for each individual injector and such a strategy leads to a satisfactory accuracy. In Figure 2.7a fuel flow estimated by the ECU is plotted against the AVL Fuel Flow Meter measurement.

CO_2 concentration in the exhaust manifold (X_{CO_2}) was also measured with a Cambustion NDIR500 system. This can be used for verifying the fuel flow estimate using the following equation:

$$X_{CO_2} = 100 \frac{w_{CO_2}}{w_f + w_{cmp}} \frac{M_{air}}{M_{CO_2}} \tag{2.1}$$

with $M_{air} = 29$ used for the average molecular mass of dry air, w_{CO_2} for the mass flow of CO_2, w_f for the fuel flow and w_{cmp} for the mass flow through the compressor. This is a rough approximation as the exhaust gas composition, especially at high loads, differs significantly from dry air. CO_2 flow can be estimated assuming complete combustion, i.e. as a result of combustion every particle of carbon from the fuel turns into carbon dioxide:

$$w_{CO_2} = w_f CF \frac{M_{CO_2}}{M_C} \tag{2.2}$$

CF stands for the fuel's carbon mass fraction. The average fuel composition was assumed to be $C_{12}H_{23}$, therefore:

$$CF = \frac{12M_C}{12M_C + 23M_H} \tag{2.3}$$

Comparison of such an estimation and the direct measurement of X_{CO_2} is shown in Figure 2.7b. Good agreement confirms that the fuel flow estimation in the ECU can be used for further analysis.

Another cross check is performed based on the exhaust oxygen concentration

measured with HORIBA EXSA. The original measurement is a dry one, i.e. when water vapour was removed from the sample. Therefore, raw measurements were corrected estimating the water vapour content using the combustion equation and the measured air-to-fuel ratio. Oxygen concentration X_{O_2} can also be estimated from the fuel flow and the mass air flow:

$$X_{O_2} = 100 \frac{Y_{O_2,amb}(w_{cmp} - AFR_{stoich} w_f)}{w_f + w_{cmp}} \frac{1}{1.11} \tag{2.4}$$

Ambient oxygen concentration $Y_{O_2,amb}$ was estimated from recorded ambient pressure, temperature and humidity conditions. The correction factor between the definition of concentration by mass and by volume varies in reality due to changing gas composition. The constant factor of 1.11 was, however, found to be an adequate approximation [Cieslar et al.].

The comparison between the measured and calculated concentrations is shown in Figure 2.7c. It is concluded that the ECU's fuel flow estimation and compressor flow measured by the MAF sensor give readings of adequate accuracy.

The differences between the mean values of the pressure in the post-compressor volume and in the intake manifold are shown in Figure 2.7d. They are caused by the pressure drop through the intercooler. At high air flow rates the difference reached about 0.15 bar. It is also worth mentioning that at these conditions, the pressure upstream of the compressor dropped to 0.9 bar and a pressure of 1.35 bar was recorded downstream of the turbine. These values suggest that assuming ambient conditions before the compressor and after the turbine is not suitable for the manoeuvres investigated.

A steady-state torque deficit at high loads and low engine speeds (as observed in Figure 2.6b) is the consequence of a limited fuel injection. This is caused by the inability of the air-path to deliver the amount of air sufficient for combustion at air-to-fuel ratios above the smoke limit. At steady-state operation the compressor surge line is the main limiting factor (as previously explained in Figure 1.7).

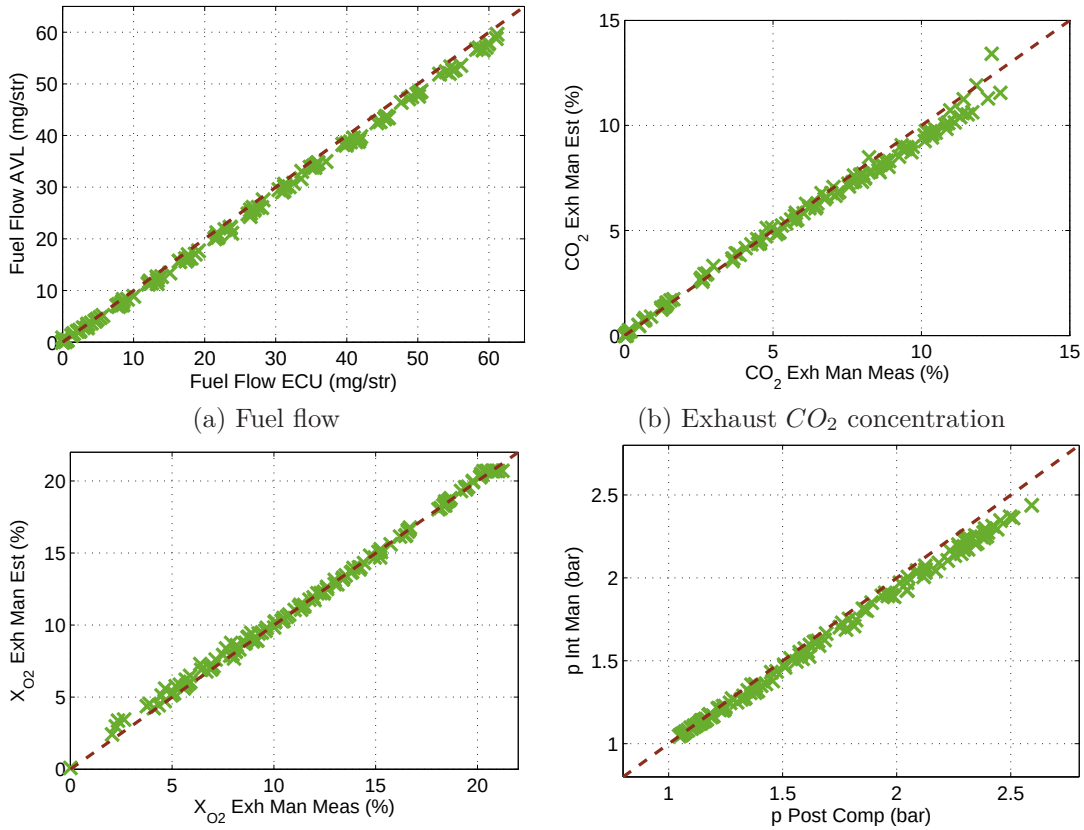

(a) Fuel flow

(b) Exhaust CO_2 concentration

(c) Exhaust O_2 concentration

(d) Pressure drop across intercooler

Figure 2.7: Summary of steady-state testing results.

2.2.5 Reference manoeuvre

Turbo-lag is most pronounced during "hard" acceleration from low engine speed. An in-gear full-load "tip-in" manoeuvre is a realistic scenario suitable for investigating the transient performance of turbocharged engines [Katrasnik et al., 2005]. Moreover, this particular transient case exercises the model throughout a wide range of rapidly changing operating points.

At the start of the manoeuvre the engine is operating at low speed and load. A step in driver torque demand is then applied. The engine response time is limited by the air-path's ability to deliver oxygen to the combustion chamber. This is due to a limit on the air-fuel ratio intended to prevent excessive engine-out smoke. As a result, the fuel quantity which can be injected into the cylinders is constrained and the torque demand can not be immediately matched (see section 3.1.1 and

Figure 3.2 for a detailed description). This manoeuvre is a version of the speed increase transient test described in detail in [Rakopoulos, 2009].

Road load model

It is desirable to simulate the load the engine would experience in a real vehicle, e.g. simulating the acceleration of the vehicle with a fixed gear engaged. To facilitate such a testing scenario, a model of road load and driveline is required. It determines the reference dynamometer speed as a function of the torque measured by the shaft torque transducer.

The model used in this work considers only the longitudinal motion of vehicle and wheel slip is assumed absent [Guzzella and Sciarretta, 2005]. The only dynamic state is the synchronised rotational speed of wheels N_{wh}:

$$\frac{dN_{wh}}{dt} = \frac{T_B r_{fd} \eta_{fd} r_g \eta_g - T_{brk} - F_{res} L_{rr}}{J_e r_{fd}^2 r_g^2 + 4J_{wh} + m_V L_{rr}^2} \tag{2.5}$$

The inertia of engine is denoted by J_e and the inertia of each wheel by J_{wh}. In the above equation, the total torque driving the wheels is calculated by subtracting the torque due to the braking system T_{brk} and the motion resistance torque $F_{res}L_{rr}$ from the propulsion torque. The latter is calculated by multiplying the engine torque T_B by the final drive ratio r_{fd} and gear ratio r_g. Transmission losses are included via the differential efficiency η_{fd} and gearbox efficiency η_g.

The motion resistance force is given by the sum of the rolling resistance F_{rr} and air drag F_{ad} forces:

$$F_{rr} = c_{rr} m_V g \tag{2.6}$$

$$F_{ad} = \frac{1}{2} \rho_{air} A_{fr} c_{ad} (N_{wh} L_{rr})^2 \tag{2.7}$$

where c_{rr} is the rolling resistance coefficient, for simplicity assumed to be independent of speed. The air drag force is modelled using the density of air ρ_{air}, the frontal area of the vehicle A_{fr} and the air-drag coefficient c_{ad}.

Values for these parameters are taken from [Fraser et al., 2009], which is based upon a European D-segment gasoline engine powered vehicle. In order to reduce

the engine speed to match the considered Diesel engine's operating range, the final drive ratio was changed from 3.94 to 3. No other changes were considered necessary for a representative transient simulation.

2.3 Engine simulation model

Models of the system under investigation are important tools in the process of controller design. There are at least two major reasons for their development: system simulation and model based control. This section describes the model used for engine simulation. In the next section, the model structure chosen for model based control is introduced.

Internal combustion engine modelling is a very broad discipline and has been recently expanding to support the design of novel engine architectures. Families of models used in ICE development can be divided into the groups shown in Figure 2.8. These various types of models are briefly reviewed based on [Varnier, 2012] and [Leufvén, 2010]):

3D CFD models use Computational Fluid Dynamics (CFD) techniques for a detailed analysis of local phenomena. This is achieved by discretising the flow domain into a great number of tiny volumes and solving Navier Stokes equations for each of them. 3D CFD models can be used to investigate behaviour of the flow in the centrifugal compressor, flow through port valves, spray formation, flame kernel development, etc.

1D models simulate the gas dynamics only along the main axis of flow solving the equations based on the principles of conservation of mass, momentum and energy. These crank angle resolved models are state-of-art for simulating the entire engine, but the calculation times are significantly slower than real-time. They allow for the investigation of gas dynamic phenomena in the air-path and at the valve ports. 1D engine models feature combustion models, complex heat transfer models and track several species. Turbocharger models are usually based on static maps.

"Real-Time" 1D models have been recently developed to allow for Real-Time simulation of engines to support Hardware-in-the-Loop (HiL) activities. RT

1D models solve simplified equations in the crank angle domain. They also have a heat transfer model, combustion model and may track several gas species. The level of simplification required depends on the hardware used for simulation. RT 1D models can be treated as lying between distributed parameter models (1D) and lumped parameter models (0D)

Filling and emptying 0D models are crank resolved, but use lumped parameters to describe the state in various sections of the air-path. They are based on principles of conservation of mass and energy, but neglect the principle of conservation of momentum. Pressures and flows in volumes exhibit pulsations due to intake and exhaust valve opening, but spatial phenomena are neglected.

0D mean value engine models differ from filling and emptying models by ignoring the engine cyclic operation. Modelled quantities are averaged over a single engine cycle. A simple engine block characterisation is used, often map-based. Phenomena caused by processes based on crank angle domain, e.g. blow through during valve overlap, are not directly simulated and need to be captured in the terms of calibrated efficiencies or correction factors. This family of models benefit from a low number of dynamic states and short calculation time.

Behavioural models: These models capture engine behaviour in the form of look-up tables, neural networks, polynomial functions, etc. They are often used for vehicle-level investigations.

Selection of the appropriate model type for a particular task is a question of finding the best trade-off between its capabilities and complexity. Very complex models not only demand significant computational power leading to long simulation times, but also require a significant calibration effort. Often the calibration parameters cannot be directly measured.

To determine the requirements of engine simulation model capabilities for the present work, the use of the intended model is reviewed. The simulation model is supposed to:

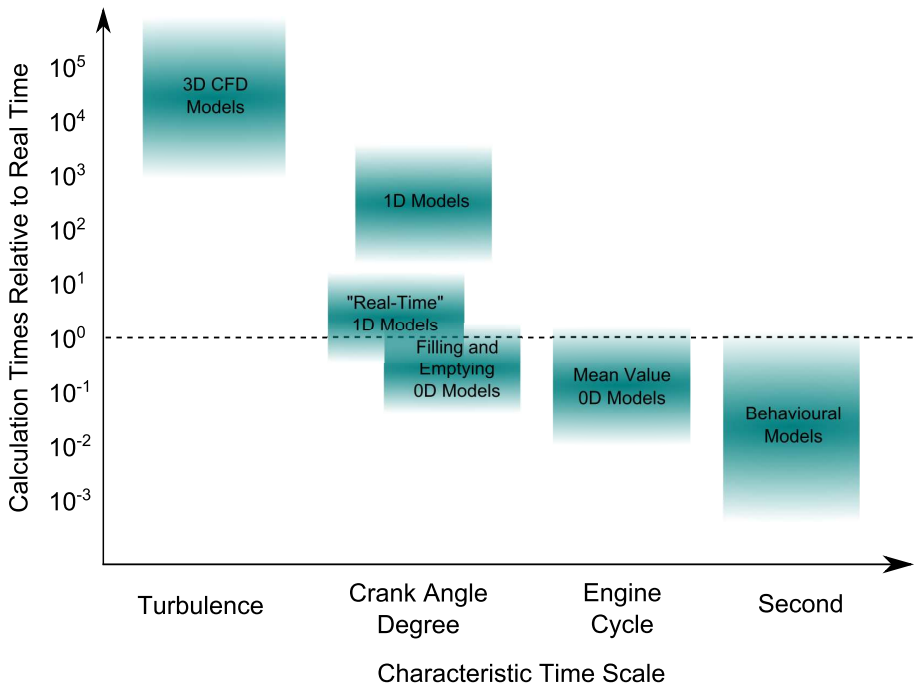

Figure 2.8: Engine models - capabilities and required computational time.

1. help in gaining insight into the most important air-path characteristics and processes during engine transients,

2. verify novel concepts prior to implementation,

3. serve as the plant model in the process of controller testing.

In order to successfully achieve the first two objectives, a simulation model should have a certain predictive capability. It should produce realistic solutions for variables which were not adjusted at the model calibration stage and for operating conditions outside of the calibration range. These are the features of models based on physical laws and conservation principles, as opposed to models derived from empirical data. A 1D engine simulation model was therefore considered to be the suitable engine simulation tool.

2.3.1 Full load model of the DW10C engine in Ricardo WAVE

Ricardo WAVE is a software package for engine and 1D gas dynamics simulations. A full-load model of DW10C engine in WAVE was supplied by Ford Motor Co. The top layer of this model is shown in Figure 2.9.

The model was set up to perform analysis around several operating points lying on the full-load curve. It featured a detailed parametrisation of the intake, EGR and exhaust systems. It used the semi-predictive Diesel Wiebe Combustion Model of WAVE with a single fuel injection and an estimation of ignition delay. This combustion model requires only two global parameters: fuel Cetane number and engine rated speed. Heat transfer parameters for the engine block and the pipework were also calibrated in the original model.

2.3.2 Turbocharger model

A standard approach to modelling static turbocharger characteristics relies on look-up tables for the compressor and the turbine. The underlying assumption is that the gas dynamic processes within the compressor and the turbine are much faster than those in the manifolds [Guzzella and Onder, 2004]. Both devices can be modelled in the same input-output convention, i.e. their interfaces with volumes upstream and downstream are identical. The traditional static description defines the steady-state relations between mass flow, pressure ratio, turbocharger speed and efficiency.

Compressor and turbine maps are generated by extrapolating data provided by turbocharger suppliers. Such data are based on gas stand testing of turbochargers. The data are usually only available for high turbocharger speeds, because at lower speeds heat transfer between the turbine and compressor housing introduces significant challenges to accurate characterisation [Moraal and Kolmanovsky, 1999], [Jung, 2003].

Under the assumption of isentropic (reversible, adiabatic) processes, the relation between the pressure (p) and temperature (θ) ratio across a compressor is

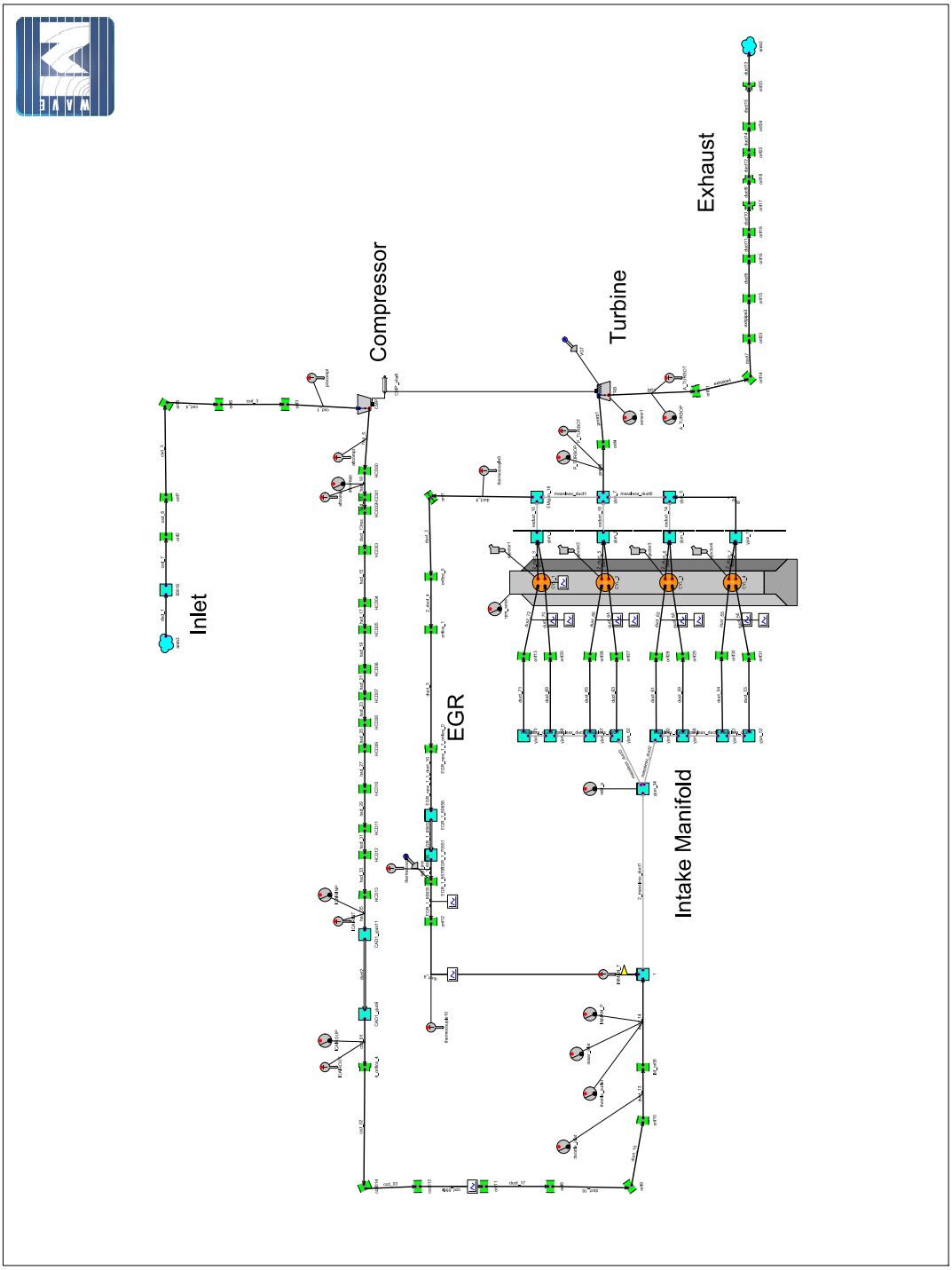

Figure 2.9: Original DW10C full load model.

defined as follows:

$$\frac{p_2}{p_1} = \left(\frac{\theta_{2,is}}{\theta_1}\right)^{\frac{\gamma}{\gamma-1}} \tag{2.8}$$

with γ for the ratio of specific heats for air.

The subscript 1 relates to the inlet conditions and the subscript 2 stands for the conditions downstream of an element. In reality, the process of compression involves losses due to irreversibilities. The effect of irreversibilities is addressed by introducing the concept of an "isentropic" efficiency η_{is}. For a compressor it relates the reversible power requirement P_{rev} to the actual power requirement P_{act} and is defined in the following manner:

$$\eta_{cmp,is} = \frac{P_{rev}}{P_{act}} = \frac{\theta_{2,is} - \theta_1}{\theta_2 - \theta_1} \qquad 0 < \eta_{cmp,is} < 1 \tag{2.9}$$

In effect, the isentropic efficiency is a correction factor for the difference between reality and the ideal.

Similarly, assuming isentropic expansion the pressure and temperature ratio across a turbine are related by:

$$\frac{p_1}{p_2} = \left(\frac{\theta_1}{\theta_{2,is}}\right)^{\frac{\gamma}{\gamma-1}} \tag{2.10}$$

and the isentropic efficiency, defined as the ratio of the actual power output to the reversible power output, is determined from:

$$\eta_{trb,is} = \frac{P_{act}}{P_{rev}} = \frac{\theta_1 - \theta_2}{\theta_1 - \theta_{2,is}} \qquad 0 < \eta_{trb,is} < 1 \tag{2.11}$$

In order to account for the pressure and temperature conditions during a mapping process, mass flow (w) and speed (N_t) data are often given in the following form:

$$\hat{w} = \frac{w\sqrt{\theta_1}}{p_1} \tag{2.12}$$

$$\hat{N}_t = \frac{N_t \frac{30}{\pi}}{\sqrt{\theta_1}} \tag{2.13}$$

In Ricardo WAVE an additional scaling utilising the gas constant R and the reference diameter D_{ref} is used to non-dimensionalise the two variables. Finally the scaled quantities will be referred to as mass flow parameter $\bar{w}$ and speed parameter $\bar{N}_t$:

$$\bar{w} = \hat{w}\frac{\sqrt{R}}{D_{ref}^2} \tag{2.14}$$

$$\bar{N}_t = \hat{N}_t\frac{\pi D_{ref}}{30\sqrt{R}} \tag{2.15}$$

The isentropic efficiency can be used as an intermediate variable for determining the temperature of the gas leaving the compressor/turbine and the absorbed (compressor) or the generated (turbine) torque. There are two drawbacks of such a formulation. Firstly, calculating physically sensible torques and temperatures in the vicinity of zero speed/zero flow conditions is challenging. For example, the post compressor temperature calculation is sensitive to low values of the compressor efficiency and will potentially give large temperature rises for pressure ratios close to unity if care is not taken when using a look-up table to capture the compressor efficiency. The torque calculation will then suffer from sensitivity to both flow and and temperature upstream of the element, which must be very accurate if sensible values are to be given as turbocharger speed approaches zero. Secondly, the torque characteristics are inherently bound up with temperature across the element. Breaking this relationship may be useful when compensating for heat transfer between the turbine and the compressor.

Temperature downstream of the compressor and torque T_{cmp} can be calculated from pressure ratio, speed, mass flow and efficiency as follows:

$$\theta_2 = \theta_1 + \frac{\theta_1}{\eta_{cmp,is}}\left[\left(\frac{p_2}{p_1}\right)^{\frac{\gamma-1}{\gamma}} - 1\right] \tag{2.16}$$

$$T_{cmp} = \frac{wc_p(\theta_2 - \theta_1)}{N_t} \tag{2.17}$$

The turbine outlet temperature and torque T_{trb} are determined using corre-

sponding formulae:

$$\theta_2 = \theta_1 - \theta_1 \eta_{trb,is} \left[1 - \left(\frac{p_1}{p_2} \right)^{\frac{1-\gamma}{\gamma}} \right] \tag{2.18}$$

$$T_{trb} = \frac{w c_p (\theta_1 - \theta_2)}{N_t} \tag{2.19}$$

WAVE manipulates the data in the mass flow/efficiency convention to generate temperature ratio and non-dimensional torque parameter maps.

$$\bar{T} = \frac{T}{p_1 D_{ref}^3} \tag{2.20}$$

This convention is directly related to the required outputs from the compressor/turbine model, as needed by the rest of the simulation (the mass flow, temperature and torque) and avoids any possibility of compounding errors when using two mapped parameters to calculate the third. If the isentropic efficiency is calculated at low turbocharger speed and pressure ratio points using this implementation, it will not give realistic values. However, this is of little importance - unlike the importance of giving sensible values for the temperature, torque and mass-flow.

The main advantage of this representation is that the performance at zero turbocharger speed is more easily extrapolated from the data provided at higher speeds. The assumption that the element acts as a throttle at zero speed also leads to the temperature ratio being unity at zero speed. Extrapolation of the torque parameter is less obvious, however it must be zero at zero speed and unity pressure ratio.

Compressor

Ricardo WAVE includes a map fitting algorithm which extrapolates the supplier's data to low speeds. The same map will be used later for the MVEM. The algorithm was set up to force the negative slopes of constant speed parameter lines. This did not have a significant effect in the range of pressure ratios considered. The result of fitting is shown in Figure 2.10.

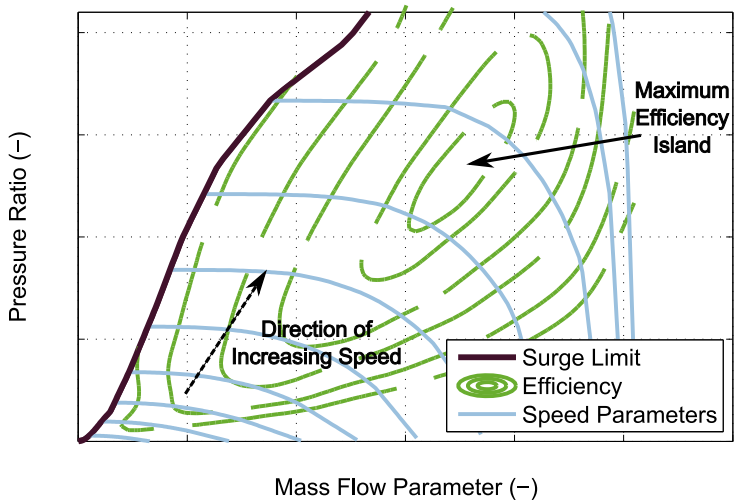

Figure 2.10: Compressor map generated with WAVE.

The non-linearity of the compressor characteristics is apparent. Considering the constant speed parameter lines it is observed that their slopes vary from almost perfectly horizontal near the surge limit to almost vertical at high flows. The contours of constant efficiency are roughly elliptical.

There are several limits of compressor operation [Watson and Janota, 1982]:

surge limit: the line defining the conditions at which fluid-dynamics instabilities destroy the regular flow pattern - this is the same phenomenon as stall of an aircraft wing and occurs when the flow no longer has enough "energy" to overcome the pressure gradient

maximum speed limit: turbocharger speed should be kept below this speed to avoid excessive centrifugal forces

choke limit: defines conditions at which the gas flowing through the compressor reaches the speed of sound

Experiments were performed on the test engine to validate the maps and the results are shown in Figure 2.11. The engine was operated to generate the characteristics along the speed lines found in the supplier's data. It is observed on the mass flow map that the experimentally determined points are indeed very close to the suppliers data. The temperature measured during experiments agrees

reasonably with the values determined from the model. Lower temperatures measured near the surge line suggest that the compressor efficiency is higher in this region. Overall, the validation of mapped compressor characteristics returned satisfactory results.

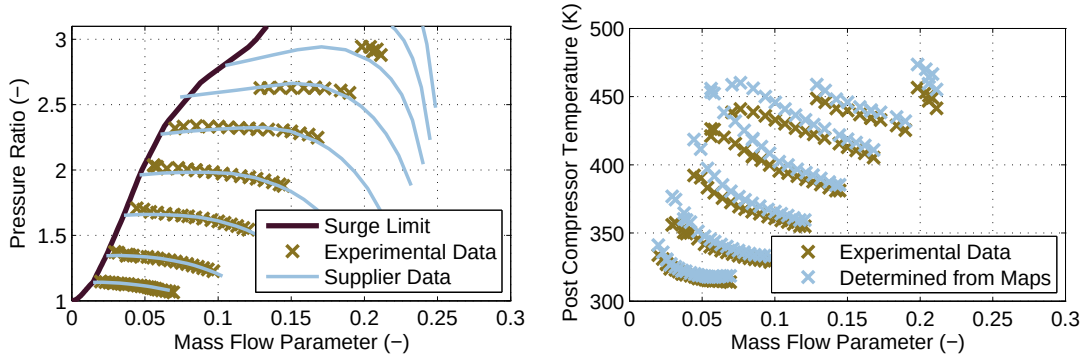

(a) Mass flow (b) Temperature

Figure 2.11: Experimental verification of compressor maps.

There exist models for simulating the compressor behaviour on the left hand side of the surge line, e.g. Moore-Greitzer model [Guzzella and Onder, 2004]. In this work it was not used as the objective is to avoid surge, rather than to stabilise a surging compressor.

Turbine

As mentioned in the general turbocharger modelling comments, the turbine is also mapped with torque parameter, temperature ratio and mass flow described as static functions of turbocharger speed and pressure ratio across the turbine.

When modelling a variable geometry turbine, there is another dimension to the maps. For several VGT rack positions the maps are generated and then linearly interpolated to calculate the final values. The turbine map generated with WAVE corresponding to a fully closed VGT is shown in Figure 2.12. A mass flow parameter for turbine is calculated in the same fashion as for the compressor (see Eq. 2.14).

The main departure from the conventions used above for the compressor lies in the fitting of the efficiency map. The angle of the incidence of the gas with regard to the turbine blade is the primary factor affecting the isentropic efficiency

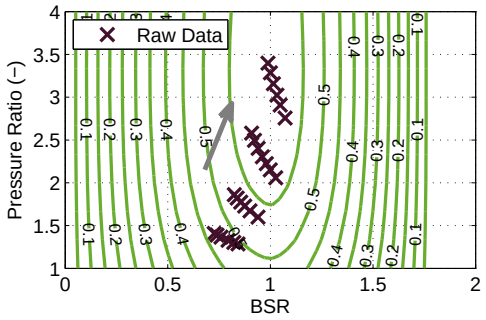

(a) Extrapolated efficiency map

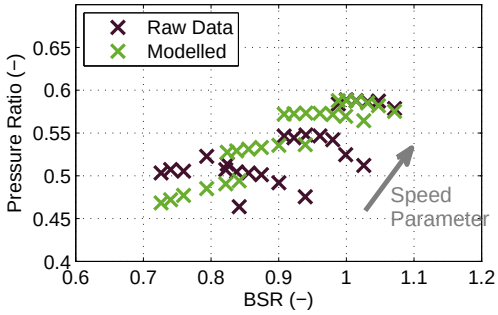

(b) Comparison of raw efficiency data to the map extrapolation

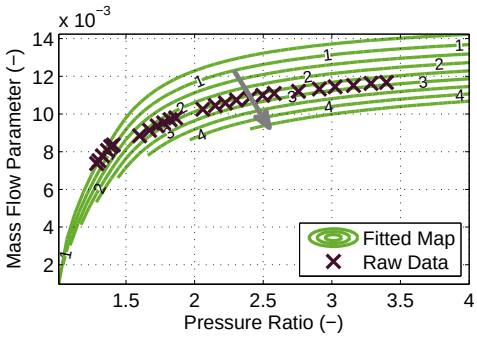

(c) Extrapolation of flow data

Figure 2.12: Example of turbine map fitting for a single VGT position.

of the turbine. This leads to mapping the efficiency as a function of blade speed ratio (BSR):

$$BSR = \frac{D_{ref} N_t}{\sqrt{2 c_p \theta_1 \left[1 - \left(\frac{p_2}{p_1}\right)^{\frac{1-\gamma}{\gamma}}\right]}} \tag{2.21}$$

As shown in Figure 2.12a, the highest efficiency for each pressure ratio is achieved at a BSR equal to 1. It is also observed that the peak efficiencies are pressure ratio dependent. The figure also shows how significant extrapolation is required. Moreover, this physically based method may result in the fitted map not necessarily passing through the experimental data (see Figure 2.12b).

The turbine maps were validated against the experimental data in a similar fashion to the compressor side. The results show a satisfactory match in flow and torque parameter. Measured temperature ratios exhibited a worse agreement. Turbine efficiency was calculated assuming equality of compressor and turbine

power. At low pressure ratios the effect of heat transfer from the turbine to the compressor housing was observed. As a result the efficiency in this region was above one (similar observations were made in [Jung, 2003]). The values at higher pressure ratios agreed with the mapped characteristics satisfactorily well. During this analysis using the measurement of temperature post turbine had to be avoided. The DOC with its significant thermal inertia is located near the turbine outlet, which makes the measurement of the temperature of the gas exiting the turbine very difficult.

The final remark in this section is that there are limitations on the accuracy of the simulations of turbocharger in 1D packages. An exhaustive investigation and discussion of such difficulties can be found in [Westin, 2005]. Being aware of such limitations, the model validation is considered to be acceptable for the purposes of this study. This is confirmed by the results presented in Chapter 4, where simulations of transient response improvements offered by injecting compressed gas into the exhaust manifold are verified experimentally.

2.3.3 Model calibration for part-load simulation

The chosen tip-in manoeuvre exercises the model across a wide range of rapidly changing operating points. The manoeuvre starts from low speed and load. Once the driver demands the maximum available torque, the engine traverses the part-load operating points to reach the full-load curve. It is, therefore, important for the simulation model to be calibrated for the operation at part-load conditions.

For this purpose steady-state data from engine test bench provided by Ford Motor Co. were used. The data included several ECU signals and some external measurements, e.g. peak in-cylinder pressure, selected temperatures and exhaust emissions.

Due to the lack of data for transient operation, the model could only be calibrated based on the available steady-state data. It was then assumed that the 1D gas dynamics code of WAVE offered sufficient prediction capabilities to produce credible results during the simulations of transient operation.

In the original model, several parameters and coefficients were set to a particular value for a certain operating point. As it is now intended to simulate the

engine's operation in transients, the parameters of interest (e.g. engine friction) will be described globally for the entire operating range.

The original model did not contain any flow restrictions (leading to pressure drops) in the exhaust pipework. In reality there exists a considerable pressure drop along the exhaust gas aftertreatment system comprising a DOC and a Diesel particulate filter. To ensure realistic boundary conditions, the diameter of one of the exhaust orifices was set to 34.5 mm. This is important at high flow operating points, when the turbine pressure ratio may be considerably affected.

Friction model

The modified Chen-Flynn model used in WAVE was chosen for the estimation of friction mean effective pressure p_{FME}:

$$p_{FME} = c_{1cf} + \frac{1}{n_{cyl}} \sum_{i=1}^{n_{cyl}} \left[c_{2cf} p_{max,i} + c_{3cf} S_{fact,i} + c_{4cf} S_{fact,i}^2 \right] \tag{2.22}$$

where $p_{max,i}$ is the maximum in-cylinder pressure and $S_{fact,i}$:

$$S_{fact} = \frac{1}{2} N_{e,RPM} L_{stroke} \tag{2.23}$$

The coefficients c_{1cf}, c_{2cf}, c_{3cf} and c_{4cf} were estimated from the validation data using the linear least squares (LLS) algorithm.

Combustion model

The most common approach to combustion modelling used in crank angle resolved models is to use Wiebe functions as an approximation to the rate of fuel mass burnt. This method has no predictive capability and the appropriate parametrisation of the Wiebe function has to be known a priori. WAVE includes a semi-predictive combustion model that calculates the rate of fuel mass burnt based on global engine and fuel parameters.

During steady-state part-load operation of the actual engine two pilot injections are used. The total quantity of fuel injected is required for simulation purposes. It is calculated simply as a sum of both pilots and the main injection.

It is also possible to simulate pilot injections in WAVE. For the sake of simplicity of calibrating the overall model, pilot injections were disabled in the WAVE model and only single injection was considered. In order to account for the lack of pilot injections, no ignition delay was assumed.

Due to the lack of information about the duration of fuel injection, values of this parameter were extracted from the full-load WAVE model. For a given engine speed it was assumed that at 0 Nm brake torque injection duration is equal to 2 crank angle degrees and at the full-load it is equal to the value found in the full-load model. At part-load conditions injection duration is linearly interpolated between these two levels.

Calibration procedure

One of the possible sets of demands for fuel injection in WAVE consists of injection quantity, injection duration and the start of injection timing (SOI). The first two quantities have already been discussed.

SOI has a direct effect on the in-cylinder pressure profile and therefore on the indicated torque and the exhaust gas temperature. In order to match the values of these three quantities simulated in WAVE with the validation data, SOI was calibrated for each operating point.

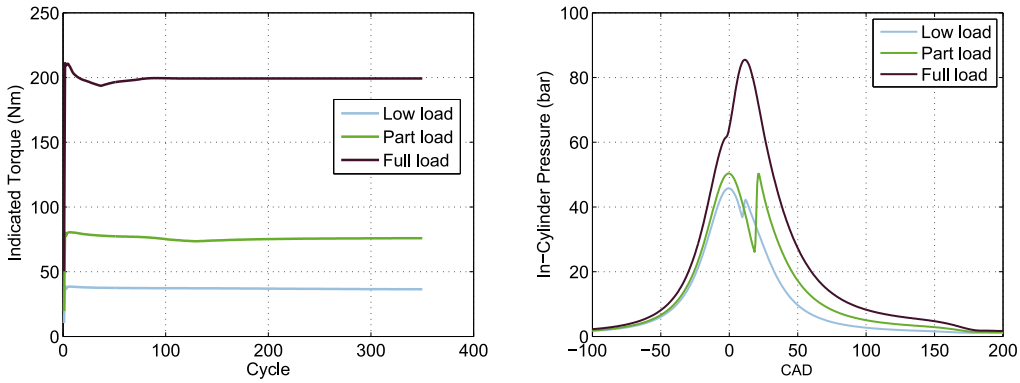

(a) Indicated torque

(b) In-cylinder pressure

Figure 2.13: Steady-state WAVE simulations.

Two simple PID controllers were added to the original model. One of them

used the VGT rack position to follow the intake manifold pressure request. The second PID drove the EGR valve to match the desired flow of fresh air. The set-points for boost and air flow were taken from the validation data.

In order to reach steady-state conditions, every operating point was simulated for 350 cycles. This was sufficient for the air-path dynamics to settle. The appropriateness of such a duration of experiment was confirmed by the plot of indicated torque (see Figure 2.13a). It shows the convergence at the engine speed of 1000 RPM. Three different levels of load are plotted and it is observed that the settling time was shorter for higher loads. Even faster convergence was observed at higher engine speeds.

Simulated in-cylinder pressures for the speed and load conditions considered in Figure 2.13a are shown in Figure 2.13b. At very low loads the peak pressure was equal to the motoring pressure and was achieved when the cylinder was at its top dead centre (crank angle degree equals zero). For a higher engine load, the pressure due to the combustion of fuel increased sharply and became higher than the motoring pressure. This remark is noteworthy, because in the SOI calibration procedure the error in maximum in-cylinder pressure was one of the factors of the cost function. It became inactive for all the loads with peak in-cylinder pressure below the motoring level.

Every operating point defined by speed and fuelling was simulated for 350 cycles with the SOI swept between -15 and 15 CAD. Three variables were used as targets:

1. Indicated torque (T_I)
2. Peak in-cylinder pressure ($p_{cyl,max}$)
3. Exhaust gas temperature (θ_x)

Turbocharger speed signal would be another good candidate, but such measurements were not available.

The $fminsearch$ function of MATLAB was used to search for the optimal

injection timing at each operating point. The cost function was universal:

$$cost(SOI) = c_1 \frac{\mid T_I(SOI) - T_{I,ref} \mid}{T_{I,ref}} + c_3 \frac{\mid \theta_x(SOI) - \theta_{x,ref} \mid}{\theta_{x,ref}} + \\ + c_2 \frac{\mid p_{cyl,max}(SOI) - p_{cyl,max,ref} \mid}{p_{cyl,max,ref}} \tag{2.24}$$

The selected penalty on peak in-cylinder pressure error was lower in comparison to the two others, because an accurate in-cylinder pressure matching is not essential for the investigation of the air-path dynamics. Indicated torque and exhaust gas temperature were more important. An example of such an optimization for a single operating point is shown in Figure 2.14.

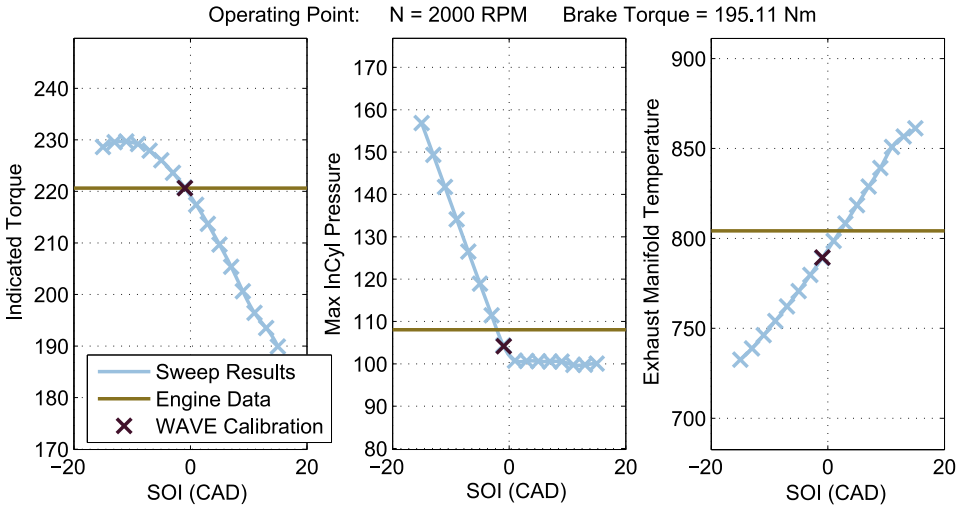

Figure 2.14: Example of injection timing calibration.

A trade-off between the level of indicated torque and exhaust temperature is clearly visible. Early fuel injection leads to high torque being available at the output shaft. Late injection is characterised by a higher portion of the available energy being dissipated to the exhaust, where it can be then harvested by the turbine.

Each operating point was simulated once again for 350 cycles with the optimized injection timing. The results are compared with the validation data as shown in Figure 2.15. Blue dashed lines indicate 10% error bands.

It is observed that the majority of the signals of interest was within the 10%

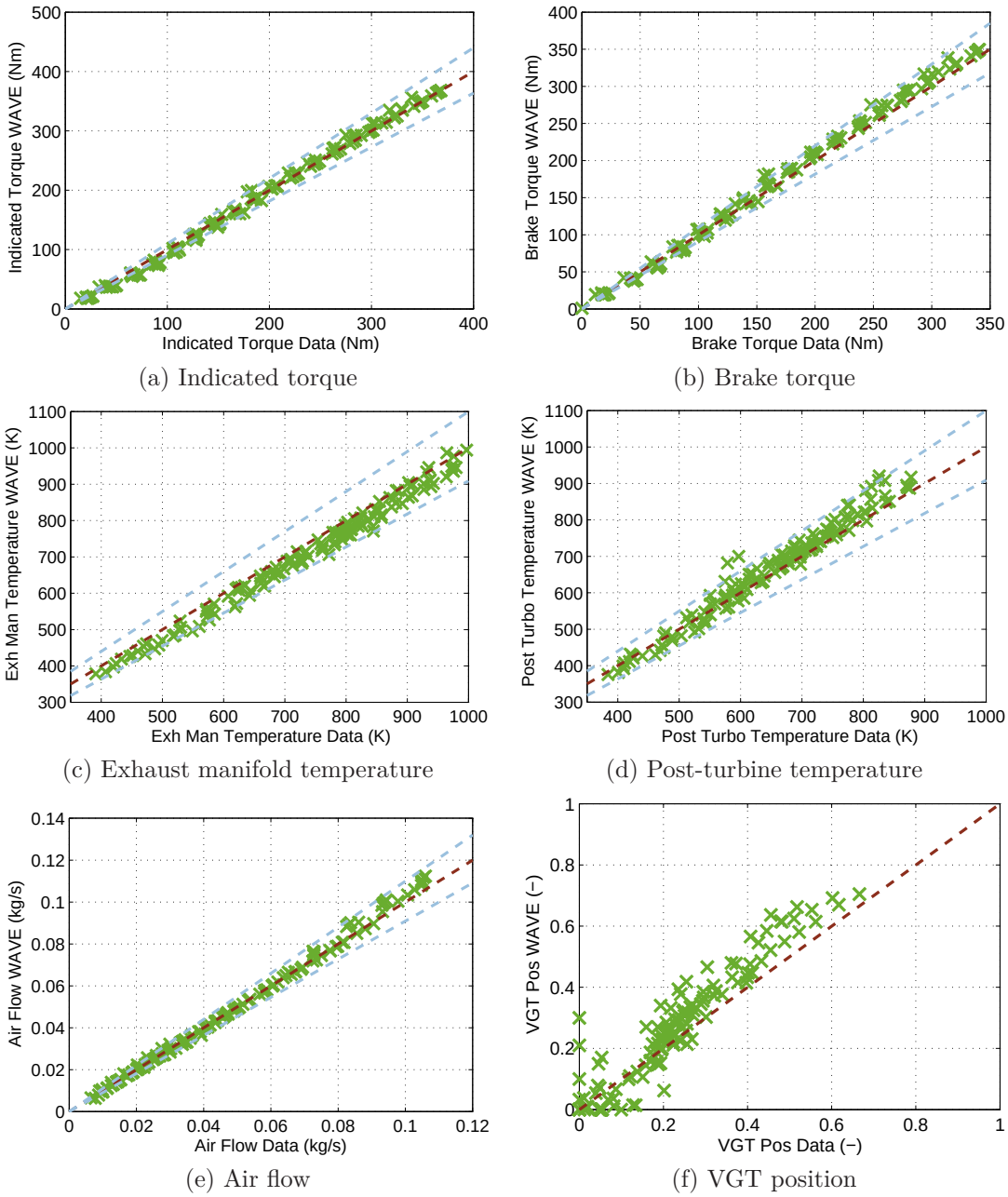

(a) Indicated torque

(b) Brake torque

(c) Exhaust manifold temperature

(d) Post-turbine temperature

(e) Air flow

(f) VGT position

Figure 2.15: Validation of WAVE model against steady-state data.

band. Very good agreement was obtained in the indicated torque. WAVE overestimated brake torques at high loads, which indicates that the friction coefficient related to in-cylinder pressure could be increased. Calculated temperatures were also satisfactory. The exhaust manifold temperatures simulated in WAVE were below the measured values. On the other hand the post-turbine temperatures were above the experimental values. This indicates a low temperature drop across the turbine. Such an insignificant difference may be caused by the improper parameters in the heat transfer model. A good agreement in simulated and measured air flows is a particularly encouraging result. A significant scatter in the figure with VGT positions suggests that a correction may be required when attempting to replicate input-output relationships during control system design.

In summary, it is concluded that the calibrated part-load WAVE model is able to produce solutions which are satisfactorily close to steady-state validation data.

2.3.4 Model modifications to include boost assistance systems

In the previous section the simulation model with the conventional air-path configuration was validated. The WAVE model can be now modified to include candidate turbocharger assistance systems (see Figure 2.16). The following concepts are considered:

1. compressed air injection upstream of the compressor
2. compressed air injection into the intake manifold
3. compressed air injection into the exhaust manifold
4. turbocharger electric assistance (TEA)

Compressed air assistance was modelled in the same way for each of its variants. Compressed air tanks were assumed to be of infinite volume with air stored at a pressure of 3 bar and temperature of 300 K. They were connected to the injection points through control valves. Connections between the standard pipework and the compressed air supply system were modelled as junctions of minimum possible volumes.

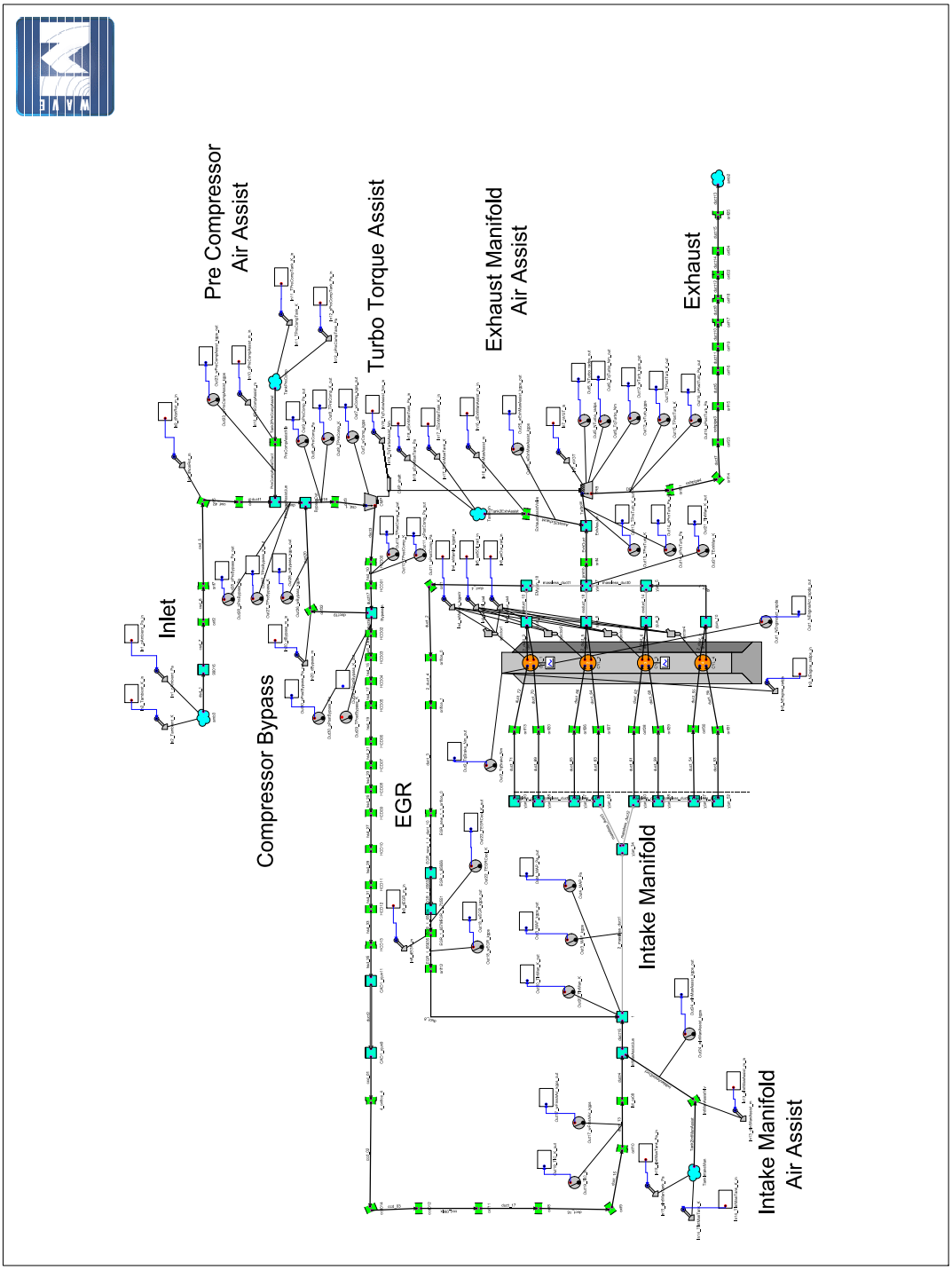

Figure 2.16: Modified part-load model in WAVE.

Injecting compressed air upstream of the compressor is a special case, because it requires an additional non-return valve. The valve was implemented upstream from the injection point and was closed fully whenever the conditions would cause the injected air to escape through the air-box.

Simulation of electric turbocharger assistance system is straightforward. This system was modelled by an actuator, which added an arbitrary torque to the turbocharger shaft. As this system will be used as a benchmark for compressed air assistance, it was assumed that the turbocharger inertia is not affected by additional electric components.

2.3.5 Co-simulation with Simulink

The MATLAB/Simulink environment was chosen as the main tool for controller development. The WAVE package includes an interface to Simulink (see Fig. 2.17). Any WAVE signal can be accessed from Simulink as long as it can be assigned to a relevant sensor or actuator.

The input signals from Simulink include: injection parameters, VGT and EGR inputs, compressed air and torque assistance inputs. Additionally, the WAVE model is supplied with ambient conditions, engine speed and compressed air supply parameters.

The set of measured signals include brake torque, turbocharger speed, turbocharger torque and all the pressures, temperatures and mass flows in various sections of the air-path.

In the Simulink environment, the WAVE model is complemented with the *EngineCtrl*, *Dyno*, *DynoCtrl*, *Driver* and *Environment* subsystems. The *Driver* subsystem is used to control both the engine model and the load model to perform specified manoeuvres. The *Environment* block can be used to set the ambient conditions. The *DynoCtrl* includes the load model, which can be switched between the road load model and fixed torque load. The *Dyno* block was intended as a subsystem for simulating the dynamometer dynamics.

Finally, the *EngineCtrl* subsystem contains two parts: a fuelling controller and an air-path controller. Fuelling parameters are determined based on the demanded brake torque and simulated engine speed. In this part of the model

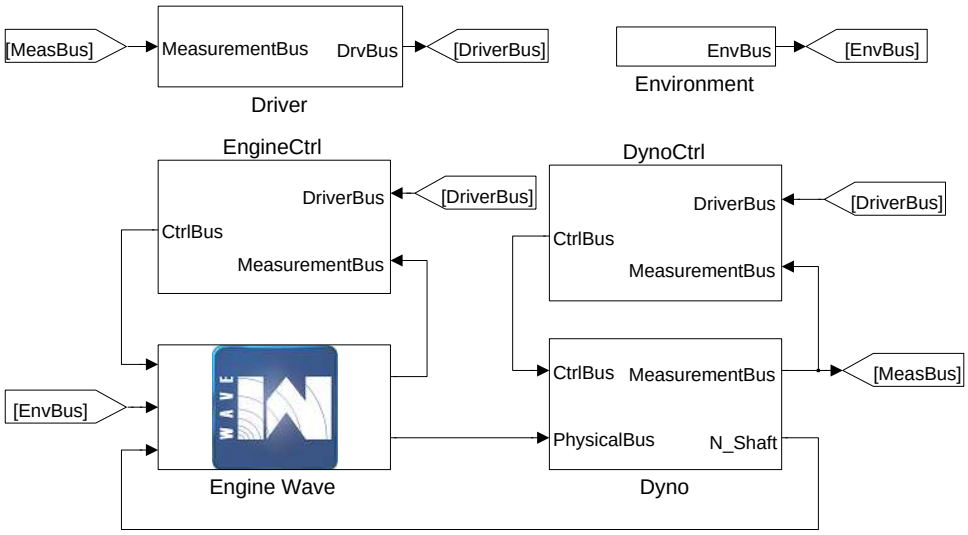

Figure 2.17: The top layer of Simulink model including WAVE model.

a smoke limit is also implemented. The air-path part of the *EngineCtrl* block allows for using open loop and closed loop control. The latter may be in the form of PID-based control or MPC control.

2.4 Mean value engine model

The MPC controller implemented in this project uses a simple mean-value engine model to calculate predictions. Mean-value engine models are well established and have been demonstrated to capture many of the fundamental characteristics of real engine operation. There are two MVEMs developed here. One of them is based upon, and calibrated to match, the results of the 1D simulation model implemented in WAVE. The second MVEM is intended for Real-Time MPC and therefore is implemented in C code. This model is parametrised and validated against the extended data set captured during dedicated engine tests.

2.4.1 MVEM equations

The approach taken here is substantially the same as described in [Hendricks, 1997], [Darlington et al., 2006], [Moulin and Chauvin, 2009] with some additions to allow the effects of boost assistance to be considered.

The overall structure of the MVEM is to consider the air-path as a number of fixed volumes with dynamic states. The flows into and out of these volumes are given by static descriptions of various components (see Figure 2.18). Turbocharger speed is the remaining dynamic state.

The MVEM described below is formulated based on the following assumptions:

- ideal gases with the specific heats of dry air
- no heat loss through manifolds, pipework and turbocharger walls

For brevity not every block of the model is described below, as many blocks share the same implementation. The notation therefore frequently reuses the subscripts 1 and 2 to refer to the upstream and downstream conditions of a block in the model.

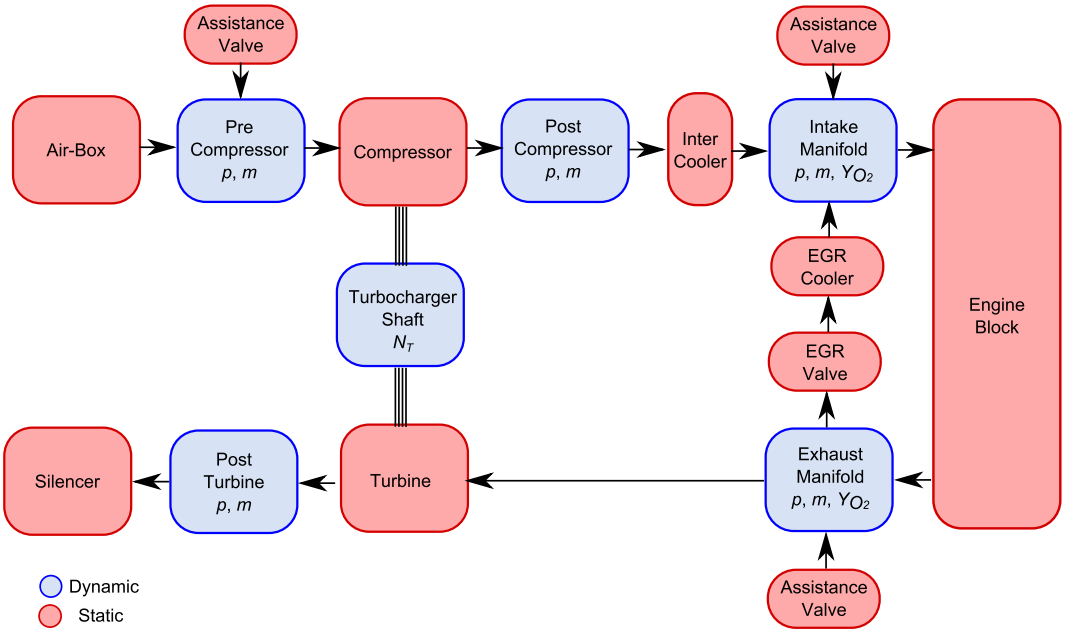

Figure 2.18: Structure of MVEM developed for the considered engine.

Orifices:

The orifice flow equation was found to be a convenient way to model the mass flow w_{or} through the air-box, intercooler, assist valves and exhaust exit:

$$w_{or} = \frac{A_{or} p_1}{\sqrt{R\theta_1}} \Psi \left(\frac{p_1}{p_2} \right) \tag{2.25}$$

where the function Ψ is defined to be:

$$\Psi \left(\frac{p_1}{p_2} \right) = \begin{cases} \left(\frac{p_2}{p_1} \right)^{\frac{1}{\gamma}} \left[\frac{2\gamma}{\gamma - 1} \left(1 - \left(\frac{p_2}{p_1} \right)^{\frac{\gamma - 1}{\gamma}} \right) \right]^{\frac{1}{2}}, & \text{for } \left(\frac{p_2}{p_1} \right) > 0.528 \\ \gamma^{\frac{1}{2}} \left(\frac{2}{\gamma + 1} \right)^{\frac{\gamma + 1}{2(\gamma - 1)}}, & \text{for } \left(\frac{p_2}{p_1} \right) \leq 0.528 \end{cases} \tag{2.26}$$

where p_1 and p_2 are pressures before and after the orifice, A_{or} is the effective area of the orifice and θ_1 is the temperature of gas at the orifice inlet. For air $R = 287$ $Jkg^{-1}K^{-1}$ is the gas constant and $\gamma = 1.4$ the ratio of specific heats.

Control volumes:

The air-path is considered to comprise five volumes: the first represents the pipework from the air-box at the start of the air-system to the entrance to the compressor; the second covers the pipework from the compressor exit to the intercooler; the third from the intercooler exit through to the intake manifold; the fourth represents the exhaust manifold to the turbine inlet; and the final volume covers the turbine exit through to the silencer at the end of the air-system.

Each volume is modelled as containing an ideal gas with constant specific heats, taken to be those of atmospheric air. Hence the state in the manifold is given by:

$$pV = mR\theta \tag{2.27}$$

Where p is the pressure in the volume, V is the volume, m is the mass of gas in the volume, R is the gas constant and θ is the temperature of the gas in the volume. Differentiating the above equation with respect to time gives:

$$\frac{V}{R} \dot{p} = \dot{m}\theta + m\dot{\theta} \tag{2.28}$$

Now, as the gas in the volume is assumed ideal, its internal energy is given by:

$$U = c_V m\theta \tag{2.29}$$

Where U is the internal energy and c_V is the specific heat at constant volume. Differentiating equation 2.29 gives:

$$\frac{1}{c_V}\dot{U} = \dot{m}\theta + m\dot{\theta} \tag{2.30}$$

Equating equations 2.28 and 2.30 therefore gives:

$$\dot{U} = \frac{c_V V}{R}\dot{p} \tag{2.31}$$

Conservation of energy and the ideal gas assumption lead to an alternative expression for the rate of change of internal energy in the volume:

$$\dot{U} = c_p \sum_{i=1}^{n} w_i\theta_i - \dot{Q} \tag{2.32}$$

Where c_p is the specific heat at constant pressure, the w_i are the mass flows in or out of the volume, the θ are the temperatures of those gas flows and Q is the heat transfer from the volume to the environment. If, following a commonly used convention, heat loss from the volume is neglected, 2.31 and 2.32 can be combined to give:

$$\frac{V}{\gamma R}\dot{p} = \sum_{i=1}^{n} w_i\theta_i \tag{2.33}$$

Where γ is the ratio of specific heats. Conservation of mass is used to give:

$$\dot{m} = \sum_{i=1}^{n} w_i \tag{2.34}$$

And together, equations 2.33 and 2.34 form the description of the volume.

The gases flowing out of the volume have a temperature determined by the ideal gas law.

Compressor and turbine:

Both the compressor and turbine are modelled by three two-dimensional maps. The maps f_{θ_r}, f_w and f_T give the temperature ratio, mass flow and torque parameters as functions of the speed parameter $\tilde{N}_t$ and the pressure ratio. The non-dimensional compressor parameters are converted to the values required by the model using:

$$\theta_2 = \theta_1 f_{\theta_r}\left(\frac{p_2}{p_1}, \bar{N}_t\right) \tag{2.35}$$

$$w = \frac{D_{ref}^2 p_1}{\sqrt{R\theta_1}} f_w\left(\frac{p_2}{p_1}, \bar{N}_t\right) \tag{2.36}$$

$$T = \frac{D_{ref}^3 p_1}{R} f_T\left(\frac{p_2}{p_1}, \bar{N}_t\right) \tag{2.37}$$

The same formulae are used for the turbine, but the pressure ratio is defined as $\frac{p_1}{p_2}$. The speed parameter $\tilde{N}_t$ is calculated as described in 2.3.2.

Turbocharger shaft dynamics:

Turbocharger shaft dynamics are calculated from Newton's Second Law:

$$\frac{dN_t}{dt} = \frac{1}{J_t}\sum_j T_j \tag{2.38}$$

where J_t is the turbocharger inertia and T_j are the torques acting on turbocharger shaft from the compressor, turbine and electric assist. Turbocharger shaft friction losses are neglected.

Coolers:

There are two charge coolers in the modelled air-path: intercooler and EGR cooler. Both describe the outlet temperature θ_2 as a function of the coolant temperature θ_{cool} and the inlet temperature θ_1:

$$\theta_2 = \theta_1 - \eta_{cool}(\theta_1 - \theta_{cool}) \tag{2.39}$$

The cooler effectiveness is given by the parameter η_{cool}.

Engine block:

The engine block is used to determine the brake torque, exhaust gas temperature, intake and exhaust mass flows. The flow from the intake manifold w_i is calculated using the speed-density equation:

$$w_i = \eta_v(N_e, p_i)\frac{N_e n_{cyl} V_{cyl} p_i}{\pi R n_{stroke} \theta_i} \tag{2.40}$$

The volumetric efficiency η_v is a two dimensional map based on the engine speed N_e and intake manifold pressure p_i. The other parameters are: the number of cylinders n_{cyl}, cylinder swept volume V_{cyl} and the number of strokes per cycle n_s. The intake conditions are defined by the pressure and temperature θ_i. The exhaust mass flow is calculated by summing the fuel flow w_f and intake flow:

$$w_e = w_i + w_f \tag{2.41}$$

The indicated torque T_I is calculated as a map of engine speed and fuelling in milligrams per stroke $\bar{w}_f$:

$$T_I = \eta_c(N_e, \bar{w}_f)\frac{w_f Q_{LHV}}{N_e} \tag{2.42}$$

where Q_{LHV} is the lower heating value for Diesel fuel. Fuel conversion efficiency η_c is again a two dimensional map scheduled on engine speed and fuel flow in milligrams per stroke. The brake torque T_B is calculated by subtracting the friction torque and transient pumping losses ΔT_P from the indicated torque. In this formulation, the fuel conversion efficiency parameter is based upon the mean value steady-state indicated torque (it is determined from the complete pressure-volume loop at steady-state operation). During significant transient manoeuvres, the instantaneous pressures in the intake p_i and exhaust p_x manifolds can be very different from their steady-state values, $p_{i,ss}$ and $p_{x,ss}$ respectively. Therefore the

increment in pumping losses due to transient operation is modelled as follows:

$$\Delta T_P = \frac{(\Delta p_i - \Delta p_x) n_{cyl} V_{cyl}}{4\pi} \tag{2.43}$$

where

$$\Delta p_i = p_i - p_{i,ss}(N_e, \bar{w}_f) \tag{2.44}$$

$$\Delta p_x = p_x - p_{x,ss}(N_e, \bar{w}_f) \tag{2.45}$$

This description of the transient pumping losses is consistent with the pumping work breakdown introduced in Heywood [1988]; it can be interpreted as the transient change in throttling work. This is a simplification of the actual phenomena as it assumes valve flow work remains constant, however it captures the main effects and fits well in the mean-value modelling framework.

The friction torque, T_F, is modelled as a second order polynomial of engine speed:

$$T_F = c_{1f} + c_{2f} N_e + c_{3f} N_e^2 \tag{2.46}$$

The final variable to be determined by the engine block is the exhaust gas temperature θ_e. This is modelled using the exhaust energy coefficient η_e:

$$\theta_e = \theta_i + \eta_e(N_e, \bar{w}_f) \frac{w_f Q_{LHV}}{c_p w_e} \tag{2.47}$$

where c_p is the specific heat capacity of air.

2.4.2 MVEM parametrisation

MVEM structure introduced in the previous section is general and can be adapted to various engines. To make it representative for a particular engine, the MVEM equations have to be parameterised and look-up tables have to be populated.

As mentioned earlier, there are two versions of MVEM used in this project. The first is used to formulate a controller for the WAVE model, whereas the second is used during engine testing. In the following section the MVEM parametrisation based on engine test results is described. It is then followed with brief comments on parametrising the MVEM for controlling the 1D model.

A description of calibrating MVEM based on a very extensive set of engine test results can be found in [Wahlström and Eriksson, 2011]. The authors use five calibration steps:

1. static parameters for each component are determined based on steady-state data
2. parametrising actuator models based on transient tests
3. effective manifold volumes and turbocharger inertia are deduced based on transient tests
4. time constants for engine torque are determined from transient tests
5. static parameters are recalibrated using the results from both steady-state and transient tests, least squares optimisation for particular components and the overall model is applied with initialising the parameters using values determined in the first step

In this section only the first and the third steps from the above list are described. A model for the VGT actuator dynamics is discussed in the next chapter. Accurate engine torque simulation using MVEM is not critical in this application.

The main parameters influencing transients of MVEM are volumes of various sections of the air-path and the inertia of the turbocharger. The WAVE-based MVEM uses the value of inertia found in the 1D model. The volumes of all the sections of the air-path were calculated assuming each duct in WAVE to be straight and of conical shape. Knowing the diameter at both ends of each duct and its overall length, the total volume can be approximated. The volumes of Y-junctions in WAVE are summed with duct volumes.

In the engine-based MVEM the values from WAVE are used as a starting point for a transient calibration.

The following parameters are determined based on steady-state test results:

η_v, η_c, η_e : engine block maps

c_{1f}, c_{2f}, c_{3f} : engine friction coefficients

$\eta_{cool,ic}$, $\eta_{cool,egr}$: EGR cooler and intercooler effectiveness

A_{airbox}, A_{ic}, A_{egr}, A_{exh} : effective areas for airbox, intercooler, EGR and exhaust exit

Turbocharger

Compressor maps generated by the algorithm implemented in WAVE were converted into the look-up tables using surface fitting. This imposes the condition that for a given pressure ratio the resulting functions of speed have to be single-valued. Furthermore, some fitting inaccuracies are observed in the vicinity of steep slopes occurring in each map at high pressure ratios. The resulting maps $f_{\theta r,cmp}$, $f_{w,cmp}$, $f_{T,cmp}$ are shown in Figure 2.19. The reference diameter is estimated by WAVE from the speed at which the maximum isentropic efficiency is achieved.

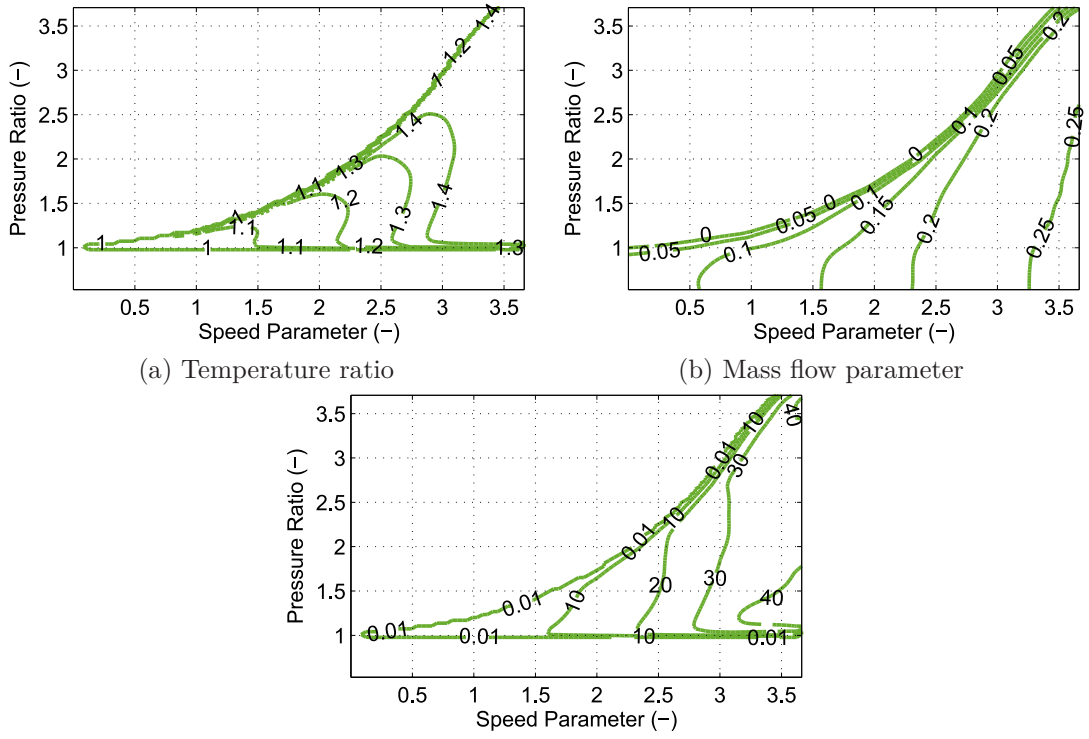

(a) Temperature ratio

(b) Mass flow parameter

(c) Torque parameter

Figure 2.19: Compressor maps used in MVEM.

The turbine maps for several VGT rack positions are formulated in exactly the same way as the compressor map. Six rack positions are parameterised and the final values of temperature ratio, mass flow and torque parameters are calculated linearly interpolating these maps.

Engine Block

The steady-state data were collected as described 2.2.4. Engine block maps were calculated according to their definitions presented in 2.4.1.

The volumetric efficiency (see Figure 2.20a) is mapped as a function of engine speed and intake manifold pressure. The top right part of the map is flat with values of about 0.9. The volumetric efficiency drops however at low engine speed and for low loads at higher engine speeds. Charge heating in the manifold and cylinder explains such characteristics [Heywood, 1988].

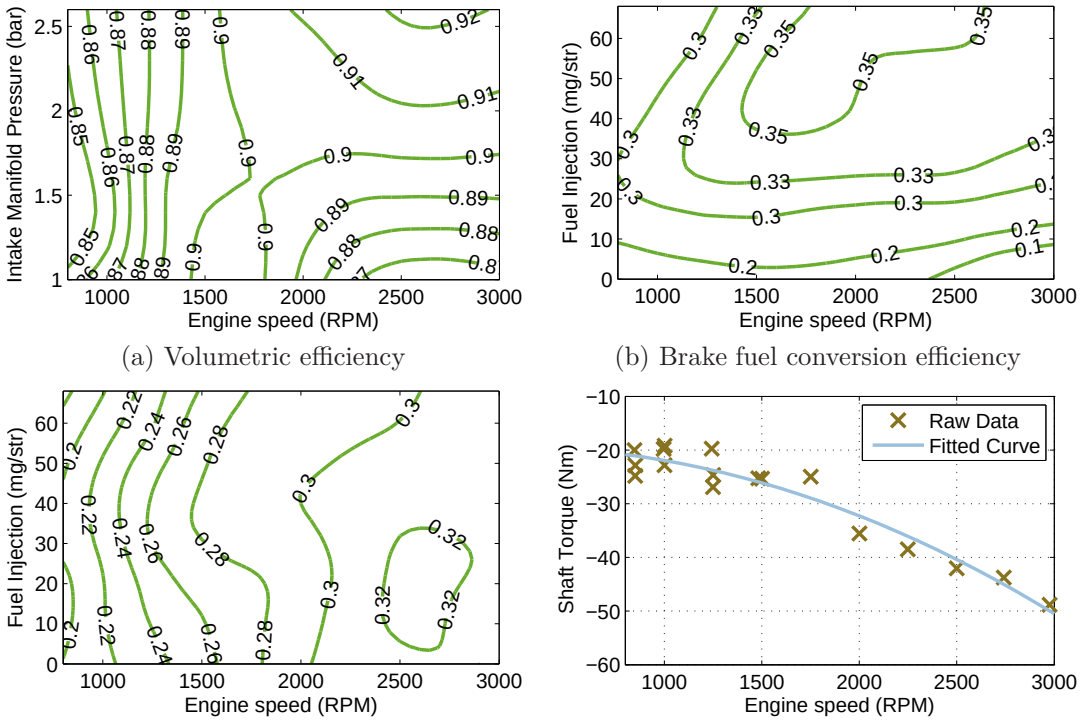

(a) Volumetric efficiency

(b) Brake fuel conversion efficiency

(c) Exhaust energy coefficient

(d) Friction parameters

Figure 2.20: Engine block maps used in MVEM.

During engine testing the brake torque was measured with a torque transducer

installed at the shaft connecting the engine with the dynamometer. Indicated torque therefore cannot be easily calculated. Instead of indicated torque used in the definition of fuel conversion efficiency (see equation 2.42), the measured brake torque is used. The resulting map is shown in Figure 2.20b. This map already includes friction and pumping losses. Friction losses increase with engine speed which explains the lower values in the map at the bottom right corner. Additionally the pumping losses are the most significant at low loads and this is why the map is flat at higher loads. Steady-state torque deficit at low speeds and high loads is observed on this map as well.

The exhaust energy coefficient is a parameter describing what portion of the fuel energy is dissipated in the form of increased exhaust gas temperature. The measurement of exhaust temperature at low loads is significantly affected by the radiative heat transfer from manifold walls and the gas temperature is increased by the heat transfer from the cylinder walls. The exhaust energy coefficient map includes also the heat losses from the gas to the manifold walls at higher loads and flows. The result is shown in Figure 2.20c.

Friction coefficients were determined using a linear least square fit of a second order polynomial in engine speed to the measured shaft torque during motoring (see Figure 2.20d).

Cooler Effectiveness

Calculating the effectiveness of the intercooler indicated a mass flow dependency. This is physically reasonable as the fixed length of the intercooler ducts has a limited heat exchange capability. This effect was captured fitting a single line to the raw data (see Figure 2.21). The effect of temperature at very low flow is of lower importance.

$$\eta_{cool,ic} = 1 - 1.4 w_{ic} \tag{2.48}$$

An accurate determination of the EGR cooler effectiveness is not critical, because during the tip-in manoeuvre EGR is fully closed. A constant parameter was used to describe it.

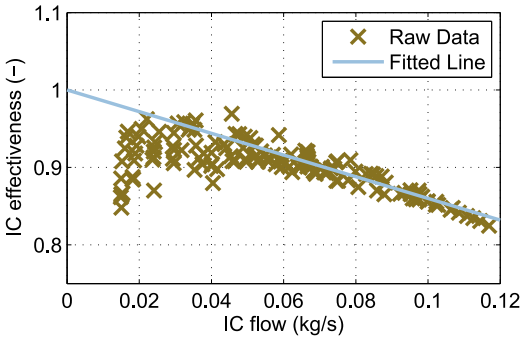

Figure 2.21: Intercooler effectiveness.

Effective areas of restrictions

At steady-state and with the EGR valve closed, flows through the air-box, intercooler and exhaust exit can be calculated from the reading of MAF sensor and the estimated fuel flow. Pressures and temperatures in all the relevant sections of the air-path are also measured. With all these data effective areas of the components modelled as orifices can be determined.

2.4.3 Steady-state validation

The complete MVEM was validated against the set of steady-state engine measurements used for the parametrisation of the components. The measured fuel injection, engine speed and ambient conditions were used as inputs. Intake manifold pressure was controlled in a closed loop using a PI controller on VGT position. The results are shown in Figure 2.22. The extended set of signals was captured during engine testing and therefore all the quantities relevant to air-path dynamics were available for validation.

Simulated values of the quantities related to the compressor operation, i.e. compressor flow, post compressor pressure and temperature, showed very good agreement with measurements. Moreover, compressor flow and exhaust manifold temperature validated well, which indicates that the volumetric efficiency and the exhaust energy coefficient map captured the engine characteristics adequately.

Simulation results showed poorer agreement in the case of exhaust manifold pressure. For the majority of operating points it remained within 10% error band,

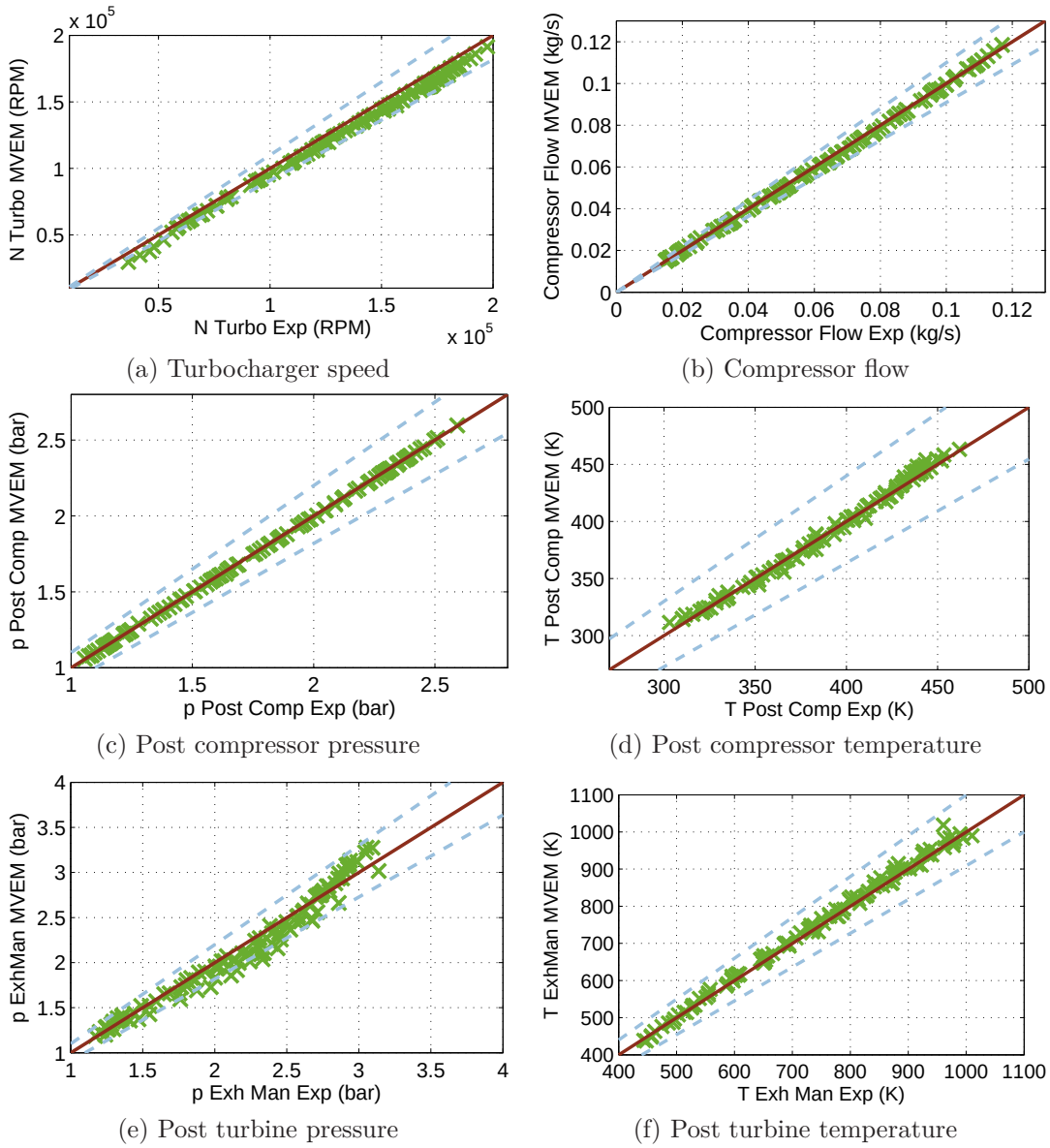

(a) Turbocharger speed

(b) Compressor flow

(c) Post compressor pressure

(d) Post compressor temperature

(e) Post turbine pressure

(f) Post turbine temperature

Figure 2.22: MVEM validation against steady-state engine test data.

but the result are worse than for any other signal. This indicated that the turbine performance was modelled with poorer accuracy.

2.4.4 VGT scaling

The range of VGT rack positions used on the actual engine is different to the range of VGT maps.

In order to determine the conversion between these two ranges, the following analysis was performed. The MVEM was simulated with engine speed, fuelling and ambient conditions measured during steady-state engine testing (with the EGR valve fully closed). The model was controlled in closed-loop: a PI controller on VGT was used to achieve the simulated boost pressure equal to the one recorded during experiments. The resulting steady-state VGT positions (see *VGT Position Sim* in Figure 2.23) were compared with experimental data (*VGT Position Exp*).

To fit the line relating the engine VGT positions to the maps, only the operating points resulting in VGT positions above 0.1 were used. The results indicated that the fully-closed and fully-opened positions of the VGT used on the actual engine are outside the mapped range.

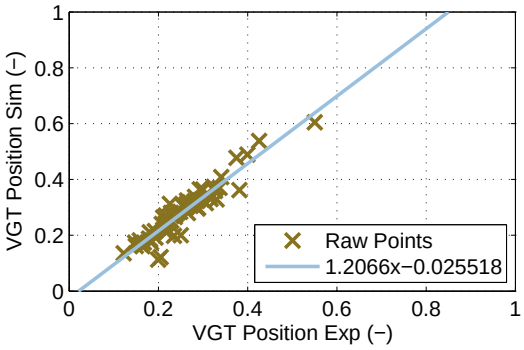

Figure 2.23: Static VGT scaling.

2.4.5 Transient validation

Once the steady-state validation of MVEM is finished, a set of variables affecting the transient response can be calibrated. The set includes volumes of various air-path sections and the turbocharger inertia. The latter introduces the slowest mode in the air-path response and can be verified based on engine test results.

For this purpose ten engine tests were performed. The engine speed was controlled to 2000 RPM and fuelling injection corresponding to a moderate load was demanded. The EGR valve was closed and a series of open loop demands in the VGT rack position was applied. Prior to the application of each step in VGT, the engine was allowed to reach a steady-state. In such conditions the turbocharger speed was about 100 000 RPM. In this region the compressor and turbine maps should not suffer from the errors due to the extrapolation of the supplier's data.

Steady-state calibrated MVEM was then fed with the recorded engine speed, fuelling and ambient conditions. The measured VGT feedback position was also applied after the scaling determined in the previous section. The response of the model was compared with the engine test results after normalising all the output variables. It was found that reducing the turbocharger inertia by 10% leads to an improved match in the measurements of interest. The volumes were not changed and the original values calculated from the WAVE model were considered to give satisfactory results.

An example of such steps in VGT is shown in Figure 2.24. It is observed that the turbocharger speed simulated with calibrated MVEM matched the engine response. Similar agreement is observed in the case of intake manifold pressure and the post compressor pressure. A considerably worse result is obtained for exhaust manifold pressure, but the shape of the engine response was preserved. Initial steep change in pressure was followed by slow conversion to a steady-state level.

There are several differences between the calibration of the WAVE-based MVEM and the engine-based MVEM. Engine block maps and engine friction coefficients are determined in a similar manner as to the engine-based version, but using the data originally delivered by Ford Motor Co. Moreover, the original WAVE model assumed that there is no drop of pressure over the intercooler - the same convention was adopted for the related MVEM. Due to this assumption, post-compressor volume and the intake manifold volume can be treated as a single one, thus reducing the number of dynamic states.

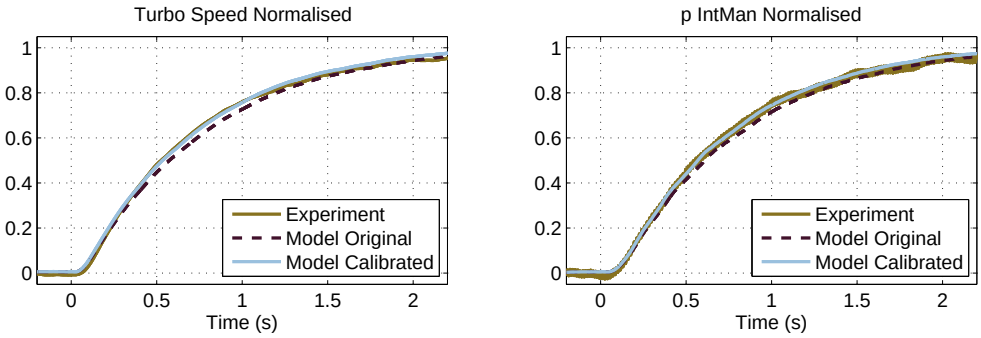

(a) Turbocharger speed

(b) Intake manifold pressure

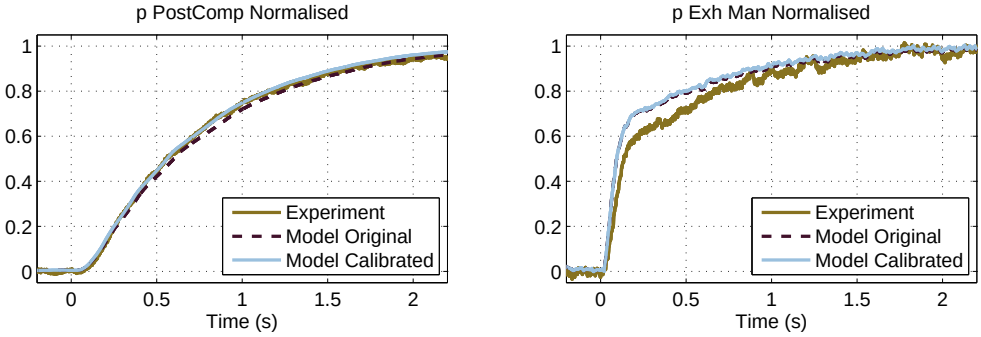

(c) Post compressor pressure

(d) Exhaust manifold pressure

Figure 2.24: MVEM validation against transient engine test data.

2.5 Summary

In this chapter, the tools and methods used to meet the overall objectives were introduced. To allow for experimental testing, the engine test bench was prepared and instrumented. A passenger car Diesel engine was installed and connected to the transient dynamometer. An extensive set of additional instruments was mounted on the engine to allow for both the calibration of models and investigation of engine operation.

Two types of engine models were described in detail: 1) A 1D engine and gas dynamics model that will be used for the verification of candidate air-path architectures, and 2) mean value engine model that will be used for model based control. Two versions of MVEM are required - one for controlling the 1D model and the other for control of the actual engine. The relative merits of both modelling conventions have been discussed.

A process of steady-state calibration for 1D model and MVEM was proposed and described in detail. Validation results for both types of models were satisfactory, but certain inaccuracies were highlighted together with reasons behind them.

In the next chapter MPC is introduced and used to investigate the transient operation of the engine.

Chapter 3

Transient response and MPC

3.1 Transient response of standard VGT/EGR air-path

The transient response of highly turbocharged engines with a single stage of pressure charging is significantly different to that of normally aspirated units. Firstly, steady-state torque at low engine speeds is affected by the compressor surge line. Secondly, meeting high torque demands at low engine speeds requires accelerating the turbocharger under low flow conditions.

The characteristics of the transient response of an engine itself (i.e. without considering the rest of a vehicle) can be visualised as shown in Figure 3.1. To generate such an image a set of full-load tip-in manoeuvres at several fixed engine speeds was performed. The measured engine shaft torque was analysed to calculate time-to-torque values. Finally, a surface was fitted to the results and displayed over a range of speeds and torques.

It is observed that the distances between the lines of constant times become smaller and smaller as the load increases. This can be interpreted as a progressively increasing difficulty of meeting high torque demands. The second observation from Figure 3.1 is that the constant-time lines become skewed creating a non-achievable triangle of torques at the top left corner of the map.

During a tip-in manoeuvre the increasing intake manifold pressure allows for injecting more fuel, which results in higher exhaust gas enthalpy. This, in turn, is

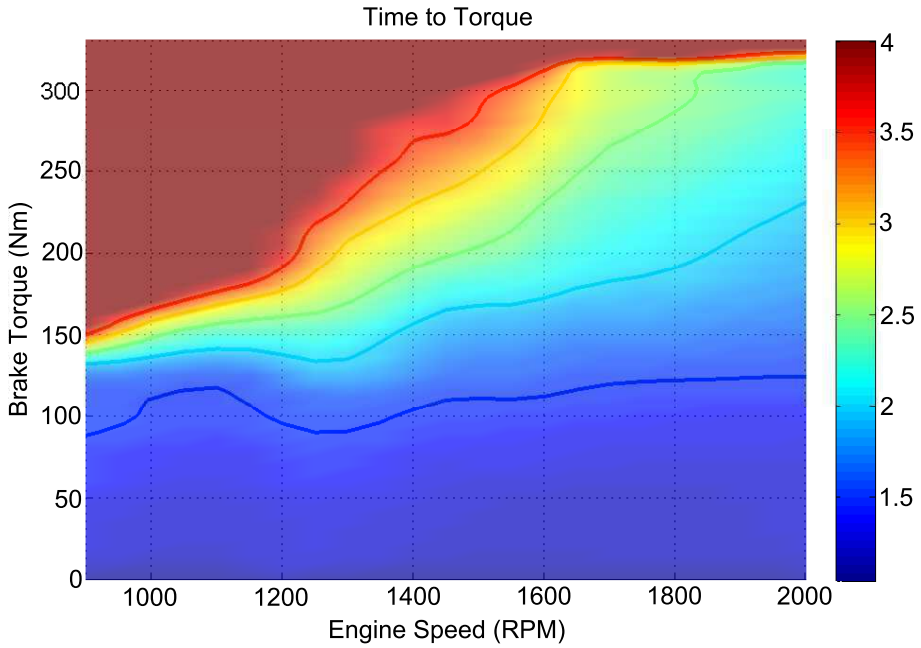

Figure 3.1: Map of time-to-torque at fixed engine speeds.

extracted by the turbine to increase the speed of the turbocharger, which leads to higher intake manifold pressures. This circle accelerates until the driver's torque demand is met or certain limits of operation are achieved. The rate of acceleration of this process is affected by the engine speed, because the mass of the gas flowing through the block (and the turbine) is closely coupled with the engine speed (see equation 2.40). At low engine speeds and high-loads the limited energy in the exhaust gas means that only a limited torque can be generated by the turbine. This prevents the achievement of high intake manifold pressures and injection of more fuel.

Certain phenomena influencing the transient response within the time-scale of one engine cycle are described in [Rakopoulos, 2009]. There exist several sources of delays preventing an immediate increase in the exhaust gas enthalpy. They include: the time between a step in torque demand and the subsequent fuel injection event, and the time to the following exhaust valve opening. These are very short time-scale effects (less than a single engine revolution and much less than any engine transient of interest here) and will be neglected during the

development of a controller.

Several simplifications were made in the WAVE model used for transient simulations in comparison to the actual engine operation. These differences are a result of fuel injection calibration, which apart from optimising the performance of the actual engine ensures reduced emissions and acceptable noise, vibration and harshness (NVH) characteristics. One of such simplifications in the WAVE model is using only one injection per stroke. During the recorded engine tests the quantity of fuel injected during pilots was found to be negligible in comparison to the main injection. Another assumption in the simulation setup is that the injection timing and duration are only static functions of the requested load and instantaneous engine speed. These functions are determined based on steady-state calibration of the model. In reality, the main injection timing during a tip-in manoeuvre is not identical to the steady-state timing for operating points the engine traverses during an acceleration.

3.1.1 In-gear acceleration and turbo-lag

The map shown in Figure 3.1 describes how much time it takes to achieve high loads at low engine speeds. To make the engine transient analysis more illustrative, tests simulating the behaviour of the engine under in-vehicle loads are now considered. In-gear acceleration on a level-road is a practical scenario suitable for investigating turbo-lag. The recorded responses of the engine controlled with the standard ECU strategy during 1^{st}, 2^{nd}, and 3^{rd} gear tip-in manoeuvres are shown in Figure 3.2a. The torque is delivered in two phases, an initial steep increase is followed by a convex shape until the demanded level of torque is met. The time to the demanded torque varies with the engaged gear - the response is slowest in the case of the third gear.

A high ratio of the first gear allows the engine to accelerate quickly even under modest levels of the engine's output shaft torque. At higher gears the engine's acceleration is reduced moving the operating points towards high torques and low speeds, which is the challenging region (see Figure 3.2b). For these reasons 3^{rd} gear tip-in manoeuvre was selected as a reference test for further investigation.

A set of signals recorded during such a test is shown in Figure 3.3. The

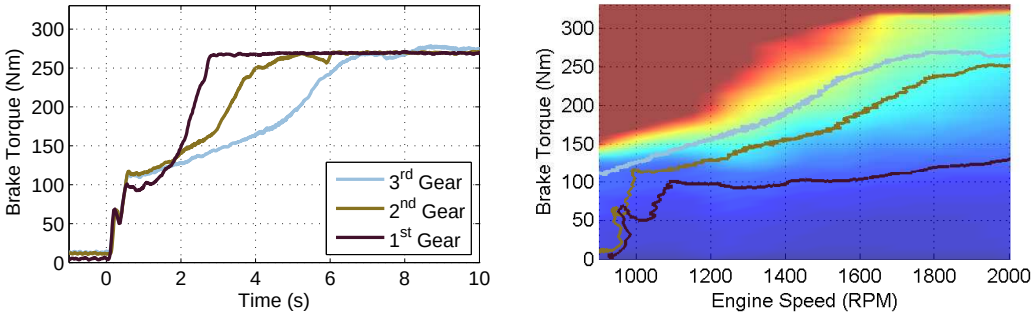

(a) In-gear tip-in in time

(b) In-gear tip-in in speed

Figure 3.2: Engine response during in-gear tip-in manoeuvres.

test starts at an engine speed near idling and finishes when the engine speed reaches 2750 RPM. The particular shape of torque delivery shown in Figure 3.2a can be explained using the plots of the fuel injection and the UEGO sensor measurements from Figure 3.3. Immediately after an increased torque demand, the fuelling reaches the level corresponding to a near-zero oxygen concentration in the exhaust gas. This means the engine operates close to the stoichiometric AFR. The fuelling is controlled in this way to avoid excessive smoke emissions. This has a direct effect on the level of generated brake torque and, therefore, on the acceleration of the engine/vehicle. A higher level of fuelling together with the fully-closed EGR valve and the appropriately modulated VGT rack position lead to the acceleration of the turbocharger. This results in a higher intake manifold pressure, higher intake flow and thus the possibility of injecting more fuel without violating the smoke limit. When the smoke limited phase is over, fuelling is controlled to the level allowing for meeting the torque demand.

The boost pressure is controlled using the VGT to ensure a suitable in-cylinder gas quantity. It is observed that the VGT is saturated during the smoke limited phase. The vanes starts to open progressively about 1.5 seconds before the boost pressure demand is met.

Thus three features of the transient response of the considered engine can be distinguished:

1. an upper limit on the maximum torque at low-speeds inherited from the steady-state torque limitation due to the compressor surge line

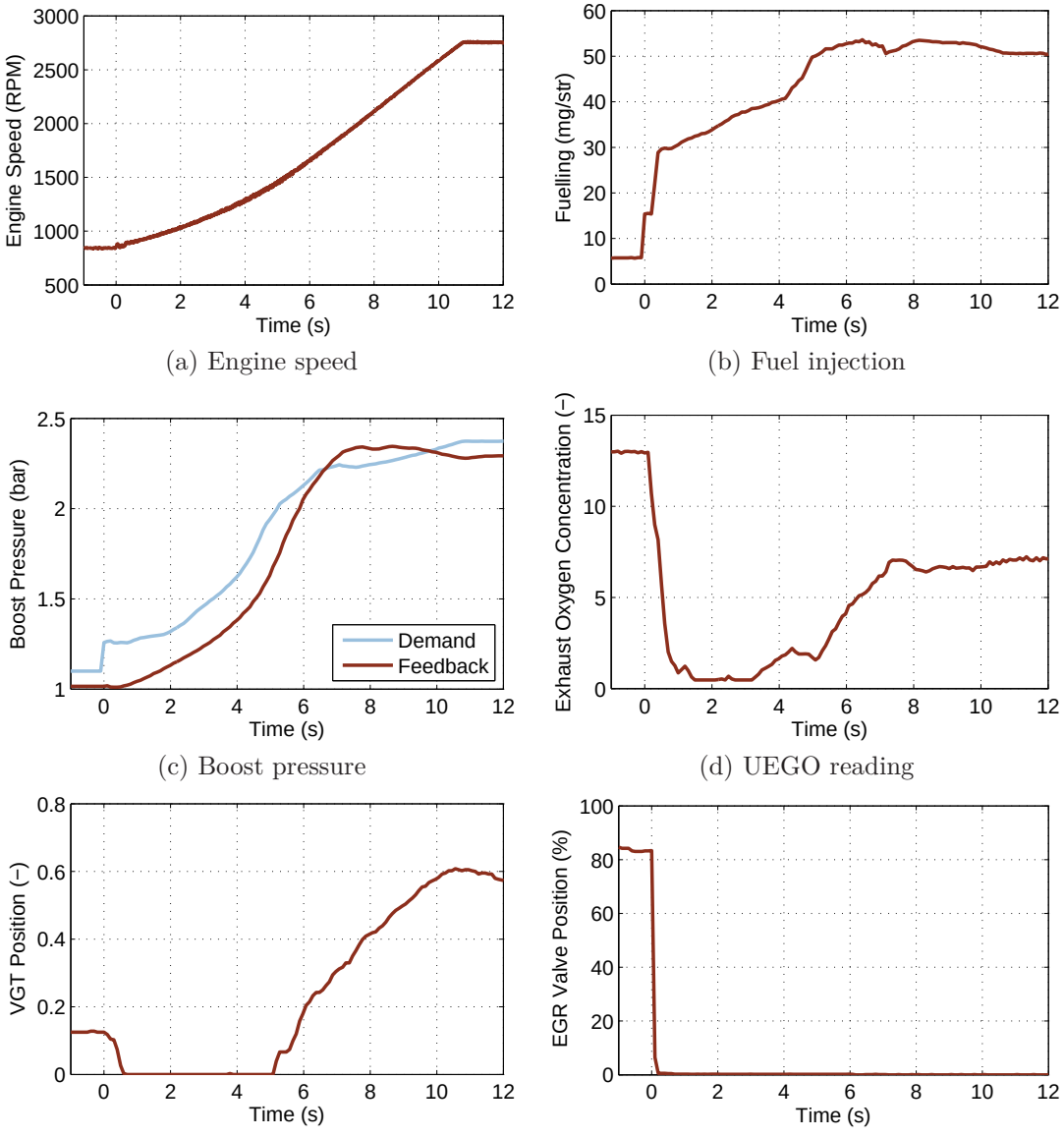

(a) Engine speed

(b) Fuel injection

(c) Boost pressure

(d) UEGO reading

(e) VGT position

(f) EGR position

Figure 3.3: Typical third gear tip-in response.

2. a smoke-limited phase caused by the air-path dynamics and its inability to deliver a sufficient intake flow

3. a phase during which the desired levels of fuelling and brake torque have been reached, but the air-path has not yet achieved the boost pressure set-point required for operating with a desired margin from the smoke limit

These three features result in a particular shape of torque delivery, which leads to a compromised vehicle driveability during significant engine transients. These characteristics of highly turbocharged engines can be perceived by the driver and is often referred to as a turbo-lag.

3.1.2 Transient measurements

The experimental setup developed for this work enables the calculation of the steady-state values for all the states of MVEM. However, the bandwidths of the installed sensors vary significantly.

The Eddy-current based turbocharger speed sensor detects each of the passing compressor blades and therefore offers very high bandwidth and resolution. Because of a significant inertia of the turbocharger, during a single engine cycle its speed varies negligibly. Therefore, the raw turbocharger speed measurements are treated as the mean values for this state. Pressures in the air-path are significantly affected by the cyclic nature of the engine operation. The bandwidth of the pressure transducers is sufficiently high to measure pressure variations during a single engine cycle. The measured peak-to-peak values in the intake manifold pressure were up to 0.35 bar (as shown in Figure 3.4b). Because only the mean values over the time of a single engine cycle will be used by a controller, the original measurement was post-processed with a non-causal cycle-averaging filter. At each sampling instant a time-window equal to two engine revolutions at an instantaneous engine speed was created and the time-average for each signal of interest was calculated. The result is shown in Figures 3.4a and 3.4b. The mean-value signals used on-line by the controller have to be determined respecting the causality and, therefore, there exists a delay between the cycle-averaged and feedback signals.

The masses of the gases stored in various sections of the air-path are the remaining states of the considered MVEM formulation. They can be calculated from the measured pressures and temperatures using the ideal gas law:

$$m = \frac{pV}{R\theta} \tag{3.1}$$

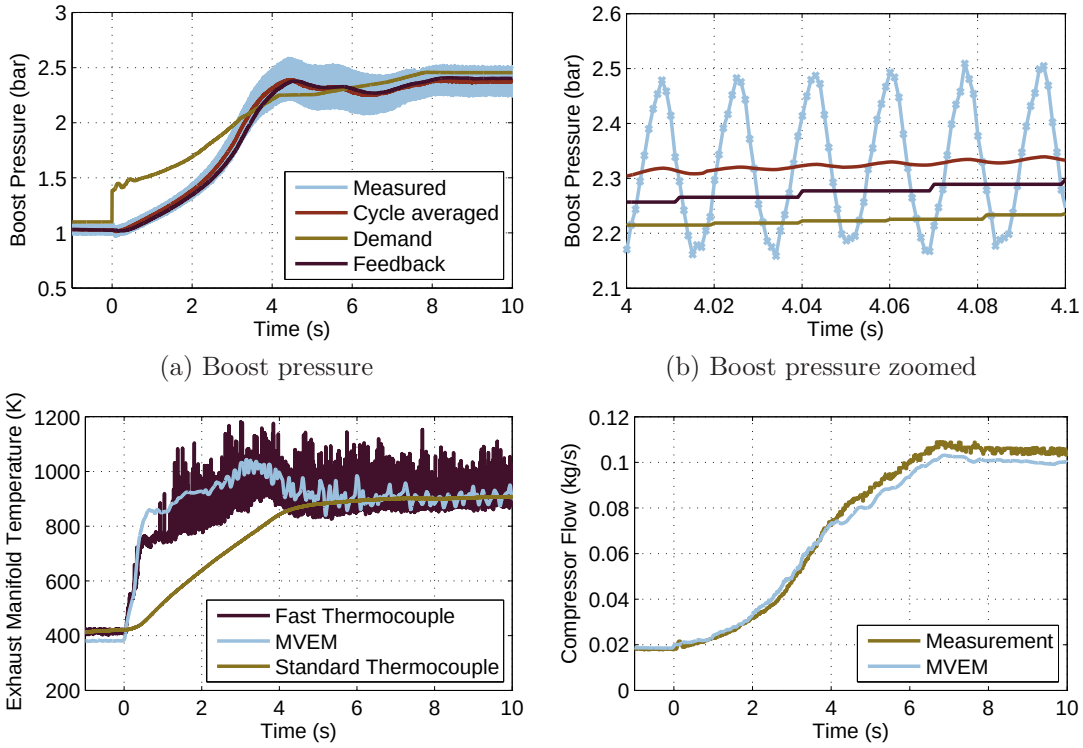

(a) Boost pressure

(b) Boost pressure zoomed

(c) Thermocouple dynamics

(d) Compressor flow

Figure 3.4: Measurements for full-state feedback - sensor system characteristics.

Calculating the feedback signals for these states relies, therefore, on the measurement of temperatures. The installed thermocouples (K type 1.5 mm) suffer from a poor bandwidth (see Figure 3.4c). The effect is most significant in the exhaust manifold, where the temperature rises immediately after a tip-in. It takes about four seconds for the standard thermocouple to give readings representative of the gas temperature. To verify this behaviour an experiment with a fast thermocouple (K type 0.07 mm) installed in the exhaust manifold was conducted. The reading showed a steep increase in temperature immediately after the tip-in, but the sensor failed at a temperature of about 750 K. High temperatures and velocities of the gas in the exhaust manifold require using more robust 1.5 mm sensors. The recorded response of the fast thermocouple can be, however, used to verify the response of the MVEM. This way it is shown that the MVEM captures the temperature (and thus the mass of the gas) dynamics well.

The compressor flow measurement is used as an additional source of informa-

tion for the analysis and model verification. The flow measured during a tip-in manoeuvre and a corresponding MVEM simulation result are shown in Figure 3.4d. It is observed that the sensor bandwidth is sufficient for measuring the mean-values of this signal and that the simulated flow matches the experimental result satisfactorily.

The MVEM requires fast measurements or estimates for several other signals. Engine speed is measured by a shaft encoder of a resolution up to a single crank angle degree. In 2.2.4 the ECU estimation for the fuel flow was found to give accurate results and is suitable for transient testing.

Actuator dynamics are discussed in section 3.4.3.

3.1.3 Turbocharger operating points

In this section, the analysis of turbocharger operating points during a tip-in manoeuvre is conducted. To recall from section 2.3.2, the turbocharger maps are non-dimensionalised to compensate for varying inlet pressure and temperature conditions. Because of the poor thermocouple bandwidth, the analysis is based on MVEM simulations, rather than on experimental results.

The compressor operating points during a third gear tip-in are superimposed over the compressor map in Figure 3.5a. Additionally, the operating points from steady-state engine tests (see Figure 2.6) are depicted as crosses. Comparing these data indicates that the air-path dynamics forces the compressor to operate further from the surge limit than during full-load steady-state operation. Closing the gap between the simulated response and the surge line should result in improved transient response.

The compressor's transient operating points superimposed on the flow map used by the MVEM are shown in Figure 3.5b. The compressor mass flow, temperature ratio and torque parameter are represented as maps in the pressure ratio and turbocharger speed parameter. The resulting transient operating points are then located at the very steep slopes of these maps. This makes the model sensitive to pressure ratio inaccuracies and is one of the drawbacks of the considered formulation.

During the first phase of a tip-in manoeuvre the VGT rack position is satu-

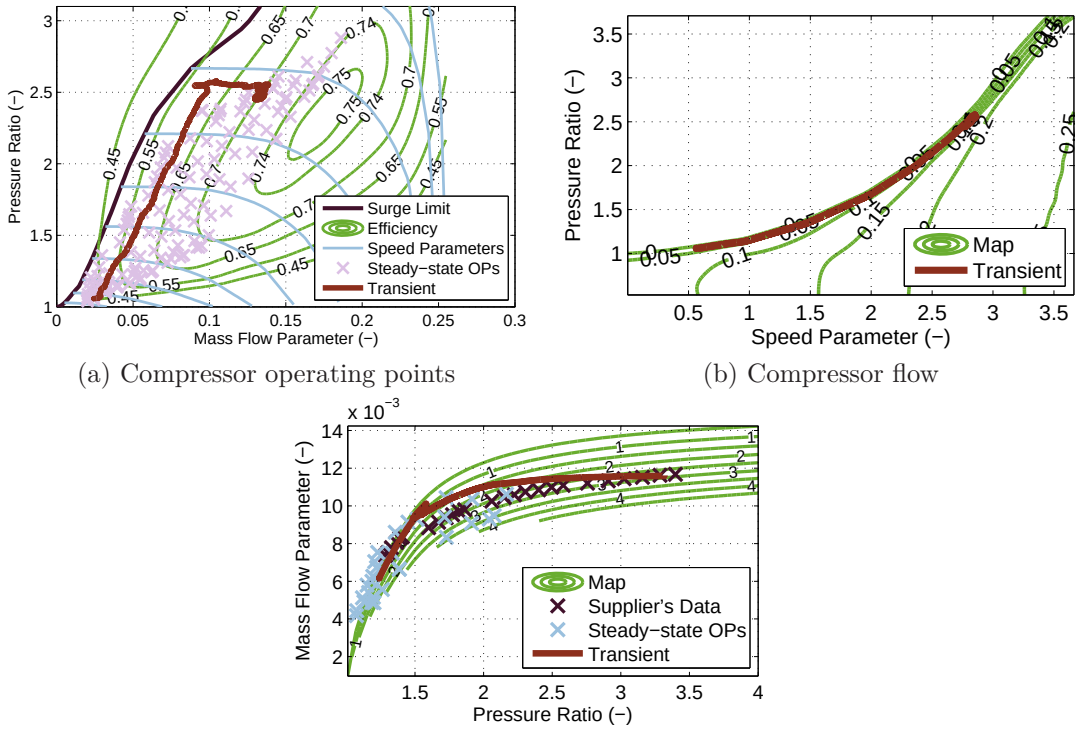

(a) Compressor operating points

(b) Compressor flow

(c) Turbine flow

Figure 3.5: Simulated turbocharger operating points during a third gear tip-in.

rated. It is therefore possible to analyse the turbine operation during this phase in a similar fashion to the previously conducted discussion of compressor operation. The turbine flow map for the saturated rack position is shown in Figure 3.5c. The steady-state engine operating points requiring fully-closed VGT are shown as blue crosses. It is observed that during the transition between initial pressure ratio and the pressure ratio of 2.5, the turbine operates further from the original supplier's data. This means that the simulation results are significantly dependent on the map fitting algorithm and the extrapolation of the these data. A positive observation is, however, that during this phase the turbine operates within the region covered by the operating points from steady-state engine testing, which can be validated against the engine measurements.

This analysis relied on the assumption that the consideration of only mean values for pressure ratios and flows across the turbine and the compressor is a valid representation of the actual operation. There are, however, reports that such

an approach suffers from neglecting the variation of the turbocharger operating points due to engine cyclic operation [Westin, 2005]. Nevertheless, an excellent accuracy is not required for deducing the direction and roughly estimating the magnitude of the shift in turbocharger operating points during transients.

3.2 Control problem

In this section some particular features of the control problem considered are discussed. General characteristics of the air-path system are first introduced. This part is based on the analysis of the MVEM. Next, the requirements for the air-path control system during tip-in manoeuvres are formulated.

3.2.1 Plant characteristics

From a modelling and control perspective, the VGT/EGR air-path is a complex system. The combination of the non-linear characteristics of compressors and turbines, the partial redirection of gas flow from the exhaust to the intake manifold and the cyclic operation of the engine block, lead to complicated non-linear dynamics. System characteristics include non-minimum phase, sign reversal and interaction between boost pressure and air mass flow control (as described in [Kolmanovsky et al., 1997]).

During significant transients the EGR channel is not active, because the generation of high pressures in the exhaust manifold is required for a fast turbocharger acceleration. In the conventional configuration the air-path system during such manoeuvres becomes a SISO system - boost pressure is controlled by modulating VGT rack position.

The MVEM formulation described in 2.4.1 results in a non-linear, continuous time system. Assuming the possibility of measuring all the states, it can be denoted as follows:

$$\begin{aligned} \dot{x} &= f(x, u, d) \\ y &= x \end{aligned} \tag{3.2}$$

where:

- state $x = \begin{bmatrix} p_a & m_a & p_b & m_b & p_i & m_i & p_x & m_x & p_c & m_c & N_t \end{bmatrix}^T$
- input $u = u_{vgt}$
- measured disturbance $d = \begin{bmatrix} N_e & \bar{w}_f & p_{amb} & \theta_{amb} \end{bmatrix}^T$

The state vector consists of gas pressures and masses in five volumes (pre-compressor a, post-compressor b, intake manifold i, exhaust manifold x, post-turbine c) and the turbocharger speed N_t. VGT position is the only input and there are four measured disturbances, which can be grouped in two categories. Engine speed N_e and fuelling in milligrams per stroke $\bar{w}_f$ are internal variables of the simulation model, but are considered as disturbances from the perspective of air-path control system. Ambient pressure p_{amb} and temperature θ_{amb} are more conventional external disturbances.

The MVEM includes dynamics of various time-scales. The fastest ones are those of pressures in the pre-compressor and post-turbine volumes due to relatively big orifice areas between the ambient and these volumes. Furthermore, the pressure dynamics are faster than the mass dynamics as the mass flows in the relevant equations are scaled by the air properties and temperatures in the volumes (compare equations 2.33 and 2.34). Because of low exhaust manifold volume, the exhaust manifold pressure dynamics is also fast. By far the slowest mode is associated with turbocharger inertia. This wide range of bandwidths makes the MVEM a stiff system. The stiffness factor for a linear system can be defined as:

$$C_{stiff} = \frac{\max\limits_i |Re(\lambda_i)|}{\min\limits_i |Re(\lambda_i)|} \tag{3.3}$$

where λ_i are all eigenvalues of the investigated system.

In order to facilitate such an analysis for the considered MVEM, the non-linear function f was linearised around steady-state operating points and the

stiffness factor was calculated for each of the obtained linear systems. The result is shown in Figure 3.6a. It is observed that the stiffness of the MVEM varies significantly with the operating point. The system is very stiff at low load and speed conditions. The system becomes less stiff with increasing engine speed and load and the lowest values for the stiffness factor are calculated for the top right corner of the map.

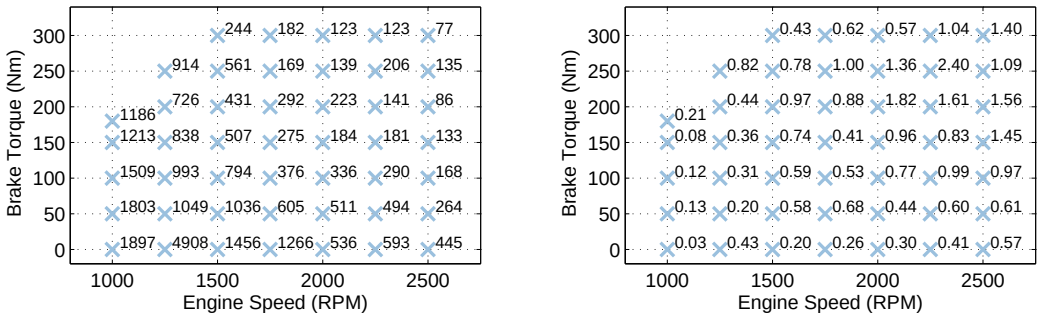

(a) Stiffness index (b) DC gains

Figure 3.6: Plant characteristics at steady-states.

The key transfer function of the MVEM is the one from the VGT rack position to the intake manifold pressure. The linear models calculated around the steady-state operating points were also used for calculation of steady-state gain of this transfer function. The results are shown in Figure 3.6b. It is observed that the variation in the gains is significant and no obvious trend in speed and load can be identified. This analysis gives an indication about the level of system non-linearity.

It is not only the static characteristics of the MVEM that are non-linear. To assess the effect of non-linearity on transient operation, the MVEM was linearised at several instantaneous operating points $(x_{0,j}, u_{0,j}, d_{0,j})$ during a tip-in simulation (as shown in Figure 3.7). The following expressions were thus obtained:

$$\dot{x}_L = f(x_{0,j}, u_{0,j}, d_{0,j}) + A_{c,j}(x_L - x_{0,j}) + B_{u,c,j}(u - u_{0,j}) + B_{d,c,j}(d - d_{0,j}) \quad (3.4)$$

where x_L is the state vector of the linearised system and:

$$A_{c,j} = \left.\frac{\partial f(x,u,d)}{\partial x}\right|_{(x_{0,j},u_{0,j},d_{0,j})} \tag{3.5}$$

$$B_{u,c,j} = \left.\frac{\partial f(x,u,d)}{\partial u}\right|_{(x_{0,j},u_{0,j},d_{0,j})} \tag{3.6}$$

$$B_{d,c,j} = \left.\frac{\partial f(x,u,d)}{\partial d}\right|_{(x_{0,j},u_{0,j},d_{0,j})} \tag{3.7}$$

These linear models were then fed with inputs and measured disturbances from the simulation of the MVEM and integrated over one second. The resulting forward linear simulations are depicted as the darkest lines in Figure 3.7. Based on these results, it can be concluded that the transient operation of the MVEM exhibits a non-linearity, but linear models determined around the instantaneous operating points give similar simulation results for about 0.5 seconds after the linearisation.

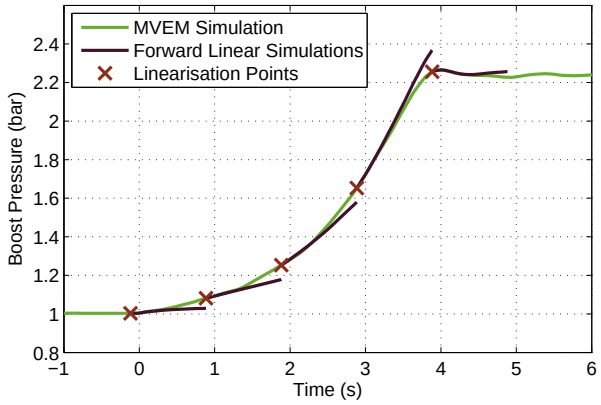

Figure 3.7: Simulations of linearised MVEM during a tip-in manoeuvre.

3.2.2 Control system requirements for tip-in manoeuvre

The closed-loop performance is a result of both the engine design and the control system.

When ad-hoc control approaches are considered, even after calibrating controller parameters, it may be necessary to modify the reference signals to pre-

vent the violation of constraints, which adds further calibration effort. Concerns about the influence of controller calibration on the results of analysis would be legitimate when using the traditional method of tuning gain-scheduled PID controllers as it relies on the subjective assessment of the calibrator. Additionally this approach is time consuming even for the standard air-path; when an additional actuator is added to the system and a number of different configurations are being considered, the calibration task could be prohibitive. Therefore one of the key requirements for the control framework used in this work is achieving close-to-optimal closed-loop performance with limited calibration effort.

The controller should also be easily reconfigurable to allow for investigation of various air-path candidates. When turbocharger assistance systems or multi-stage turbocharging configurations are considered, additional inputs are available and a control allocation problem has to be solved.

When investigating the full-load tip-in response, a control system is required to ensure that the operation of the engine lies within a number of physical constraints. The most critical constraint is the surge line of the compressor. Because of the design margins considered during the process of turbocharger matching, the surge limit is never active during a tip-in manoeuvre with the conventional engine configuration at nominal conditions, but is important when certain assistance systems are considered.

Turbocharged engines have some advantages over naturally aspirated ones when operating at high altitudes. Forced induction system allows for ensuring the intake gas conditions similar to those achieved at the sea level. The same intake manifold pressure requires, however, higher pressure ratios across the compressor and a higher turbocharger speed. In the case of high ambient temperature, the temperature of the gas post-compressor may become excessive. Therefore upper limits on turbocharger speed and post-compressor temperature are required. Other relevant constraints include absolute intake manifold pressure, exhaust manifold pressure and the pressure ratio across the turbine.

The tip-in manoeuvre is a test which exercises the engine over a set of rapidly changing operating points, which are far from steady-state equilibria. As a consequence state derivative offsets $f(x_{0,j}, u_{0,j}, d_{0,j})$ (see eq. 3.4) play an important role in approximating the engine behaviour with linear models.

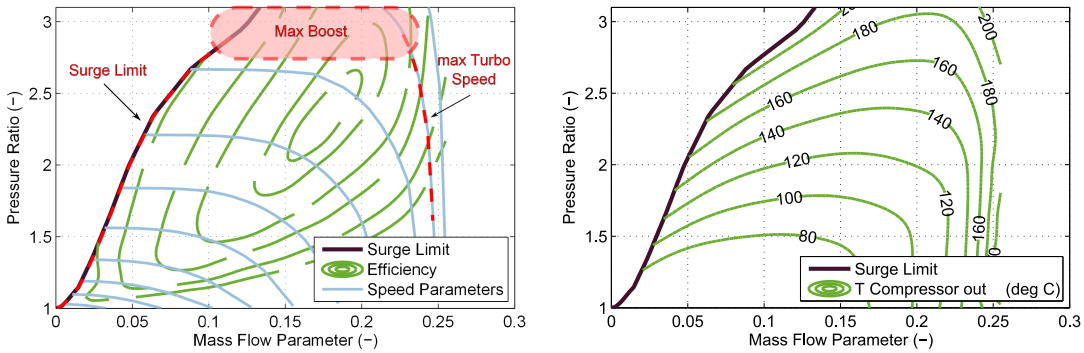

(a) Surge limit and turbo speed

(b) Compressor out temperature

Figure 3.8: Some physical limits of operation relevant to tip-in manoeuvres.

When a linearised system is simulated, contributions to the final result from inputs ($x_{B_u}(t)$), disturbances ($x_{B_d}(t)$) and state derivative ($x_f(t)$) can be separated.

$$x(t) - x_0 = x_{B_u}(t) + x_{B_d}(t) + x_f(t) \tag{3.8}$$

with

$$x_{B_u}(t) = \int_0^t e^{A_c(t-\tau)} B_{u,c} \left(u(\tau) - u_0\right) d\tau \tag{3.9}$$

$$x_{B_d}(t) = \int_0^t e^{A_c(t-\tau)} B_{d,c} \left(d(\tau) - d_0\right) d\tau \tag{3.10}$$

$$x_f(t) = \int_0^t e^{A_c(t-\tau)} d\tau f(x_0, u_0, d_0) \tag{3.11}$$

Such an analysis during a tip-in manoeuvre is shown in Figure 3.9. The results of linear simulations (the dark solid lines) are split into the inputs driven, disturbances driven and non-zero state-derivative driven components of the overall response. The values of the boost pressure for the linearisation points are shown as dashed lines for reference. It is observed that the response due to state derivative offsets dominates the simulations during the considered transition. This is an important feature of this control problem, as determining the appropriate values for state derivatives during engine operation is challenging.

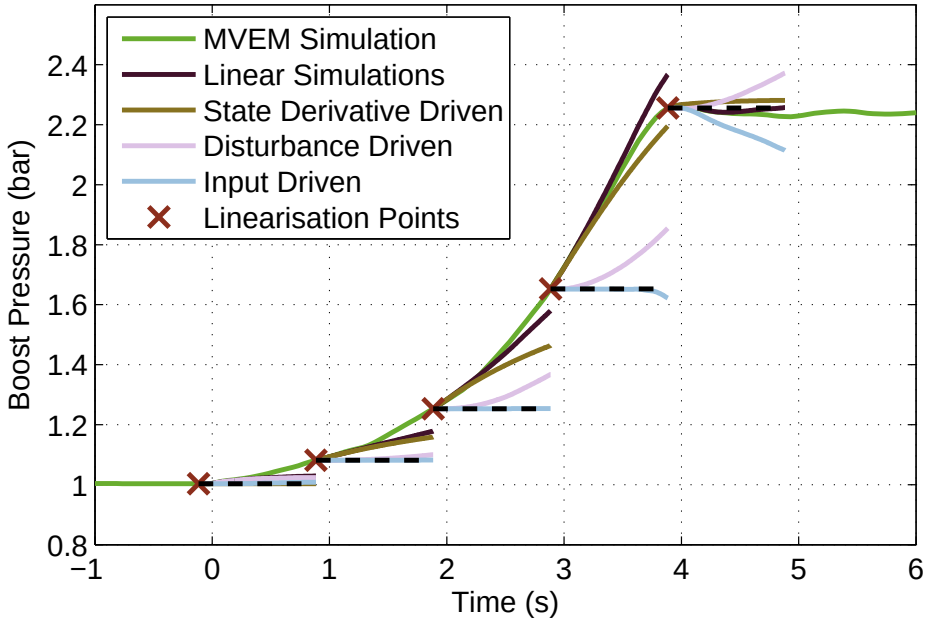

Figure 3.9: Significance of non-zero state derivatives at linearisation points during a tip-in manoeuvre.

Whilst computational complexity is an important consideration for the real-time control of actual engines, it is not significant when applied to a 1D engine model with a long execution time. Similarly, because the assessment of various air-path configurations is based on simulations, the stability and robustness guarantees of the controller are of less importance provided stability is indeed achieved.

When operating below the compressor surge limit the standard VGT air-path system is open loop stable, i.e. there exists an equilibrium for every set of engine speed, fuelling and VGT position [Kolmanovsky et al., 1997]. Therefore, the controller is never required to stabilise the system. When operating in the vicinity of the surge line, the controller is rather used to avoid compressor surge. Instabilities can thus be only induced by too aggressive control, which in the case of the considered formulation was avoided by appropriately selecting controller parameters.

3.3 Model predictive control

To tackle the challenging plant characteristics and ensure a close-to-optimal closed-loop performance for all of the investigated air-path configurations, Model Predictive Control (MPC) is employed here. It is an optimisation based control framework that explicitly includes input/state/output constraints and is applicable to multi-input multi-output (MIMO) systems [Maciejowski, 2002]. Potential drawbacks include significant computational complexity and limited stability and robustness guarantees in the case of non-linear systems.

In this section, the *locus* of the control approach investigated in this study in the broad field of automotive powertrain control is indicated. The following review of current powertrain control activities is not intended to be exhaustive, but only to outline the main directions of development.

3.3.1 Prior art in predictive control of engines

There exist a number of very informative surveys of control approaches used in automotive research. The introduction to control problems for gasoline engines, Diesel engines and alternative powertrains is the subject of [Guzzella and Onder, 2004] and [Guzzella and Sciarretta, 2005]. More concise description of various control loops and requirements for particular powertrain configurations can be found in [Cook et al., 2006].

A review of standard Diesel engine control tasks and approaches is presented in [Guzzella and Amstutz, 1998]. Regulating EGR and VGT to reduce toxic emissions and ensure satisfactory driveability (e.g. MAP/MAF tracking problem) is a control problem that attracted particular attention of automotive control community due to its multivariable nature and direct effect on emissions levels. Several concepts utilising control algorithms of limited computational complexity were compared in [van Nieuwstadt et al., 2000]. The authors argued that generating appropriate set-points for controlled variables is key in achieving satisfactory results, i.e. the performance of a feedback controller has only a secondary effect on emissions as it can not significantly improve the NOx-PM trade-off. Feedback controllers are, however, required to ensure control robustness.

Engine models have become an invaluable tool in the controller development

process due to the increasing complexity of IC engines and their control strategies. It is necessary to distinguish between two similar notions: model-based controller development/design and model-based controllers. The first refers to utilising engine models for engine simulations at the controller calibration stage (e.g. PID calibration) or verifying controller strategies using engine models developed, for example, in MATLAB/Simulink. In model-based controllers, a system/plant dynamics model, often simplified, is used to calculate the control inputs. Models are, therefore, internal and inherent components of controllers. This approach has many benefits, because the controllers can be tailored to specific plant characteristics. Achieving sufficient accuracy of the internal models can, however, be challenging [del Re et al., 2010].

Control oriented models can be developed based on the laws of physics, obtained from experiments using system identification techniques or via a mixture of these two approaches. The controller formulation investigated in this work utilises a mean-value engine model. This family of models belongs to the physics-based category and is a well-established technique - its brief history can be found in [Hendricks, 1997]. During early 2000s, various formulations of MVEM were extensively used for engine controllers based on the $\mathcal{H}_\infty$ theory [Christen et al., 2001], [Jung et al., 2002] and other approaches to Diesel air-path [Darlington et al., 2006]. To exploit the achievements of linear control theory, a highly nonlinear MVEM can be simplified and converted to the linear parameter-varying (LPV) form. Among others, this method was applied to the AFR control of variable cam timing gasoline engine [Genc, 2002] and Diesel air-path control [Jung, 2003].

The LPV method is equally applicable to models obtained via system identification. In [Wei and del Re, 2007] the identified model was scheduled with engine speed and VGT position to formulate a $\mathcal{H}_\infty$ controller for the MAP/MAF tracking control problem.

The opportunities for engine control offered by MPC were considered from an industrial perspective in [Stewart and Borrelli, 2008]. The possibility of a systematic approach to the development and calibration of multivariable controllers with an explicit treatment of constraints was found to be a key advantage over the traditional procedures. In particular, the advantages were envisaged for scenarios

in which the engine operates in a wide range of operating points and "close to the boundary of the set of admissible states and inputs". The analysis also identified several challenges:

- state estimation
- offset-free tracking
- limited ECU memory and computational power
- time-varying actuator and state constraints
- constraint satisfaction under steady-state disturbances leading to infeasible optimisation problems

As it was previously shown, the Diesel engine air-path is a highly non-linear system. Therefore, applying non-linear MPC (NMPC), which involves solving non-linear optimisation problem at each controller execution step, seems natural. This approach was investigated in [Herceg et al., 2006]. The reported simulation results confirmed that NMPC outperforms linear and non-linear state feedback controllers, which suffered from saturations due to input constraints. The computational complexity of this controller concept meant that it could not be executed in Real-Time. A simplified NMPC was also discussed in [Ortner et al., 2009]. In this simulation-based study, QP problems were formulated with matrices varying during the prediction horizon. They were obtained by integrating the model with optimal control input calculated at previous sampling instant. Approximate solutions to the MAP/MAF tracking formulated as an optimal control problem was investigated in simulations in [Sassano et al., 2012]. The air-path in this work was modelled around a single fixed speed and load operating point using identified NARX models.

The computational complexities of the above approaches are too high for Real-Time applications and could only be investigated in simulations. In order to allow for verifying the MPC benefits during engine experiments, simplifying the setup to linear MPC was extensively investigated. The first experimental tests of MPC for Diesel engine air-path used the explicit formulation. In such a setup, the state-space is partitioned into polyhedral regions, which are characterised by different

sets of active constraints. For each of these regions, the MPC solution takes the form of an affine state feedback control law [Bemporad et al., 2002]. This allows for calculation of the MPC solutions off-line and storing them in a database. The required computational power for executing such a controller is greatly reduced, but the amount of memory required for storing the pre-computed solutions may be prohibitive. Furthermore, finding the database entry corresponding to the current state still requires significant computational effort.

Nevertheless, a successful implementation of an explicit MPC on dSpace rapid prototyping system for MAP/MAF tracking was reported in [Ortner et al., 2006] and [Ortner and del Re, 2007]. To cope with the system non-linearity, the operating range was divided into 12 regions and for each of them a linear model was identified. In spite of the control horizon of only 1 step, improvements over a standard ECU strategy were observed. [Langthaler and del Re, 2007] used similar setup to investigate the potential of reducing emissions by controlling intake oxygen concentration instead of mass air-flow. [Langthaler and del Re, 2008] investigated in simulations several approaches to ensuring robustness of MPC-based engine control approach.

The implementation of the explicit MPC on a common industrial ECU was reported in [Stewart and Borrelli, 2008]. EGR and VGT were used as inputs to track boost pressure and mass air-flow demands with constraints on NOx emissions. The MIMO model was developed with dynamics of each channel approximated with a first order transfer function. The sampling time of 100 ms was used with the control horizon of 1 step and the prediction horizon of 40 steps.

The same experimental setup and control problem were considered in [Ferreau et al., 2007], where QP problems were solved on-line with an active set solver and the sampling time of 50 ms. Only a limited range of engine operation was considered and the LPV model was developed based on two identified linear models. The active set solver was extended to cope with matrices varying during the prediction horizon. This technique allowed a control horizon of 5 steps.

The trade-off between computation power and memory required for implicit and explicit MPC solvers was discussed [Borrelli et al., 2010]. The authors also considered a semi-explicit algorithm to show that there exist possibilities of balancing these two factors to meet particular requirements.

The MAP/MAF tracking problem for a Diesel engine was also considered in [Maruyama et al., 2011]. The MPC controller was formulated based on a plant model comprising of 2^{nd} order system and Pade approximations for pure delays in VGT and EGR actuator responses. The algorithm was executed on a rapid-prototyping system with the sampling time of 16 ms. The experimental results showed an improvement in performance when compared with a PID controller. Another Real-Time MPC controller for the Diesel air-path with an EGR valve and a throttle used as actuators is described in [Iwadare et al., 2009].

[Karlsson et al., 2010] used an identified linear model around a fixed engine operating point to implement a high-level MPC for the complete engine. Instead of using intermittent variables, the controller was set-up to directly track high-level set-points, such as meeting torque demand, limited in-cylinder pressure derivatives and toxic emissions. The results were promising, though it is worth remarking that non-standard sensors including in-cylinder pressure transducers and an opacimeter were used in that study.

An interesting alternative in the form of parameterised MPC is introduced in [Murilo et al., 2009]. The authors proposed restricting the set of admissible open loop control profiles, which can be described with a limited set of parameters. The simplified optimisation problem is then formulated using these parameters and solved on-line by the sequential QP (SQP) method. The setup was validated experimentally using a rapid prototyping system.

In [Behrendt et al., 2011] several enhancements of active-set QP solver were described. The proposed algorithm was executed on an ECU and used successfully for a high-level torque control of a SI engine. Several other publications reported applying MPC to gasoline engines [Lee, 2009], [Amari et al., 2010], [Kristoffersson, 2006].

Several studies investigated the application of MPC to the transient control of engines ([Lujan et al., 2007], [Papalambrou and Kyrtatos, 2009]). They have shown that these problems are challenging due to the difficulty in capturing the system non-linearity by identified prediction models.

3.3.2 Approach investigated

The approach taken in this work is to develop a simplified engine model and at each controller time-step to linearise the simplified model at the current engine operating point. This linearisation allows the formulation of quadratic programming (QP) problems, for which efficient solvers exist. Such an approach can be regarded as a LPV-MPC, because the structure of the model remains the same, only its parameters vary at each controller execution instant.

Work has been reported concerning MPC formulation based on successive linearisation of a non-linear plant dynamics model. [Palmieri et al., 2010] investigated the control problem of ensuring vehicle handling stability. The effectiveness of the approach was demonstrated in simulations. Application to active steering control of autonomous vehicle was considered in [Falcone et al., 2007] and verified experimentally. The assessment of LPV approach to MPC described in [Keviczky and Balas, 2005] proved this technique to be promising in the field of UAV guidance. The stability analysis of such MPC formulation was investigated in [Falcone et al., 2008], where an additional quadratic constraint was proposed to ensure closed-loop stability.

Continuing the description of the setup investigated in this work, the optimal inputs resulting from the solution of the QP problem are applied and at the next controller time-step the process is repeated. In this way the non-linearity of the engine air-path system is addressed while retaining an easily solvable optimisation problem. The simplified engine model used by the MPC controller is a mean value engine model (MVEM). Including additional actuators in MVEM is straightforward and this way a very flexible controller configuration is achieved.

The investigated controller concept and its application have many commonalities with the ideas presented in [Mueller et al., 2005]. The authors of that paper intended to exploit the benefits of a non-linear MPC to investigate a turbocharged Diesel engine air-path with two EGR loops. The details of the solver and results were, however, not disclosed.

In this work, the optimisation of the MPC code for Real-Time implementation is not pursued. Therefore, for example, full MVEM was used during the entire investigation and model reduction techniques were not considered. Further-

more, linearisation code was not tailored to each particular air-path configuration. Throughout the work, the formulation assumed full-state feedback and observers were not used.

The main objective for the developed system is to be easily reconfigurable. Ensuring close-to-optimal performance with limited calibration effort is another desired feature of the investigated control strategy. To examine this capability, MPC performance is compared to a related optimal control problem (OCP).

3.3.3 Transient response as optimal control problem

As a benchmark for the closed loop performance of the MPC controlled engine, a related optimal control problem (OCP) is examined. This OCP is formulated and solved with the MVEM rather than the WAVE model as the plant. The same transient is subsequently repeated, however with the MVEM controlled using the MPC algorithm. Comparing these results reveals that an appropriately tuned MPC controller achieves close-to-optimal performance for this problem.

The optimal control problem formulated for this investigation is concerned with finding the open loop trajectory for the inputs of a dynamic system that optimise an associated cost function Φ over time T. The solution must of course satisfy the system dynamics equation f, initial conditions (represented by the function r) as well as constraints imposed on inputs u and states x (defined by the function s). In general, this is an off-line process and the OCP for the engine transient can be defined as:

$$\max_{u(kT_s)} \Phi(T, x(0)) \qquad k = 0, 1, \ldots, \frac{T}{T_s}$$

$$\begin{aligned} &\textit{subject to}: \\ \forall t \in [0,T] \quad &0 = f(\dot{x}(t), x(t), u(t)) \\ &0 = r(x(0)) \\ \forall t \in [0,T] \quad &0 \geq s(x(t), u(t)) \end{aligned} \tag{3.12}$$

The above definition assumes that the input u is discrete with interval T_s and applied using a zero order hold.

When the problem is formulated in this way, the engine speed and fuelling are internal to the model and the system will therefore comprise both the original MVEM and the driveline model.

The OCP was solved numerically using the ACADO Toolkit (see Houska et al. [2011], Houska and Ferreau [2009–2011]), which implements the sequential quadratic programming (SQP) method. A selection of integrators are offered by the ACADO Toolkit and as the MVEM is a stiff model (the turbocharger inertia dynamics are significantly slower than the gas dynamics in the small volume of the exhaust system) the Backward Differentiation Formula (BDF) was chosen. The time range was set to 6 seconds and the controller input was determined every 200 milliseconds. In addition, two constraints were specified: the VGT rack position takes values between 0 and 1 and the intake manifold pressure is limited above to 2.4 bar.

The states of the MVEM model are initialised with values corresponding approximately to idling at 800 RPM. With the engine operating at this steady condition a step change to full load is made in the fuelling demand. However, during the tip-in manoeuvre the fuel injection quantity is limited to take into account the smoke limit (and the actual injected fuel quantity ensures the air-fuel ratio remains above 14.5:1).

During the tip-in manoeuvre it is assumed that the driver wishes to accelerate as quickly as possible. For a fixed time horizon this can be interpreted as a desire to achieve the maximum possible terminal vehicle speed. The first set of tests with OCP attempts to investigate the degree to which the latter is equivalent to maximising the intake manifold pressure (the aim of a production style control system).

In the first test the OCP was set up to maximise the terminal vehicle speed over a 6 second interval. The result is plotted in Figure 3.10 as OCP Setup I. This plot shows the entire manoeuvre and a typical tip-in response is observed. During the first 4 seconds the VGT remains fully closed in all three of the considered cases. This is consistent with the findings of [Black et al., 2007], where the possibility of leaving the vanes open during the full-load tip-in for reduced

pumping losses was investigated experimentally. It was found, however, that the deterioration of the boost pressure caused by this approach limits the amount of injected fuel leading to an overall worse tip-in response. The author of [Flärdh, 2012] investigated the optimisation of the transient response of a 1D model of a gasoline engine. Controlling the ratio of the exhaust manifold pressure to the intake manifold pressure for reduced impact on volumetric efficiency was found to be more important than generating the highest possible intake manifold pressure.

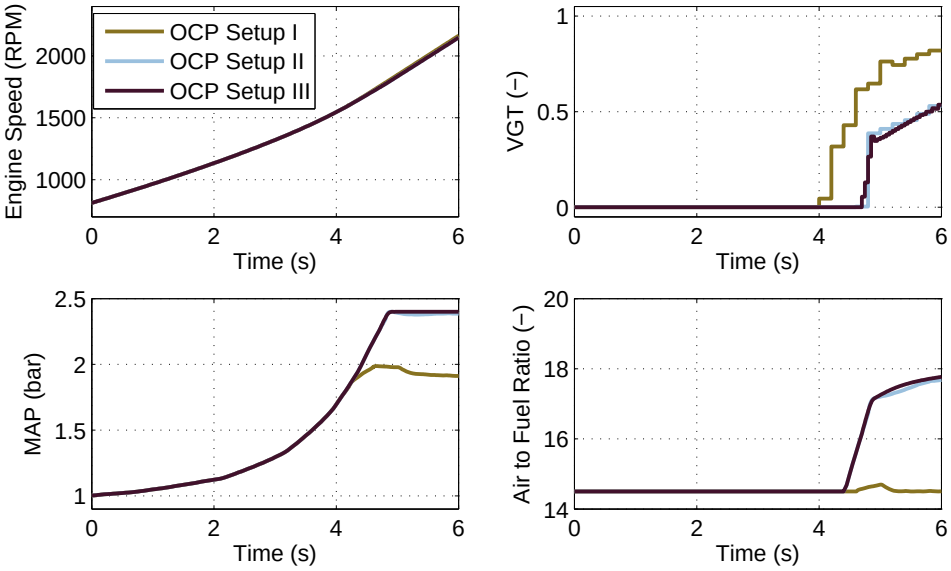

Figure 3.10: The solutions to the Optimal Control Problems. Setup I: maximising terminal vehicle speed ($T_s = 200$ms). Setup II: maximising terminal vehicle speed, no incremental exhaust pumping losses ($T_s = 200$ms). Setup III: maximising the integral of the intake manifold pressure ($T_s = 50$ms). EGR valve fully closed at all times.

From the first OCP result it can be concluded that the highest vehicle speed is achieved with the boost pressure not exceeding 2 bar. In the MVEM the engine brake torque is affected by several parameters: fuel flow, fuel conversion efficiency map, friction and pumping losses. The most critical is the fuel flow, which is limited to the lesser of either maximum fuelling level for the considered engine (66 milligrams per stroke) or to give an air-fuel ratio of 14.5. The air

mass flow in this first case (OCP Setup I) is sufficient to allow the maximum fuel quantity to be injected (i.e. exactly at the smoke limit). This solution is preferred to one with a higher boost pressure as the VGT remains more open leading to a reduction in engine pumping losses.

Although the solution to the first problem is physically sensible, it is not necessarily practical. Even at full-load operation the particulate emissions must not be excessive and hence the air-flow must be raised to keep the AFR further from the smoke limit. The second test therefore attempts to determine how much influence the incremental exhaust pumping losses have on the maximum engine speed achieved. To evaluate this the same optimisation was repeated, but ignoring the exhaust pumping effect. The result is shown in Figure 3.10 as OCP Setup II. It is observed that this time the intake manifold pressure was controlled to its maximum allowed level. As expected, the increased pumping losses resulted in a lower final engine speed, but the difference was marginal. The speed plots in Figure 3.10 cannot be distinguished and the above conclusions had to be verified by inspecting the numerical results of simulations.

A production style control system typically maximises the intake manifold pressure at each point in time during the tip-in manoeuvre. The third OCP is formulated to more closely resemble this behaviour by defining the cost function to be the integral of the intake manifold pressure over the entire transient. Due to the difficulties with convergence of the optimisation algorithm, the problem was initially solved for 30 input steps. The number of input steps was then iteratively increased and the new optimisation hot-started using the result from the previous iteration. The final result with 120 input steps is shown in Figure 3.10 as OCP Setup III. This approach gives the same engine speed as Setup II and furthermore, due to the increased number of input steps, gives a smoother intake manifold pressure profile.

Within the limits of the simplified model used, the results from the three optimal control problems support the intuitive idea that the standard production air-path control approach (demanding maximum intake manifold pressure) is indeed analogous to a driver demand for maximum acceleration during the tip-in manoeuvre. Furthermore, the results from Setup III (VGT input updated every $T_s = 50$ ms) are selected to act as a benchmark against which the performance

of the MPC controller will be evaluated.

3.3.4 MPC formulation for simulations

The MVEM described in 2.4.1 is a non-linear system with 11 states. In the MPC setup considered here, full state feedback is assumed and virtual measurements are taken every T_1 =10 ms. The controller itself is executed every $T_S = 50$ ms and includes linearisation of the MVEM at the current operating point (x_0, u_0, d_0), discretisation of the linear model and solving the linear MPC optimisation problem. As the controller is being assessed during a transient manoeuvre, the model is not necessarily linearised around a steady-state operating point and therefore an offset $f(x_0, u_0, d_0)$ appears in the equations:

$$x_{k+1} - x_0 = f(x_0, u_0, d_0)T_S + A(x_k - x_0) + B_u(u_k - u_0) + B_d(d_k - d_0) \quad (3.13)$$

$$y_k - y_0 = C(x_k - x_0) \quad (3.14)$$

The controller will be used for transient operation of both the 1D model and the MVEM. Although the system matrices must be obtained from linearisation of the MVEM, the offset term can be taken directly from the plant output. Therefore at each sampling instance approximate state derivatives Δx_0 are calculated by subtracting the latest measurements from the ones obtained at the previous sampling instance:

$$\Delta x_0 = \frac{x(t_0) - x(t_0 - T_1)}{T_1} T_S \quad (3.15)$$

where t_0 is controller execution instant. This pragmatic approach was found to give better steady-state reference tracking than when the state derivatives were calculated directly from the MVEM.

Constant system matrices and constant disturbances (i.e. $d_k - d_0 = 0$) are assumed throughout the entire prediction horizon. The optimisation problem can be therefore expressed as:

$$\min_{u_0,u_1,\ldots,u_{N_C-1}} \Phi(x_0, d_0, \Delta u_0, \Delta u_1, \ldots, \Delta u_{N_C-1})$$

$$\begin{aligned} s.t. \quad & \forall k \in [0, N_P - 1] \\ x_{k+1} - x_0 =& \Delta x_0 + A(x_k - x_0) + B_u(u_k - u_0) \\ 0 \geq& s(x_k, u_k) \end{aligned} \tag{3.16}$$

where

$$u_{k+1} = u_k + \Delta u_k \tag{3.17}$$

The cost function $\Phi(x_0, d_0, \Delta u_0, \Delta u_1, \ldots, \Delta u_{N_C-1})$ is quadratic in the boost reference tracking error and the rate of change of the input during one controller sampling period. The constraint function s is linear. The control horizon N_C may be shorter than the prediction horizon N_P and in such a case:

$$u_{N_P-1} = u_{N_P-2} = \ldots = u_{N_C} = u_{N_C-1} \tag{3.18}$$

The cost function, therefore, takes the following form:

$$\begin{aligned} \Phi(x_0, d_0, \Delta u_0, \Delta u_1, \ldots, \Delta u_{N_C-1}) = & \sum_{k=0}^{N_P-1} (r_k - \bar{x}_k)^T Q (r_k - \bar{x}_k) + \\ & + \sum_{k=0}^{N_C-1} \Delta u_k^T R \Delta u_k + (r_{N_P} - \bar{x}_{N_P})^T P (r_{N_P} - \bar{x}_{N_P}) \end{aligned} \tag{3.19}$$

where $\bar{x}$ stands for the state vector extended by the magnitude of the input:

$$\bar{x} = \begin{bmatrix} x \\ u \end{bmatrix} \tag{3.20}$$

The cost function Φ is implicitly dependent on d_0, because disturbances affect the linearisation, thus system matrices used in each consecutive optimisation. Furthermore, in this simplified approach, the terminal cost P was assumed to be

equal to the penalty on reference tracking Q.

MPC has been successful in real-world applications largely because such an optimisation can be rewritten as a quadratic programming (QP) problem and solved efficiently. The algorithm described above was implemented using the Model Predictive Control Toolbox in MATLAB.

To assess the performance of this setup, MPC control was initially applied to the MVEM. The driveline model was not a part of the prediction model and the engine speed and fuel injection were therefore treated as measured disturbances by the controller. In the considered formulation, using a long prediction horizon was not beneficial. Linear time invariant models used for predictions were only valid in the proximity of the linearisation point (see Figure 3.9). On the other hand the horizon should be long enough for predictions to capture the relevant dynamics. A prediction horizon of 10 samples (i.e. 0.5 s) and a control horizon of 5 were found to be suitable. To ensure that the solution of MPC remains feasible, the desired boost pressure and the constraint on the maximum boost pressure were set to 2.4 and 2.6 bar, respectively. To improve the numerical behaviour and calculations the magnitudes of states and actuators were scaled: pressure states were expressed in bar, masses stored in volumes were multiplied by the factor of 100 and the turbocharger speed was divided by 10000. This configuration was then compared with the results from OCP Setup III.

In Figure 3.11 the engine speed achieved using this technique can be seen to be very close to the one calculated from the OCP. In the case of OCP, the VGT was opened progressively starting at 4.7 seconds (about 150 ms before the reference boost pressure of 2.4 bar was achieved). The optimiser had sufficient information to predict the effects of the changing engine speed and VGT rack position on all the states of the MVEM and a smooth transition, in both actuator commands and output variable, was observed. A major difference between the OCP and the MPC setups is that in the case of OCP, the full vehicle model including fuelling and engine speed dynamics is a part of the formulation. In the MPC case, not only the linearised system behaviour is predicted over a finite time horizon, but also the controller assumes a fixed level of fuelling and a constant engine speed. As a result the VGT was actuated earlier in the MPC case, starting from the time of 4.45 seconds, but the rest of the actuator trace was observed to be similar to

the OCP result. The steady-state level of boost was tracked without any error.

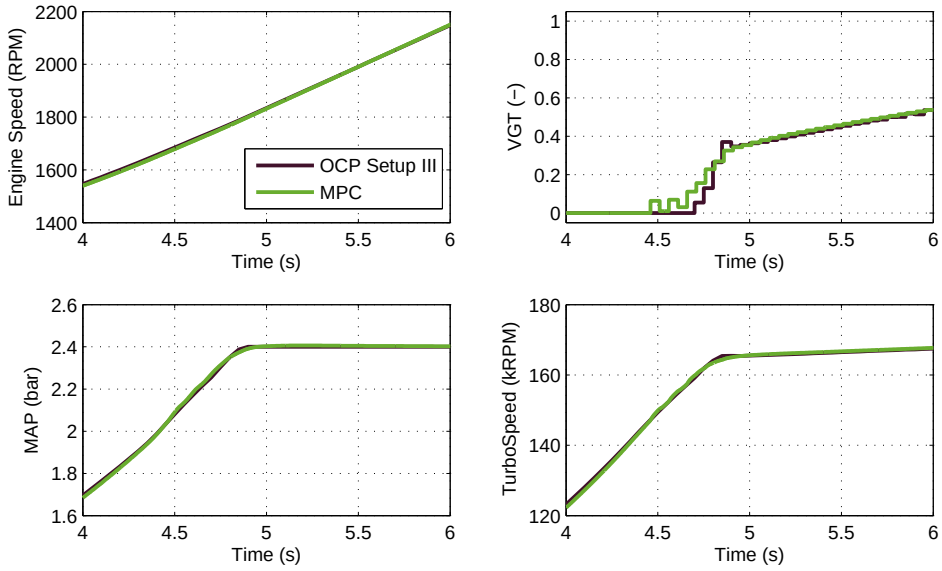

Figure 3.11: The comparison of the results of OCP maximising the integral of the intake manifold pressure and MPC control.

The above analysis gives some insight into the characteristics of the controller; because of the simplified system model used for prediction, the actuation of VGT is less smooth around the knee region. A more detailed analysis of MPC calculations and the influence of simplifications used in this particular formulation can be found in the Appendix C.

3.3.5 MPC control of 1D engine model

The MPC control approach outlined in the previous section is now applied to the WAVE 1D engine simulation model described in 2.3. The weightings in the MPC cost function are the same as in the original setup. Sensors for the turbocharger speed and the pressure and temperature corresponding to each of the MVEM volumes are added to the WAVE model. The sensors are set to give the cycle-averaged values of measured quantities, which is implemented as a sliding window filter. Such fast temperature measurements would not be practical in reality due

to the longer time constant of standard thermocouples.

The focus of the remaining results is on the air-path control system performance. To allow for a better comparison with the previous results the engine models are now operated using the engine speed and fuelling taken from the OCP results. If the models were operated with the driveline included, the absolute response times would be affected by differences in the treatment of the combustion process.

Figure 3.12 shows the results for both the new setup and the case when the MPC controls the MVEM. The boost pressure from the MPC controlled WAVE model shows a satisfactory tracking performance with a less sharp knee region. No overshoot, undershoot or steady-state error in reference tracking are observed. The latter feature is ensured by using the estimate of the state derivatives from measurements (see eq. 3.15). The simplifications present in the MVEM can be seen in the differences in the final turbocharger speed but overall, the results confirm that the 1D engine model can be effectively controlled by MPC based on a related MVEM.

Controlling the engine within constraints

In the previous section it was shown that the controller ensures close-to-optimal operation of 1D engine simulation model. In this part, the controller's capability of ensuring the engine's operation within physical limits is considered.

Control system requirements for tip-in manoeuvres and some related physical limits were discussed in 3.2.2. Here, three constraints of a different nature are considered:

maximum exhaust manifold pressure - The dynamics of pressure in the exhaust manifold is one of the fastest in the MVEM, because of a small volume of this part of the air-path. Additionally, this was the state, for which MVEM validation was the poorest (see Figure 2.22).

maximum turbocharger speed - Turbocharger speed dynamics is the slowest mode of the air-path

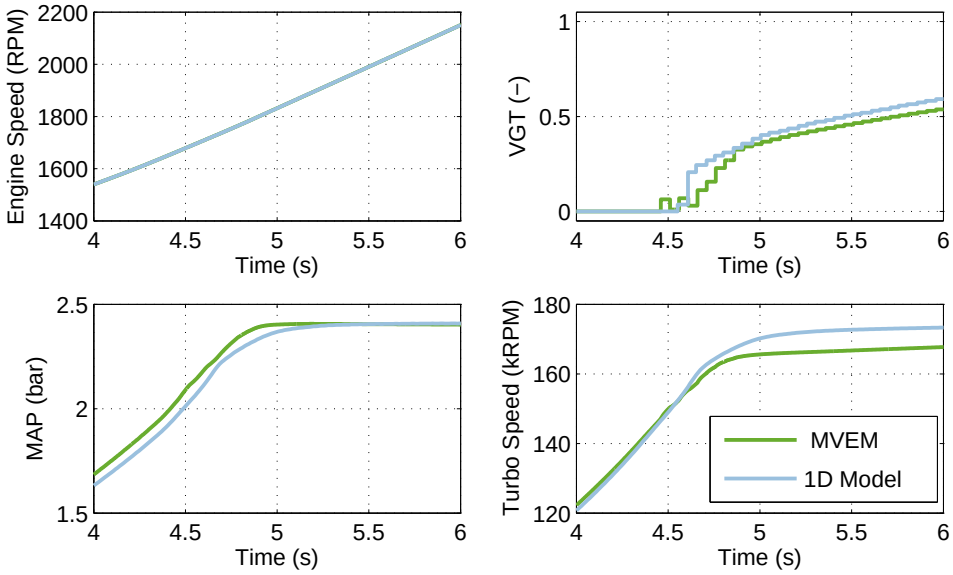

Figure 3.12: The comparison of the closed-loop performances of the MVEM and WAVE models controlled with the same MPC controller. Close to optimal performance of 1D model is achieved using the MPC controller based on a related MVEM.

compressor surge limit - This is a state-dependent constraint sensitive to actuator operation

Operation at high altitudes

Matching a turbocharger to an engine is a compromise. On the one hand, the selected combination is required to achieve excellent performance in nominal ambient conditions. On the other hand, the system has to be capable of operating at high altitudes and a significant range of temperatures. This requires ensuring certain margins in the design. Therefore, in the case of the tip-in manoeuvre at nominal ambient conditions (pressure ∼1 bar and temperature ∼20 deg C), the system usually operates with a safe margin from the limits of operation.

Simulations of 1D model with ambient pressure of 0.8 bar are now investigated. This pressure corresponds to the altitude of about 2000 metres above the sea level. To satisfy the same boost pressure demand as at the sea level, the required

turbocharger speed is significantly higher. The compressor and the turbine needs to operate at much higher pressure ratios.

Two constraints are now investigated: the maximum exhaust manifold pressure of 4 bar and the maximum turbocharger speed of 210000 RPM.

Both variables are states of the MVEM and the required limits can be readily added to the MPC controller. Soft constraints were used in this setup. This allowed, but heavily penalised, the exhaust pressure and the turbocharger speed exceeding their limits, but ensured the feasibility of optimisations. Exceeding the limits is often unavoidable, because of the mismatch between the prediction model and the actual plant.

The results of such simulations are shown in Figure 3.13. It is observed that the demanded pressure of 2.4 bar was achieved significantly later than it was in the case when nominal conditions were investigated. Meeting the boost demand required accelerating the turbocharger to higher speeds. Before this was achieved, the pressure in the exhaust manifold had become very high and the MPC controller had generated a demand for opening the VGT. Maintaining a constant boost pressure required progressive opening of the VGT which resulted in a drop in the exhaust pressure. Soon after that, the turbocharger speed achieved its maximum permitted value. The MPC controller sacrificed the reference tracking to keep the turbocharger speed at the specified limit.

3.3.6 Surge avoidance control

When simulating operation at high altitudes, consideration of compressor surge is necessary because of increased pressure ratio across this element. Several definitions are possible as shown in Figure 3.14. Considering the instantaneous compressor operating point denoted with the cross, a natural definition of the surge limit would be to express it as the shortest distance in the flow parameter and pressure ratio coordinates to the compressor surge line (*absolute distance* in Figure 3.14). Simpler definitions consider only one coordinate: *pressure distance* and *flow distance*. An alternative method is to define the surge limit using turbocharger speed parameter, but this approach suffers from the fact that at high pressure ratios, the slopes of constant speed parameter lines become positive near

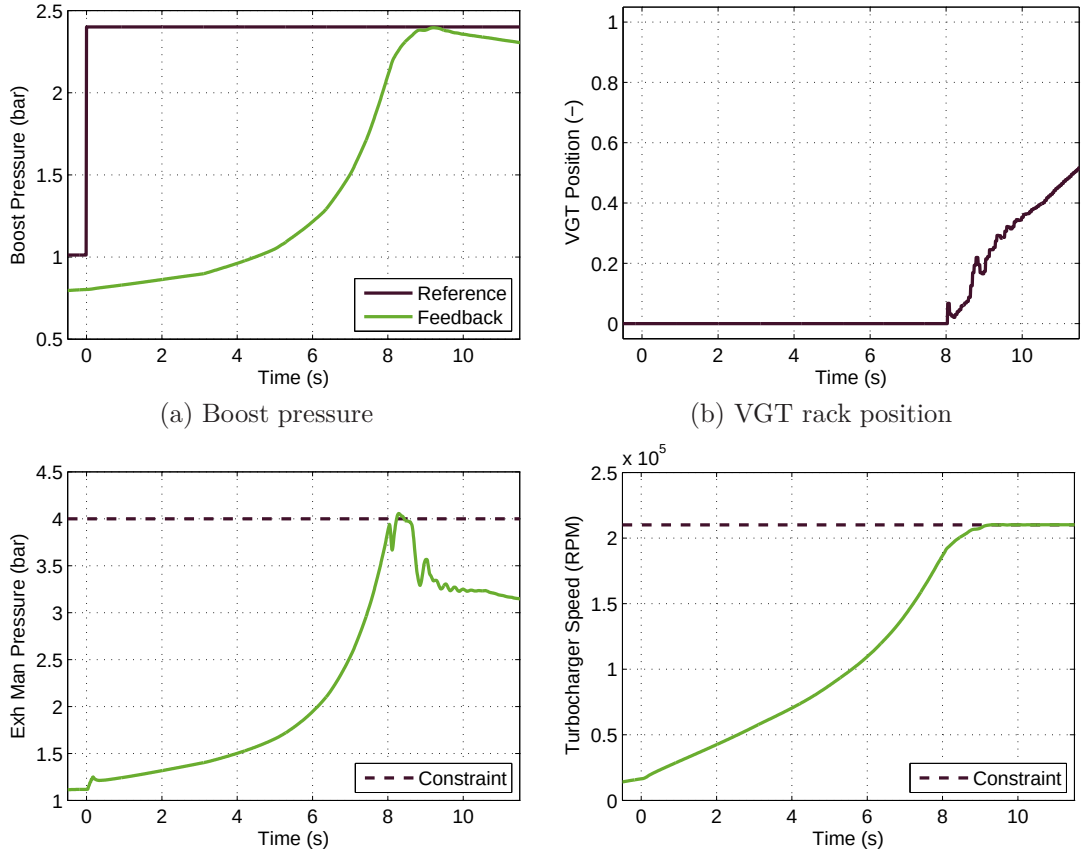

(a) Boost pressure

(b) VGT rack position

(c) Exhaust manifold pressure

(d) Turbocharger speed

Figure 3.13: Simulating 1D operation at high altitudes - MPC satisfies the exhaust manifold pressure and turbocharger speed limits.

the surge line.

In this work, the definition of the surge limit as a pressure distance is used, because it can be relatively simply accommodated in the investigated controller. The surge limit is stored as a look-up table between the mass flow parameter and the pressure ratio. The WAVE model includes sensors for compressor flow, pre-compressor pressure, temperature and post-compressor pressure. This allows the instantaneous compressor flow parameter and pressure ratio to be calculated, thus the surge limit to be expressed as a post-compressor pressure. In the MVEM used by the controller, the compressor surge limit can be calculated in a similar fashion.

Two methods for avoiding surge were investigated:

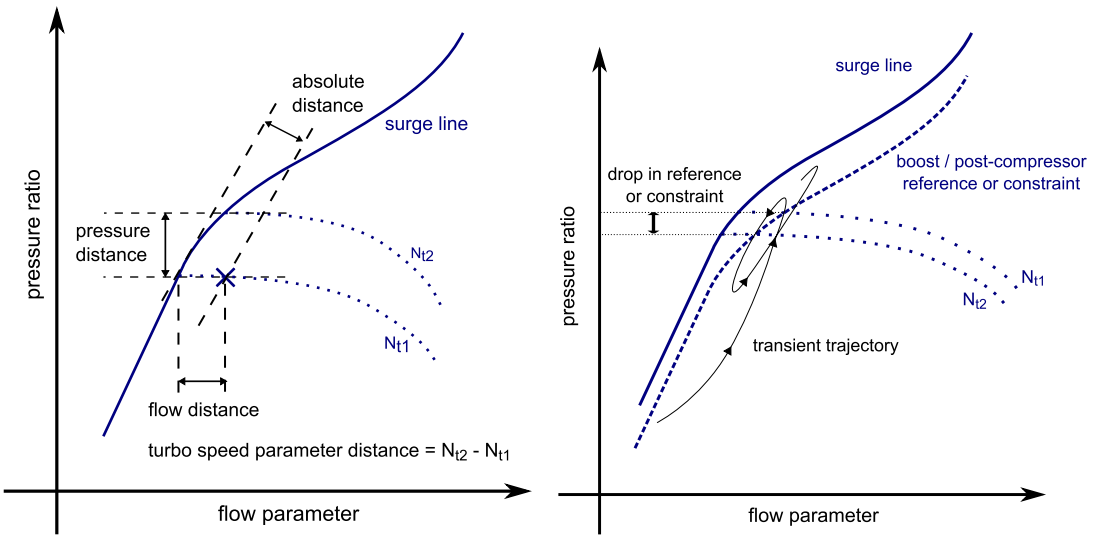

(a) Surge limit defitions (b) Control induced oscillations

Figure 3.14: Definition and challenges with compressor surge limit.

1. Setting the boost reference as the minimum of the demanded pressure and the surge limit.

2. The difference between the surge limit and the boost pressure was defined as one of the system outputs. The evolution of this difference within the prediction horizon of MPC and its dependency on inputs were in this way included in the actual optimisation procedure. A constraint of 0.15 bar was imposed on this output.

A particular difficulty with compressor surge avoidance is highlighted in Figure 3.14b. This is valid for both approaches described above. Boost reference or constraint is specified with a certain margin in pressure from the surge line. Considering a transient trajectory starting at the bottom left corner, initial turbo-lag pushes the operating points further from the surge line. Once the turbocharger is spinning faster, the actual boost pressure overshoots the reference or closes the gap to the constraint. As a result VGT is opened and the turbocharger slows down. This leads to lower compressor flow parameter and as a result the boost reference/constraint has to drop as well. The actual pressure needs to fall below this value, before it may continue rising to the demanded level.

Such behaviour was observed during the simulations of the 1D model with the

ambient pressure of 0.8 bar. The tests shown in the previous sections (see Figure 3.13) were conducted without surge limit avoidance control and resulted in the operation shown in Figure 3.15a. In fact, the surge limit was briefly exceeded between 8 and 9 seconds.

To avoid such a situation, the two methods described above were implemented. The first one, relying on limiting the boost reference to the surge limit, was not effective and unreliable due to the previously described difficulties.

Better results were obtained when the difference between the boost pressure and the surge limit was treated as a system output (*Surge Ctrl A* in Fig. 3.15). The problem with the dependency of the constraint on the state and the input was still visible (see Figure 3.15b). The relatively low penalty on VGT actuation from the original MPC calibration, resulted in an abrupt VGT rack position change (as shown in 3.15d). This led to a characteristic drop in the value of the constraint, which was, however, not exceeded. The boost pressure had to be then recovered from value below 2 bar.

MPC was then recalibrated with an increased weight on the VGT rate of change (from 20 to 100). The resulting response is shown as *Surge Ctrl B* in Figure 3.15. This time the VGT was not actuated as abruptly as previously and the drop in constraint and boost pressure was avoided.

This confirms that in this idealised setup (ideal sensors and actuators) an effective surge avoidance control can be realised for 1D models using a MPC controller. The necessity of finding a suitable trade-off in VGT actuation penalty was explained. On one hand a low penalty is preferred for fast boost tracking. On the other, too aggressive actuation results in controller induced oscillations in the vicinity of the surge limit.

3.4 Real-Time MPC for engine experiments

In the previous section MPC formulation for control of 1D simulation model was introduced. Applying a similar concept for Real-Time control of the actual engine requires a number of modifications. Some of the challenges of implementing MPC in the ECU were considered in [Stewart and Borrelli, 2008]. In this applications, the code will be executed on rapid prototyping system and the following issues

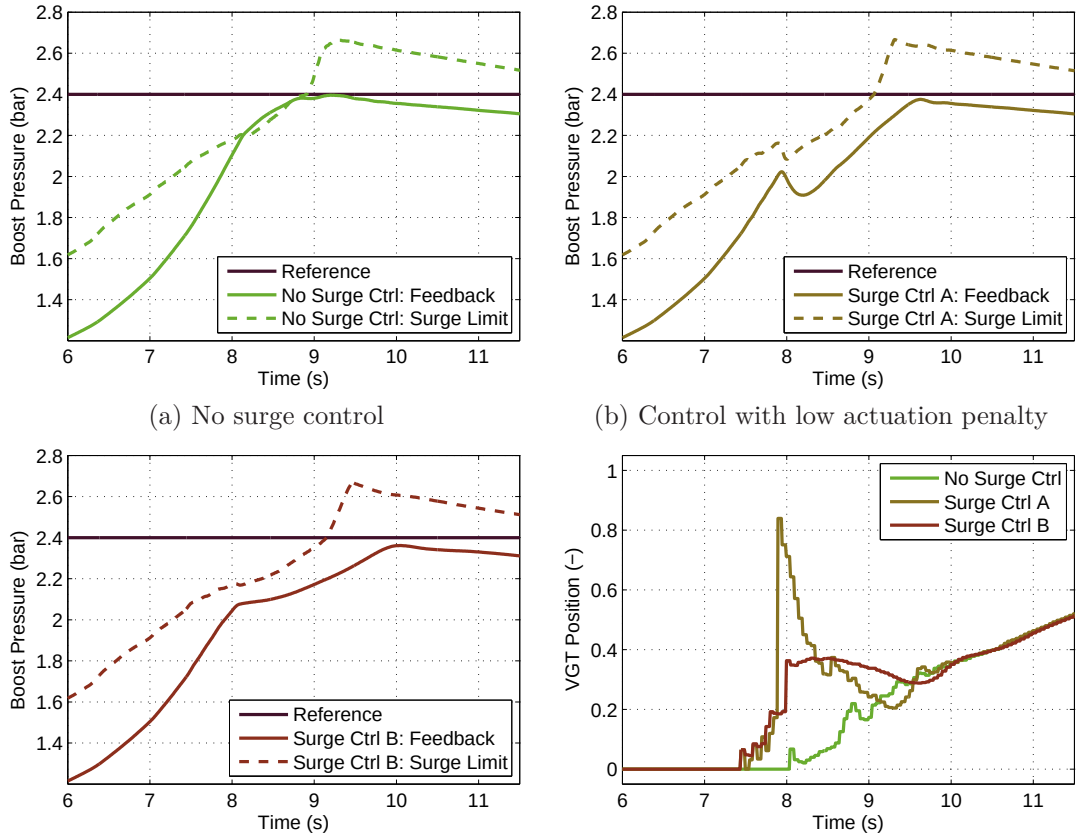

(a) No surge control

(b) Control with low actuation penalty

(c) Control with an increased actuation penalty

(d) VGT positions

Figure 3.15: Surge avoidance control for 1D simulation model.

are relevant:

1. the implementation of a QP solver has to be suitable for Real-Time execution
2. fast pressure measurements are affected by engine cyclic operation
3. temperature measurements suffer from low sensor bandwidth
4. the assumption of ideal actuator is not valid

In this section, the approach to address the above list of challenges is described.

3.4.1 QP solver

A dedicated solver was implemented in M-code and autocoded to C using Code Generation for MATLAB [1]. The solver used the dual active-set algorithm introduced in [Goldfarb and Idnani, 1983]. The QP matrices were built up in an efficient way, but the algorithm did not exploit the exact problem structure. It allowed however for improved traceability between the design in MATLAB/Simulink and the final execution code. Furthermore, it was possible to calibrate cost function weights and adjust constraints during on-line execution.

To realise the described control concept, the communication between the engine control unit (ECU) and the dSPACE rapid prototyping system was established via CAN Calibration Protocol, which allowed for the exchange of signals at the rate of 10 ms. The fuelling quantity was read from the ECU to linearise the MVEM around the appropriate operating point. The MPC result in the form of VGT position demand was then written to the ECU.

3.4.2 Full-state feedback

The investigated MPC formulation assumes full-state feedback. There are three types of measurements required: pressures in all five volumes, temperatures in the volumes to allow for calculating the stored mass of gas and turbocharger speed.

In the simulation environment the sensors implemented in the 1D model were noise-free, of instantaneous response and set to indicate cycle-averaged values. In the real application the bandwidths of sensors and the characteristics of measured signals cannot be neglected.

Measuring turbocharger speed during transient conditions is the simplest in this set. A fast digital sensor is used to determine the speed of the compressor wheel, which due to a significant turbocharger shaft inertia does not show considerable variations during single engine cycle. Therefore, a raw signal from the sensor can be used for feedback.

[1] The code of the solver was supplied by Dr Edward Hartley.

Cycle-averaged pressure measurements

As it was shown in Figure 3.4, a high bandwidth of pressure transducers allows measurement of variations in pressure during a single engine cycle. In the discussion presented in the section 3.1.2 a non-causal cycle-averaging filter was used. For on-line execution two approaches were considered. The first option was to apply a discrete time filter (DTF). The filter parameters were determined discretising a 1^{st} order continuous time low-pass filter with the time constant τ given by:

$$\tau = \frac{2\pi}{N_e} = \frac{t_{ct}}{2} \tag{3.21}$$

The engine speed N_e is expressed in radians per second and t_{ct} is the duration of a single engine cycle.

The second method involves integrating the measured pressure during one engine revolution and dividing the result by the time of integration. One engine revolution rather than the entire cycle is used in order to reduce the time delay introduced by this approach. Nevertheless, this method is referred to as cycle-average filters (CAF). This method, however, suffers from implementation difficulties. The pressure signal is sampled by the rapid prototyping system with the step of 1 ms. The shaft encoder attached to the crankshaft triggers the integrator reset every engine revolution. This period is speed dependent - 60 ms at 1000 RPM and 21.8 ms at 2750 RPM. As a result the resolution of capturing the pressure variations becomes worse at high engine speeds, which is then reflected in the resulting cycle-average value.

The results obtained applying the two methods to intake manifold pressure measurements are shown in Figure 3.16. Two sections of the tip-in manoeuvre are shown: a part of the manoeuvre with a steep increase in the intake manifold pressure (Figure 3.16a) and the steady-state operation at full load (Figure 3.16b). It is observed that during steady-state operation results obtained with CAF are significantly better, i.e. the variation of calculated signal is smaller.

To improve our understanding of the effects these two methods may have on the MPC controller, the time instances of the controller execution are marked with crosses. It is observed that both approaches returned similar values during the

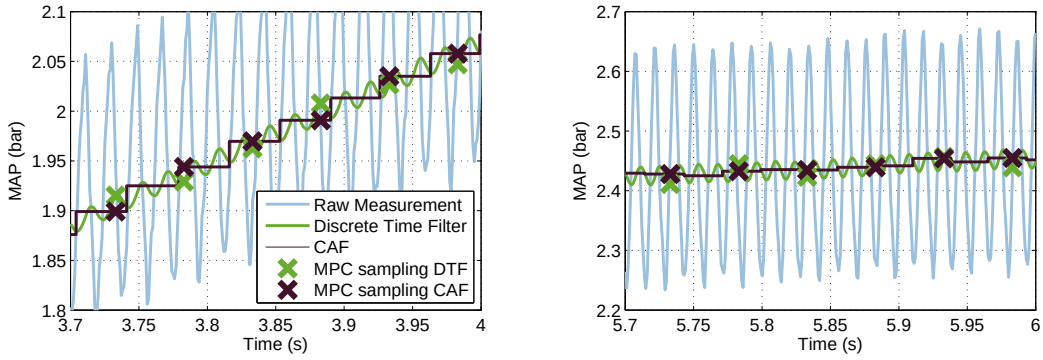

(a) Boost pressure A

(b) Boost pressure B

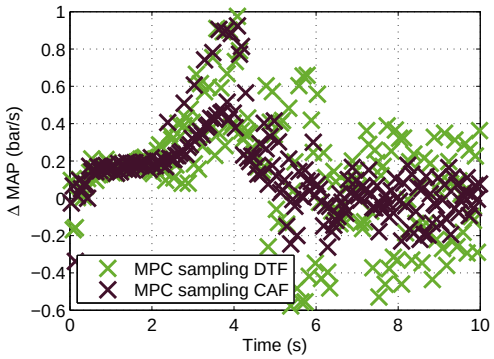

(c) State derivatives

Figure 3.16: Measuring pressure states and their derivatives.

test. However, the formulated controller also approximates state derivatives from last two measurements. The approximate state derivatives for the intake manifold pressure calculated during the entire manoeuvre are shown in Figure 3.16c. The plot can be divided into two parts - a big transient in pressure happening before the time of 5 seconds, and from 6 seconds onwards, when the pressure was controlled to a constant value. The differences in state derivative estimates for the two methods, especially during the second part of the test, indicate that the CAF approach is more suitable.

Calculating temperatures for state-feedback

Measuring temperatures in the air-path volumes during transients is difficult due to the low bandwidth of the sensors (see discussion in 3.1.2 and Figure 3.4c). In order to maintain the general controller structure, estimated temperatures

were calculated based on the steady-state characteristics of the elements prior to a considered volume. For example, the temperature of the gas in the post-compressor volume was estimated multiplying the pre-compressor temperature by the compressor temperature ratio. These characteristics are mainly based on the pressures across a considered element, turbocharger speed, engine speed and fuelling level. All these signals can be effectively measured during transient engine testing.

The results of such calculations (*Static*) were compared with the temperatures determined from solving the full MVEM (*Dynamics*) in Figure 3.17. This comparison was performed for the simulation of a tip-in manoeuvre using the MVEM as an engine simulator.

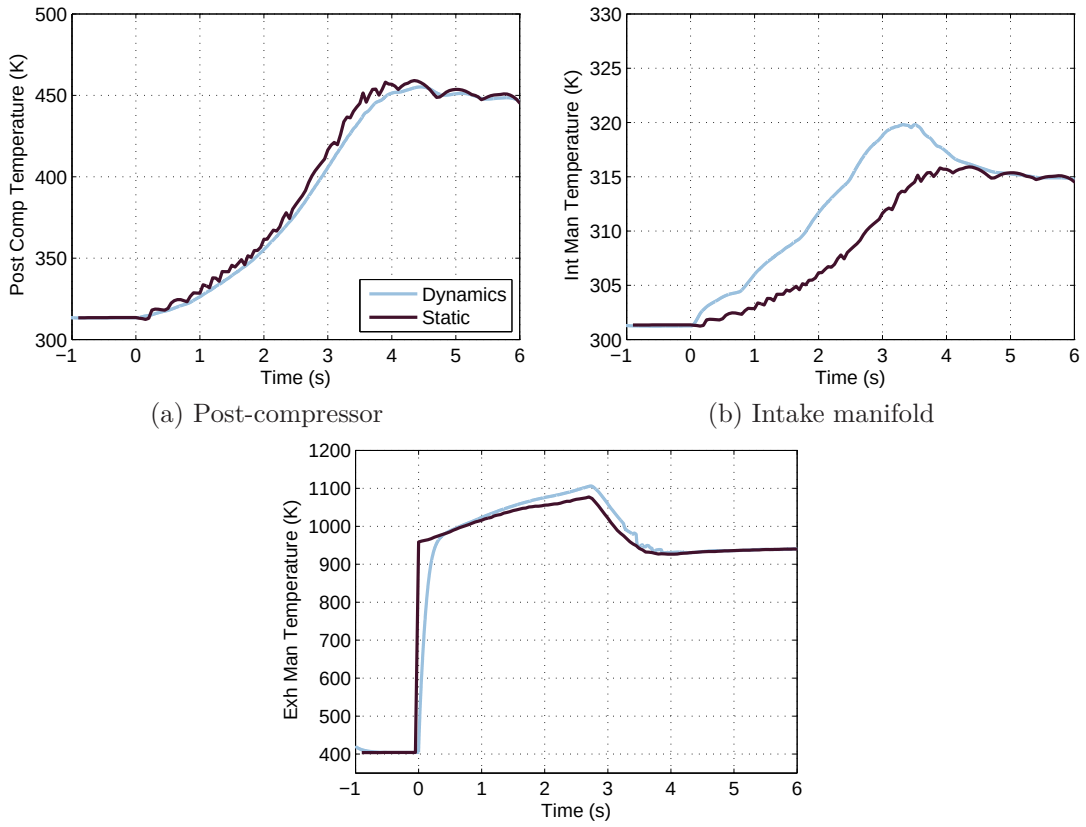

(a) Post-compressor

(b) Intake manifold

(c) Exhaust manifold

Figure 3.17: Estimating the temperatures using steady-state characteristics.

It is observed that the effect on the pre compressor temperature is not sig-

nificant. The intake manifold temperature estimation is worse, but does not affect the overall operation significantly considering the scale of the temperature changes and the relative error. Omitting the temperature dynamics in the exhaust manifold has a considerable effect. However, comparing the error introduced by such calculation to temperature measurements shown in Figure 3.4c), leads to the conclusion that using the calculated values for feedback is superior to using the raw thermocouple readings.

3.4.3 VGT dynamics

In the previous two sections, practical challenges to the proposed control strategy introduced by the measurement system were described. The characteristics of the VGT actuator are now considered. At this stage of investigations this is the only actuator used by the controller.

The engine used for the experiments is equipped with a pneumatically actuated Variable Geometry Turbine. A detailed description and modelling of such an actuator can be found in [Mehmood et al., 2011]. The authors also proposed and verified experimentally a feedback control strategy with friction compensation. Such an approach was shown to perform significantly better than a linear PID controller.

In the setup considered in this work, the MPC controller is used to determine the reference for the valve position. Tracking of this reference is ensured by the original low level controller implemented in the ECU. The dynamics of this low-level control loop and its performance cannot be neglected in the overall strategy. It was found that the assumption of an ideal actuator leads to an unacceptable controller performance, especially when the MPC is used to satisfy operating constraints.

Several tests involving open loop steps in the VGT demand position were performed to characterise the actuator. To investigate the directional dependency of response, steps of 10% were applied as shown in Figures 3.18a and 3.18b. It was observed that actuation during VGT opening was considerably more aggressive than during VGT closing. In the first scenario, the response resembled an under-damped system, whereas during closing an over-damped characteristics

were recorded. There was also a 50 ms delay (MPC controller execution period) between the demand from the MPC block and the demand signal recorded in the ECU.

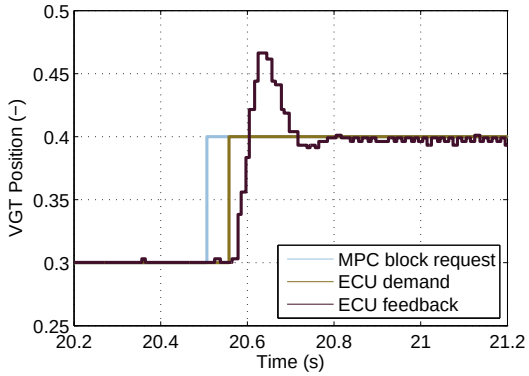

(a) Directional dependency: opening

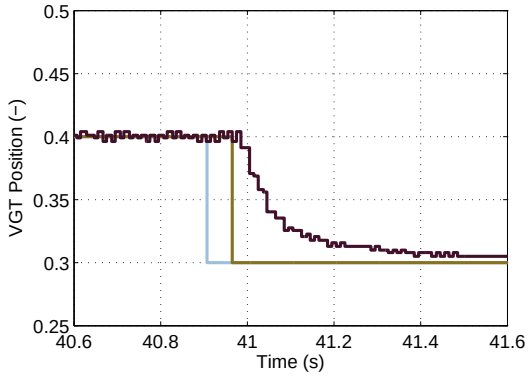

(b) Directional dependency: closing

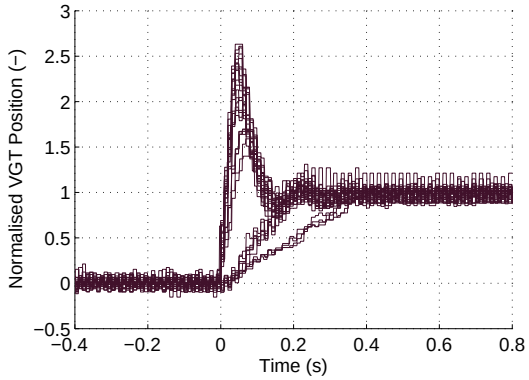

(c) Operating point dependency: opening

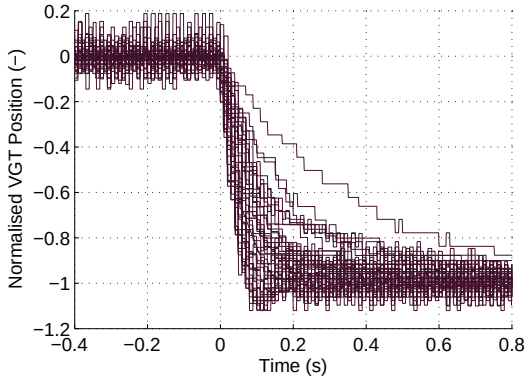

(d) Operating point dependency: closing

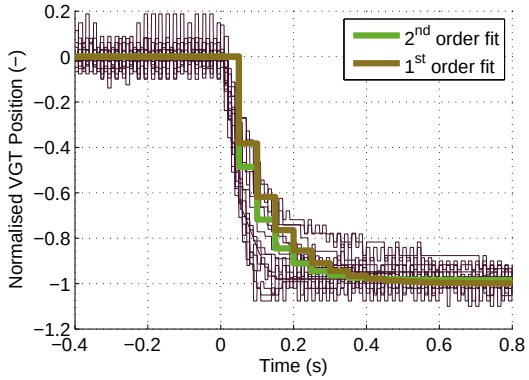

(e) Model fitting

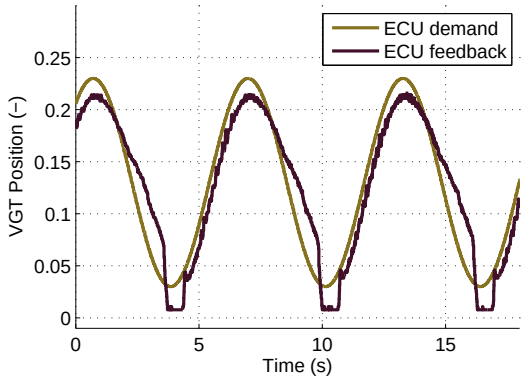

(f) Non-linearity near the fully closed position

Figure 3.18: VGT actuator: characteristics and dynamics.

In the next set of experiments, several series of steps of various magnitudes (in the range from 5 to 15%) and at three different engine operating points were applied. This showed the dependency of the response on the VGT operating point. The results were normalised and can be found in Figures 3.18c and 3.18d. A significant variation in the measured positions was observed. The closing dynamics was more consistent. Several traces measured during VGT opening were significantly different to the majority of under-damped responses. These "outliers" were observed when opening the valve from almost fully-closed positions.

In order to account for such actuator characteristics in the MPC controller, it was desirable to approximate them with a simple model. To facilitate such a simplification, 1^{st} and 2^{nd} order transfer functions were fitted to a selection of recordings from VGT closing tests. The parameters of these transfer functions were calculated using the linear least square algorithm.

To ensure the durability of the actuator and to avoid the variable vanes mechanism hitting the safety end-stop, the actuator was forced to saturate when the demand was near to fully-closed position. This introduced a non-linearity as shown in Figure 3.18f.

To conclude, the prediction model in the MPC formulation used during engine testing was extended with the modelled VGT dynamics. The model was in the form of 1^{st} order low-pass transfer function. In spite of this significant simplification of the actual actuator response, it was sufficient to improve the capability of the MPC controller: overshooting the specified constraints was considerably reduced as it is shown in following sections. Because of the way the controller was implemented, the result of calculations for a given controller execution instant was actually applied during the subsequent controller execution. To compensate for this one step delay, the initial state of the prediction model was calculated simply multiplying the effective state derivatives by the controller sampling time.

3.4.4 Comparison to standard ECU control

The performance of the RT-MPC is evaluated by comparing the achievable engine response during the 3^{rd} gear tip-in with the one under standard ECU control.

For the purpose of this analysis, the internal ECU boost demand was overwrit-

ten with a step from 1.1 bar to 2.4 bar as shown in Figure 3.19a. Furthermore, the engine fuelling demand was modified to remove all the limitations except of the smoke limit and the dual mass flywheel protection. It is, therefore, necessary to emphasise that the ECU controller operates in the regions it has not been calibrated for.

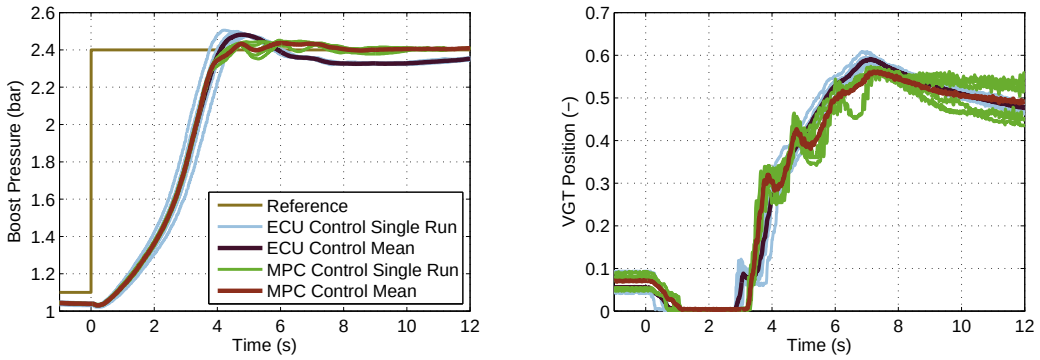

(a) Boost pressure (b) VGT

Figure 3.19: Comparison of engine performance under MPC and standard ECU control.

The experimental results of the boost control performance are presented in Figure 3.19a. During these tests, the only constraints were the operating limits of the VGT actuator. The RT-MPC controller was calibrated with the following values:

- prediction horizon of 15 steps (0.75s)
- control horizon of 10 steps (0.5s)
- penalty $Q(i_{p_i}, i_{p_i})$ on boost tracking error squared of 10
- penalty $R(i_{\Delta u_{vgt}}, i_{\Delta u_{vgt}})$ on the square of VGT position change over one sampling time of 20

where i_{p_i} is the index of the state vector entry corresponding to intake manifold pressure and $i_{\Delta u_{vgt}}$ is the index of the input vector entry corresponding to VGT actuation.

A discussion of the controller calibration can be found in Appendix A.

Six repetitions were performed under MPC and ECU controllers to verify the repeatability of the results. Each single run under the ECU control is shown in bright blue and each run under the MPC is plotted in green. The single recordings for each set of tests are averaged and also presented. It is observed that the MPC was able to better regulate the boost pressure around the set-point of 2.4 bar. Negligible steady-state error was recorded with relatively low overshoot and undershoot. The control action (see Figure 3.19b) was in this case more energetic than under the ECU control. Furthermore, the tests with MPC controller resulted in a bigger spread in actuator plots. This was caused by the influence of noisy state derivative estimates (as shown in Figure 3.9).

3.4.5 Satisfying constraints with RT-MPC

The next set of experiments was conducted to verify the MPC capability of ensuring the operation of the engine within some imposed constraints. To perform such tests, the constraints were set artificially low:

- Maximum exhaust manifold pressure = 2.8 bar
- Maximum turbocharger speed = 165 000 RPM

Three scenarios were considered - operation without state constraints, operation with the exhaust manifold pressure constraint only and operation with the turbocharger speed limit only. Similarly to the setup with 1D simulation model, slack variables (soft constraints) were used to ensure the feasibility of optimisation. Each scenario was repeated three times and the results of the tests can be found in Figure 3.20.

The tests without any state constraints resulted in a peak exhaust manifold pressure of about 3.5 bar and turbocharger speed of 175 000 RPM. When a limit on the maximum exhaust manifold pressure was imposed, the peak value did not exceed 3 bar. This indicates that soft constraints in MPC have to be defined with a certain margin from the actual physical limits. Nevertheless, in all three repetitions, the MPC was able to reduce the peak pressures. This was achieved by an earlier VGT opening and lead to a delayed achievement of the boost pressure set-point.

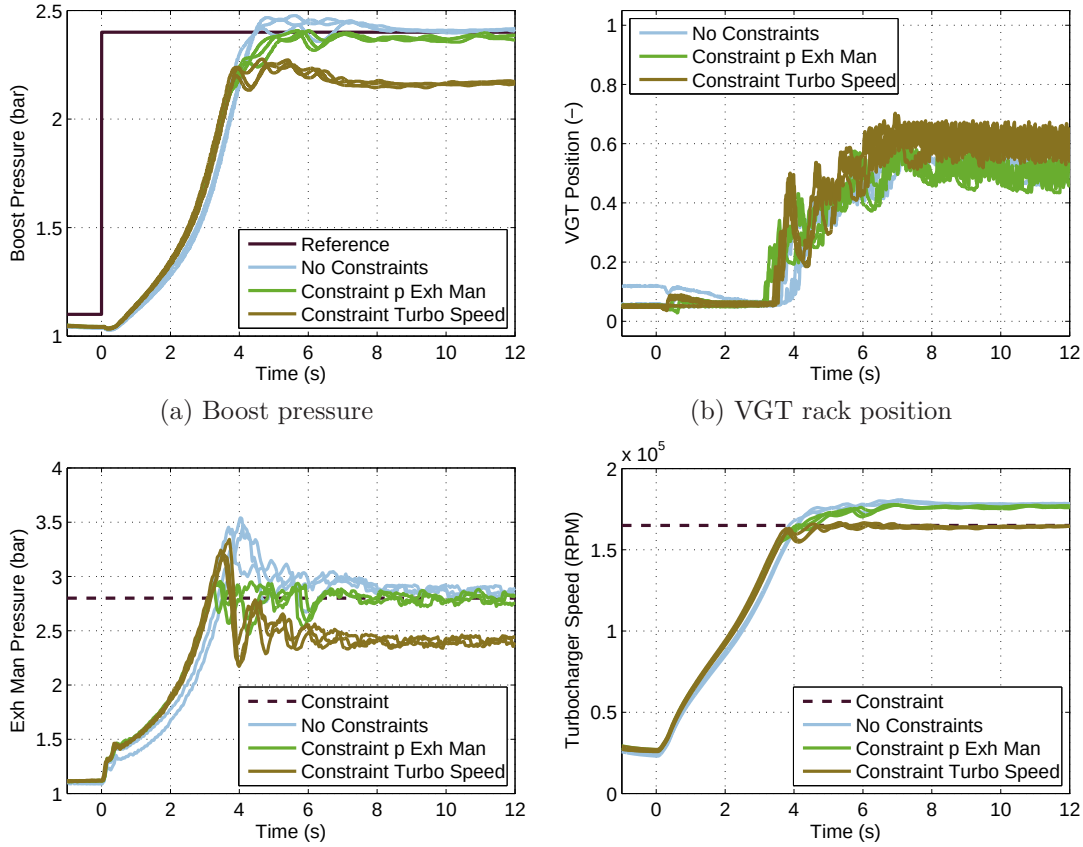

(a) Boost pressure

(b) VGT rack position

(c) Exhaust manifold pressure

(d) Turbocharger speed

Figure 3.20: MPC ensuring the operation of the engine within imposed constraints.

When the turbocharger speed limit was introduced, a more severe impact on the achievable boost pressure was observed. The maximum of 165 000 RPM allowed for delivering only about 2.2 bar of intake manifold pressure. Again, the MPC controller was able to satisfy the imposed constraints.

3.5 Summary

In this chapter, a systematic procedure was used to assess the closed-loop performance of a standard Diesel EGR/VGT air-path system. The standard transient response was discussed and some difficulties of transient measurements were considered.

The system including the plant and the control requirements during tip-in manoeuvres was then discussed from a control perspective. In order to satisfy the imposed requirements the MPC control framework was selected.

The controller builds on a relatively simple Model Predictive Control formulation and uses a prediction model based on the well studied family of Mean Value Engine Models. This technique was initially evaluated in simulation environment to show that it can deliver close-to-optimal performance and ensure operation within physical limits. In this way 1D physical modelling, MVEMs and MPC can be combined to quickly investigate the achievable performance of a particular air-path configuration whilst retaining high fidelity simulation results to support design decisions. This approach is used in the next chapter for assessing various boost assist options.

Moreover, the implementation of a discussed controller for Real-Time engine testing was presented. This required some attention to account for the characteristics of the VGT actuator and of the applied measurement system. The experiments confirmed both that the MPC can be used for Real-Time testing of the engine transient performance and that during such tests it can satisfy the imposed physical constraints.

Chapter 4

Boost assistance systems and BREES

A relative lack of "bottom-end" torque has always been an important issue for turbocharged engines (both spark and compression ignition) and has prompted significant research and development into basic turbo-machinery performance as well as innovative systems to increase torque at low engine speed. The desire to mitigate turbo-lag and operate the turbo-machinery under more favourable conditions has led to widespread adoption of VGTs in Diesel engines. The higher temperature of the exhaust gas in SI engines results in significantly more severe requirements on the properties of the turbine material and makes VGTs less popular in this type of engine. Mechanical superchargers are very effective in improving the transient performance, but suffer in terms of their impact on brake specific fuel consumption and cost. Some manufacturers have introduced lightweight materials to overcome the problems associated with turbocharger inertia, as well as more complex solutions involving multiple compressor and turbine stages, and electrical assistance (see section 1.4 for a brief review of these technologies).

In this chapter, the engine simulation model, the engine test rig and control tools developed in the previous chapters are utilised to investigate boost assistance systems. First, the effectiveness of several concepts based on compressed air and electrical assistance are evaluated in simulations. For this purpose the 1D engine model was modified to include compressed air injection ports and an ideal

electrical assist, i.e. additional torque available at the turbocharger shaft with no impact on its inertia. The MPC controller was then employed to assess the transient response improvement offered by each of the options considered. Further study revealed how these improvements depend on the available resources and system parameters. Injecting the compressed air into the exhaust manifold was found to be both an effective and rarely considered method.

The exhaust manifold assist was then verified experimentally on the engine test rig described in section 2.2. The air was supplied from a workshop reservoir. MPC was used to control the modified air-path automatically coordinating the VGT position and the assist valve. In this way, the effectiveness of the exhaust manifold assist was confirmed. Calibrating the MPC with various weightings on the assist valve actuation and modifying the compressed air supply pressure enabled parametric studies of the investigated system.

Finally, a concept for charging the compressed air tank during braking and providing assistance during acceleration was developed and implemented in the test cell. It was shown experimentally that the benefits of exhaust manifold assist can be realised with a limited number of additional components and with only minor changes to engine operation. This study used a simple control algorithm, which can be easily implemented on the existing ECU. The chapter finishes with a discussion of opportunities and challenges to practical implementation of such a system.

4.1 Simulation-based assessment of boost assist systems.

Two possible types of boost assistance are considered here: electrical torque assistance directly to the turbocharger shaft and compressed air assistance. Both Turbocharger Electrical Assistance (TEA) [Arnold et al., 2005],[Ibaraki et al., 2006] and air-assistance schemes have been previously presented in the literature.

An illustration of the engine configuration along with the assistance methods considered in this work is shown in Figure 4.1.

The effect of the electric assistance was incorporated by assuming some addi-

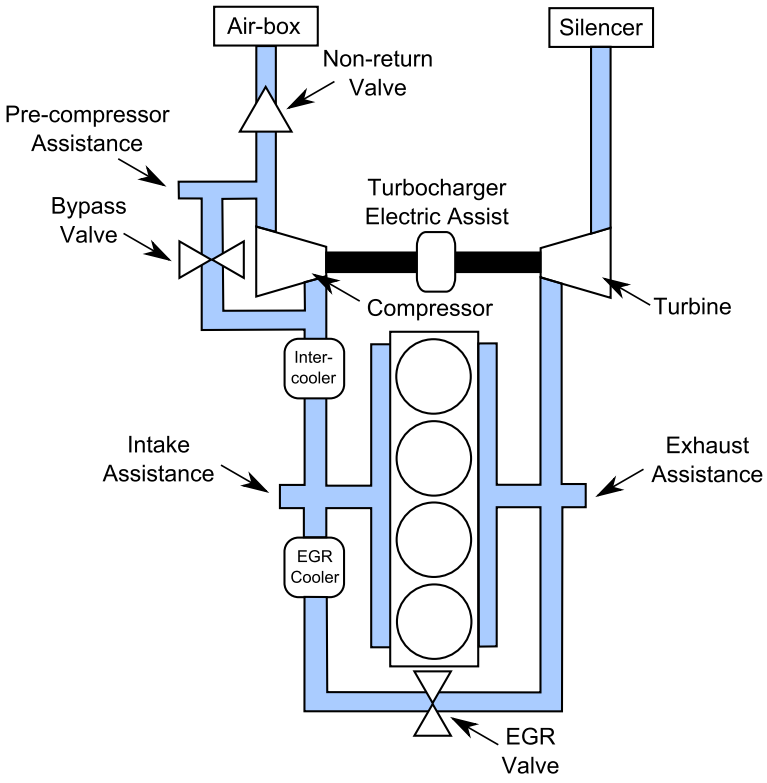

Figure 4.1: System layout illustrating the boost assistance methods.

tional torque available at the turbocharger shaft up to a given maximum power. The additional torque took values up to 0.32 Nm and the total power ranged between 1-3kW. These assumptions are consistent with the values in [Ibaraki et al., 2006], [Pfister and Perriard, 2010], [Noguchi et al., 2007], [Tavcar et al., 2011]. Compressed air assistance was simply the addition of air at some point in the engine's air-path. The simulation model was set up for air-assistance in three locations: before the compressor, directly into the intake manifold (after the compressor) and into the exhaust manifold. To allow air to be injected before the compressor a non-return valve was added between the air-box and the pre-compressor volume. Air was assumed to be available from a reservoir at 3 bar and 300K. At this stage the focus was on the relative performance benefit that could be achieved rather than on the implementation of the additional hardware required for these assistance options.

The discussion of the results starts with some comments on the control system performance to demonstrate that it gives sensible behaviour. The remainder of this section is focused on the investigation of the proposed boost assistance methods.

4.1.1 Control system verification

The aim of this study is to compare the performance of four different boost assistance options. As the overall system performance depends on both the physical components and the control system, it is desired to have a single control method that delivers close to optimal performance for all the considered configurations. If this can be achieved, concerns about the influence of controller calibration can be minimized.

Both the calibration effort and the control system performance were found to be satisfactory when using the MPC approach. The main controller design choices include the selection of appropriate control and prediction horizons, as well as weighting penalties on the control effort and tracking performance. For each engine configuration a single controller setup was sufficient for all operating points encountered during the tip-in manoeuvre without any need for parameter scheduling.

The MPC setup explicitly includes the constraints on the actuators: VGT and assistance valves can only take values between fully open and fully closed. The intake manifold pressure is the only controlled variable in this application. It is not possible to achieve the demanded steady-state pressure immediately after the driver requests full load due to various characteristics of the air-path including the compressor surge limit, the smoke limit on air-fuel ratio and the dynamics of the air system. Nevertheless the general objective during this phase is to increase the mass of oxygen entering the cylinders as quickly as possible to allow the maximum fuel injection (and therefore torque).

In practice it is necessary to ensure there is some margin between the intake manifold pressure and the surge limit. If the surge limit is approached too closely, instability can be observed as any drop in the boost reference value causes the flow to fall, thus resulting in an even greater drop in the reference value. In this

study the controller weights were selected to avoid operating in this region.

The phase of the transient, when the controller is used to match a desired steady-state boost demand value, is significantly simpler. The compressor now operates further from the surge line and by selecting an appropriate penalty on the inputs it is possible to ensure that turbocharger assistance is not used unnecessarily at steady-state.

Figure 4.2a shows the reference intake manifold pressure, actual pressure and surge limit. During the first stage it can be seen that the boost pressure rises and closely follows the surge limit. To achieve this close tracking it is necessary to apply an increasing amount of assistance (in this example adding the compressed air to the intake manifold) as shown in Figure 4.2b. In the second phase of the transient, the constant level of boost can be achieved without any assistance and in fact requires VGT to be opened to avoid over-boosting.

The actuator positions show that the MPC controller gives the behaviour that might be expected: it reduces the level of assistance and gradually opens the VGT, and the coordination of the actuators gives minimal overshoot at the transition between the two stages.

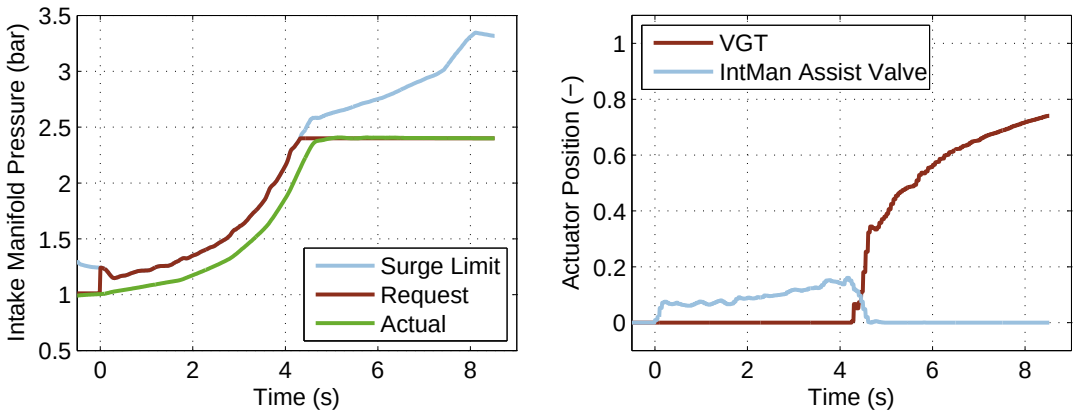

(a) Boost control

(b) Coordination of actuators

Figure 4.2: Controller verification.

Boost Assistance Method	Acceleration Time (s)
No assist	8.70
Intake manifold air-assist	8.40
Exhaust manifold air-assist	7.54
Turbocharger electric assist	7.49
Pre-compressor assist	6.16

Table 4.1: Acceleration times for each of the five engine configurations.

4.1.2 Comparison of boost assistance options

The maximum achievable performance from the four assistance methods is now evaluated using the 1D model. The obvious baseline for the results is the performance of the standard engine. Figure 4.3a shows the compressor map operating points during a full-load acceleration for each of the engine configurations considered. When no assistance is used, there is a significant gap to the surge line and it is this gap that leaves open the opportunity for boost assistance to improve the transient torque response. The exception is pre-compressor air-assistance as this approach effectively bypasses the compressor during the transient. For all the other boost assist options the compressor surge line is the limiting factor on the engine's transient performance.

For pre-compressor air-assistance, the surge line does not limit performance at all. The combination of a non-return valve and compressor bypass valve means that the pre-compressor pressure rises as well as the post compressor pressure. As a result the compressor pressure ratio is negligible. The system's performance is therefore determined in this case by the filling/emptying dynamics of the pre and post compressor volumes and the intake manifold pressure constraint. However, this scenario can be considered unrealistic because it requires the entire air flow to the engine to be delivered from the assistance reservoir. It is nevertheless useful to include this scenario in the results as it represents an upper limit on achievable transient performance from boost assistance.

Figures 4.3b and 4.3c show the simulated full load acceleration response of the engine. The resulting acceleration times from the initial engine speed to 2750

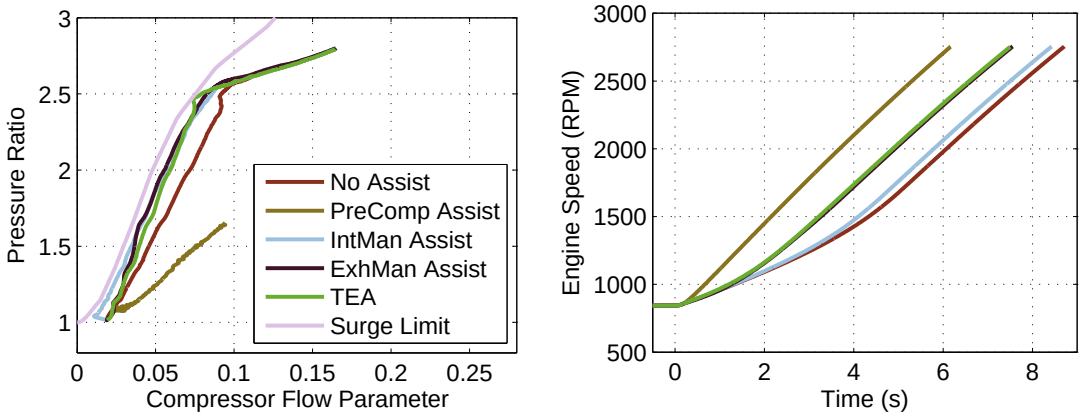

(a) Compressor operation

(b) Engine speed

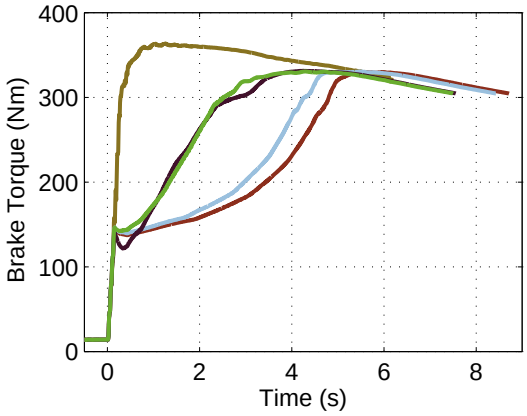

(c) Brake torque

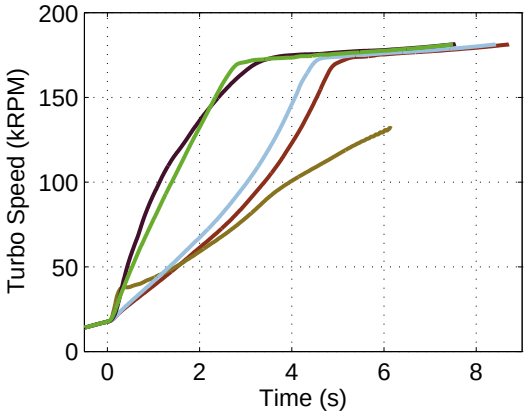

(d) Turbocharger speed

Figure 4.3: Comparison of maximum achievable improvements with various boost assist options.

RPM are given in Table 4.1. In the unassisted case, torque can be seen to rise very rapidly after the initial increase in driver demand (up to the smoke limit), however this is then followed by a much slower rise in torque while the turbo speed and pressure ratio across the compressor increase.

The turbocharger electric assist (TEA) and the exhaust assist show similar level of performance as they both increase the turbocharger speed as fast as possible subject to the constraint imposed by the surge limit. The intake assist method is also limited by the surge line, however because it does not spin up the turbocharger as quickly (see Figure 4.3d) and reduces the flow through the compressor, the response is significantly slower than those for the exhaust assist

and electric assist methods.

4.1.3 Relative merits of compressed air based options

The exhaust manifold compressed air assistance has been shown to significantly outperform the intake air assistance. This result may seem counter-intuitive and is therefore examined in more detail. To keep the comparison fair the results from simulations that used the same quantity of injected air: 0.02 kg, are considered.

When using exhaust manifold assistance, the injection of the compressed air results in a higher pressure ratio across the turbine. This increases the mass-flow (and enthalpy) of the gas flowing through the turbine, resulting in a higher turbocharger shaft torque, and therefore, a higher turbocharger acceleration rate. As the turbocharger shaft speed increases, the compressor generates a higher mass-flow which gives a corresponding increase in the intake manifold pressure. The fact that the exhaust manifold assistance manifests itself via an increase in the turbocharger shaft torque explains the similarity in the achievable performance when compared to electric assistance.

In the case of intake manifold assistance, at the beginning of the tip-in manoeuvre the injection of compressed air leads to an increased pressure ratio over the compressor and a reduction of compressor flow (see Figure 4.4a). The compressor operating point is therefore moved closer to the surge limit. As the turbocharger accelerates, air can be injected at higher rates, but the overall engine performance is significantly worse than in the case of exhaust manifold assistance.

Another interesting feature of the exhaust manifold assistance scheme is its influence on the brake torque. The rapid increase in exhaust manifold pressure leads to both an increase in pumping losses and a reduction in volumetric efficiency. This is particularly noticeable at the very beginning of the tip-in manoeuvre and can be observed in Figure 4.3c. Over the first few hundred milliseconds, the brake torque is significantly lower than in the other cases, which may have a negative effect on driver perception of vehicle response.

Finally, the effect of exhaust manifold assistance on the exhaust gas temperature must be considered due to its influence on correct operation of the after-treatment system. The compressed air reservoir in these simulations is assumed

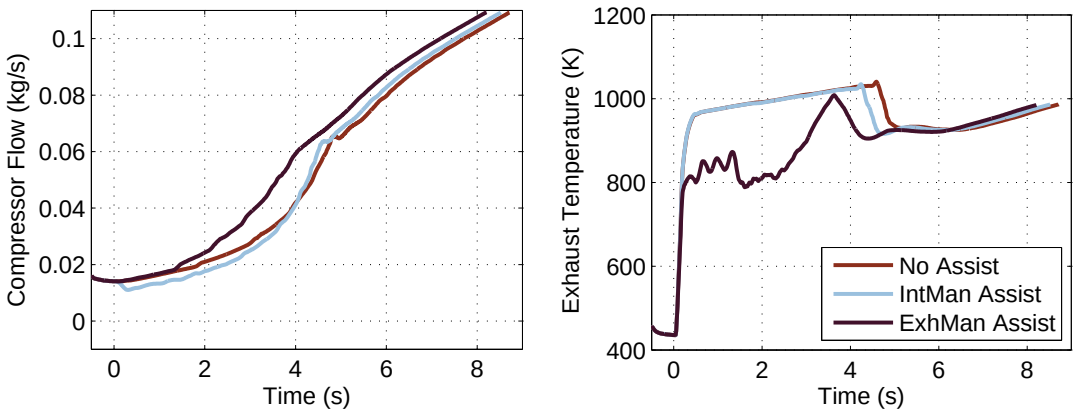

(a) Compressor flow

(b) Exhaust temperature

Figure 4.4: Relative merits of intake and exhaust manifold compressed air assist.

to contain gas at 300 K and therefore the use of exhaust manifold assistance will lead to a reduction in the exhaust gas temperature. For the transient simulated here it can be observed (Figure 4.4b) that the effect is not sufficiently large to raise immediate concerns over applicability of the method.

4.1.4 Usage of resources

For all of the boost assistance methods it is important to consider not just the ultimate performance improvement possible but also how much resource (e.g. mass of air at a certain pressure or electrical work performed with an available power) is required for a given level of performance. To help in this assessment it is necessary to define a measure for the transient performance. Various time-based metrics can be found in the literature [Arnold et al., 2005], [Ibaraki et al., 2006], [Tavcar et al., 2011]. Here the rise time from the initial brake torque value up to 90% of the full load value is used.

For the compressed air assistance methods, the quantity of air used can be adjusted by modifying the penalty on the assistance actuator in the MPC formulation. The assistance air flow is then integrated over the entire transient manoeuvre to give the mass of injected air. It is noted that this setup is not equivalent to optimising the performance over the entire tip-in manoeuvre subject to a constraint on the total amount of available air. Nevertheless the results

presented here do provide some insight into how efficiently the air from the reservoir is used in the cases of intake and exhaust assistance.

Figure 4.5 shows the results of simulations for several magnitudes of the assistance actuator penalty as well as two reference levels. The lower reference value is the torque rise time calculated for the pre-compressor assistance and can be considered as the upper limit of the achievable performance. A second reference level is shown representing turbocharger electric assistance with the torque limited to 0.16 Nm and the power limited to 2 kW. The first points for each assistance option, at the far left of the figure, correspond to a very high penalty and therefore negligible assistance. In subsequent simulations, the penalty is progressively reduced until the controller begins to open the VGT (to prevent the violation of the surge limit) thus wasting the assistance resources.

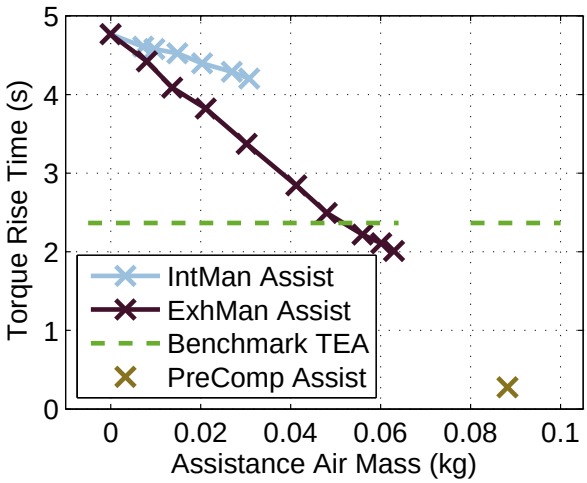

Figure 4.5: Performance achieved with varying levels of compressed air assistance.

This exhaust air assistance allows a significant improvement in transient performance, reducing the torque rise time down to just 2 seconds; whereas the lowest possible torque rise time in the case of intake manifold assistance is about 4.2 seconds. A more interesting observation is the fact that for any given quantity of assistance air, exhaust assistance will deliver a greater improvement in performance. Finally, it can be seen that the electric torque assistance benchmark can be matched by exhaust manifold assistance if 0.05kg of air is used.

For the electric torque assistance case it is appropriate to consider the resource usage slightly differently. The upper limit on the available electric motor torque is explicitly included in the controller setup and was varied between 0-0.32 Nm. In addition, the total power from the electric motor was limited to 1, 2 or 3 kW in the simulations. This range of options was motivated by the designs reported in the literature [Arnold et al., 2005], [Ibaraki et al., 2006], [Pfister and Perriard, 2010], [Noguchi et al., 2007], [Tavcar et al., 2011].

It can be seen in Figure 4.6 that a significant improvement in performance can be obtained even with a 1 kW machine. The 2 kW machine offers a further increase in performance, but the 3 kW motor gives very little additional benefit. Similarly, increasing torque initially has a dramatic effect on transient performance, but levels above 0.2 Nm see diminishing returns. This can be explained by the fact that once the system becomes limited by the compressor surge line, no use can be made of additional power or torque. Other results found in the published literature are consistent with trends observed here and following [Arnold et al., 2005], it is envisaged that higher power electric assistance motors would be required for engines with higher swept volume (which are equipped with the turbochargers of higher inertia).

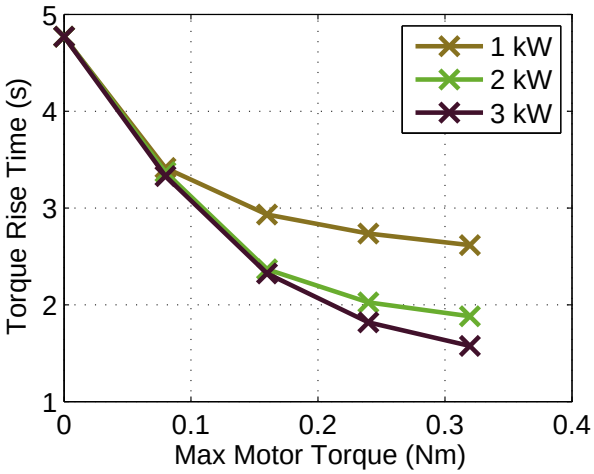

Figure 4.6: Tip-in performance for different electric motor characteristics.

4.1.5 Practical considerations

Using any of the boost assistance schemes will incur a cost and weight penalty due to the additional hardware required. All of the air-assist methods would require a reservoir of air. The intake air assist system would be simplest to implement, requiring only a control valve to allow air into the relatively cool intake manifold. Exhaust assistance would likely have increased costs as the additional hardware would need to cope with the high temperatures in the exhaust manifold. Pre-compressor assistance avoids the high temperatures but necessitates the addition of non-return and bypass valves. Turbocharger electrical assistance would most likely require some alteration to the vehicle's electrical system such as larger or separate batteries and possibly a larger alternator. As with any new vehicle system, considerable expense and effort would also be required to ensure the long term durability and lifetime costs associated with the new hardware.

It is also important to note that while all of the systems provide an improvement in performance in the 3^{rd} gear acceleration simulated, 3 of the 4 assistance methods would make relatively little difference in other important driving situations. This is because performance with assistance systems (after compensating for turbo lag) is essentially limited by the surge limit of the compressor. Therefore in slower transients, such as higher gear accelerations or when lugging a heavy load, these boost-assist schemes can offer only a small improvement on the standard engine performance, even for short bursts. Further improvement would require shifting the surge limit to the lower flows and some work in this area has been recently reported in [Ibaraki et al., 2012]. The only method out of the 4 considered that could significantly boost the steady-state performance at low engine speeds is the pre-compressor air-assistance method, however the quantity of air required would likely be prohibitive.

A final consideration for the exhaust assist method is the effect on the after-treatment system. The addition of cold air on the exhaust side will cause the temperature of the catalyst to drop, potentially deactivating it. The results of these simulations indicate that for all the exhaust assist cases the catalyst temperature will not drop below acceptable levels.

4.2 Experimental verification

This section presents the experimental verification of the transient response improvement offered by injecting compressed air into the exhaust manifold. During the conducted tests the engine was controlled with the MPC formulation based on consecutively linearised Mean Value Engine Model (MVEM) as described in 3.3.4 and 3.4. The algorithm was implemented in C code and executed on a rapid prototyping hardware. The main benefit of the MPC approach in this case lies in the simultaneous coordination of multiple actuators to ensure the boost reference tracking. Furthermore, once a suitable MVEM is available, the calibration effort of such a controller is significantly reduced in comparison to more conventional approaches. As discussed earlier, the considered MPC formulation requires relatively high computational power and does not explicitly address the controller robustness with regard to closed loop stability and performance. Therefore, the technique discussed is primarily aimed to be a systematic methodology for hardware evaluation in a laboratory environment.

The turbocharger assistance was provided by compressed air injection into the exhaust manifold via an additional gas fitting (see Figure 4.7). The rate of injection was modulated using a controllable valve. For this purpose a standard Diesel EGR valve with position feedback was used. A Proportional Integral (PI) controller with a pre-emptive offset was implemented for a low-level valve position control. The valve suffered from a minor leakage during fully closed position and a considerable pressure ratio dependent hysteresis (see Figure 4.8). Such characteristics affected the achieved accuracy of the valve control.

The practical aspects of collecting and storing the air are not considered at this stage. The air was supplied from a workshop reservoir and regulator used to maintain the working pressure.

The results of the tests performed with the described setup are divided into the following three sections. Firstly, the boost pressure control in the case of standard engine and that with exhaust manifold assistance are compared. Next, the transient torque performance improvement offered by compressed air assistance is assessed. Finally, the effectiveness of such assistance as a function of the quantity of injected air and the pressure of the air supply is investigated.

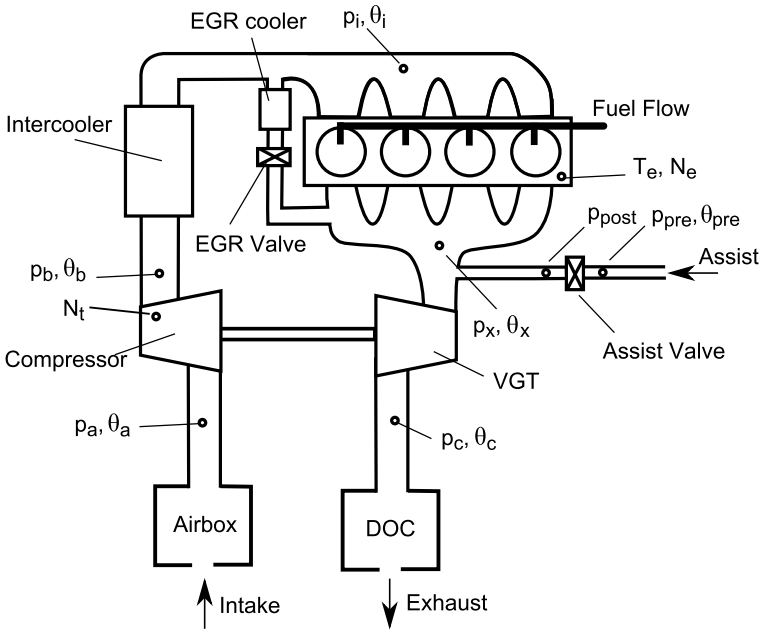

Figure 4.7: Additional port and instrumentation for experiments with compressed air injection.

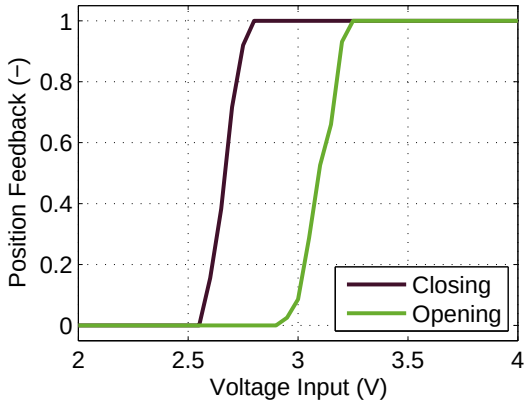

Figure 4.8: Hysteresis of the assist valve.

4.2.1 Assessment of transient response with boost assistance

The improvement in transient torque delivery offered by the compressed air assistance is shown in Figure 4.9a. It is observed that the level of brake torque in the conventional configuration was significantly limited during the first 4 seconds after the tip-in. As it was previously discussed, this behaviour was caused by the limitation of the fuel injection due to the smoke limit. During this period the VGT actuator remained saturated and the air delivery was affected by the turbo-lag effect.

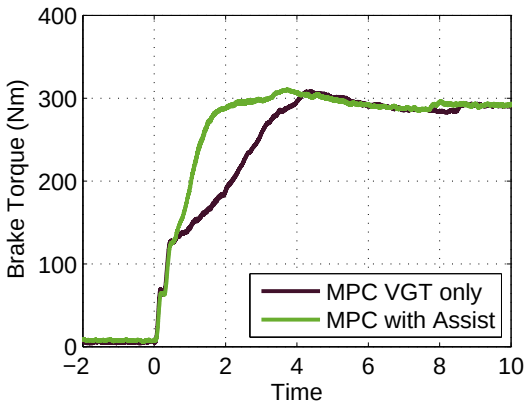

(a) Brake torque

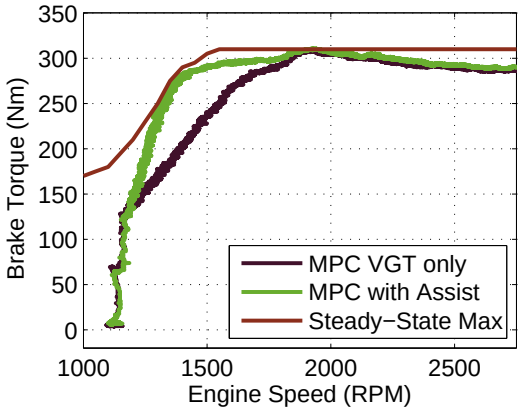

(b) Engine operating points

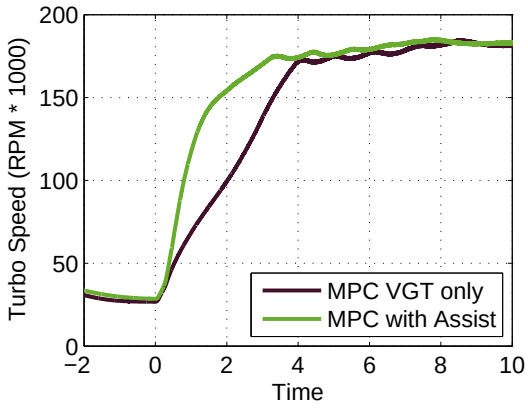

(c) Turbocharger speed

Figure 4.9: Recorded improvement in transient response.

The compressed air assist improved the engine response significantly. The

recorded brake torque rose sharply up to ∼90 % of its maximum value, which was achieved within 2 seconds. At that moment the engine speed was 1350 RPM (as shown in Figure 4.9b). Comparing this result to the steady-state characteristics of the engine, it is observed that during the transient with assistance enabled the maximum steady-state torques were matched from significantly lower engine speeds.

The improvement during the tip-in manoeuvre was possible because of increased quantity of intake air. The reason behind this enhancement can be deduced from Figure 4.9c, where the turbocharger speed is presented. As a result of the increased exhaust manifold pressure, the turbocharger accelerated immediately and quickly achieved the speed required to overcome the smoke limit. The amplitude of the post-compressor pressure oscillations during assisted operation was not higher than in the standard case and therefore it was deduced that compressor surge was avoided.

4.2.2 Boost control of engine with assistance

Injecting the compressed air into the exhaust manifold enables an improved tracking of the reference boost pressure during 3^{rd} gear tip-in manoeuvre. A comparison of boost pressures and actuator positions recorded during a non-assisted and assisted operation is shown in Figure 4.10. The two tests used the same weightings on boost pressure tracking error and VGT actuation. In the case of assisted operation, both the absolute position of the assist valve and its rate of change were penalised.

With the assistance enabled, the boost pressure rose significantly faster than in the non-assisted case. The biggest difference was observed in the first phase of the transient. During both tests the recorded VGT positions were very similar in spite of slightly different initial positions. Figure 4.10c shows how the assistance valve was actuated during this test. A sudden increase in injection was recorded immediately after the tip-in. It peaked after about 0.5 second and was then progressively withdrawn. Once the demanded boost pressure was achieved, the assist valve was closed and the VGT started to open to control the pressure around its set-point.

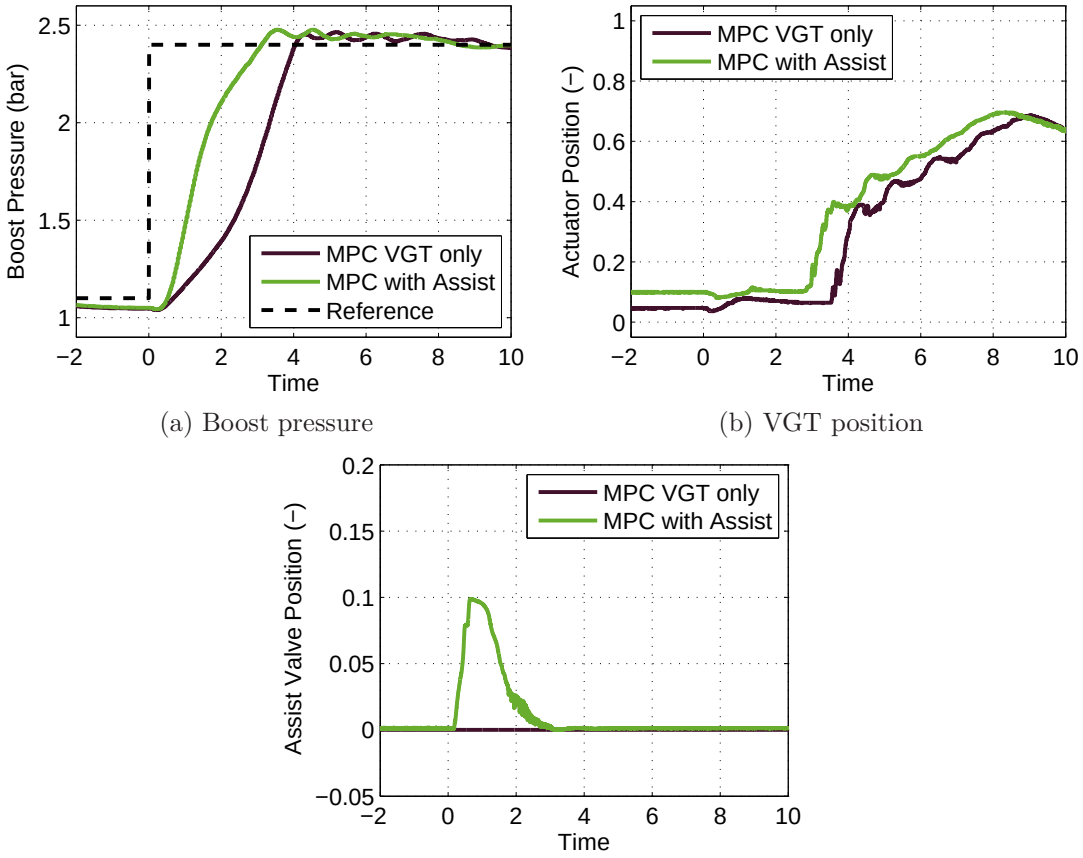

(a) Boost pressure

(b) VGT position

(c) Assist valve position

Figure 4.10: Comparison of boost pressure control under various scenarios.

The performance of the low-level assist valve control is shown in Figure 4.11a. The MPC demand was to abruptly open the valve immediately after the tip-in and then phase it out gradually from 0.5 seconds. The valve opened reasonably quickly, but remained open more than desired. For this reason the obtained transient response cannot be treated as optimal for the amount of air injected during the test. Another interesting plot is shown in Figure 4.11b. The supply pressure is observed to drop slightly during the injection period. This was due to the dynamics of the installed compressed air supply system.

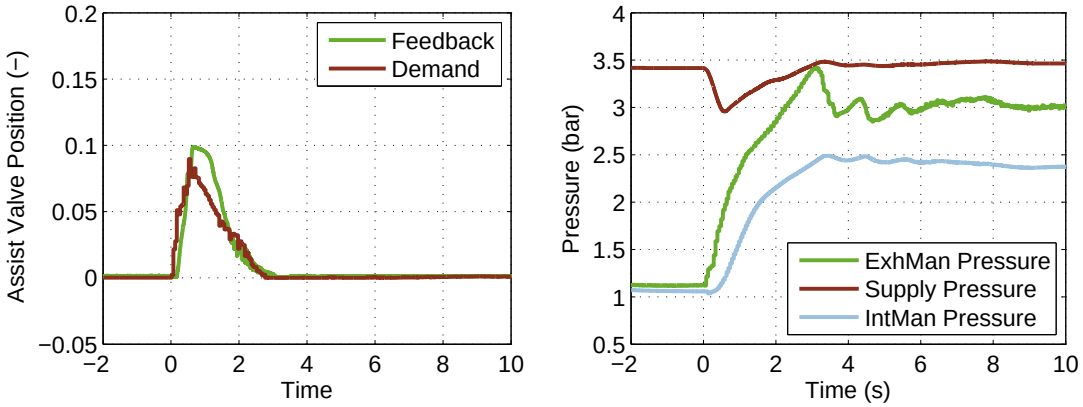

(a) Assist valve control

(b) Air-path pressures

Figure 4.11: System operation with compressed air assistance.

4.2.3 Assistance effectiveness

The effectiveness of the assistance for various quantities of injected air and compressed air supply is now investigated. The engine tests were repeated for three different set-points of the pressure regulator in the compressed air supply: 2.5, 3 and 3.5 bar. Similarly to the simulation-based assessment, the quantity of the injected air was not directly controlled. Instead, for various runs the weighting on the assist valve position in the MPC cost function was modified. Therefore, in a strict sense this procedure does not optimise the performance of the engine for a given quantity of air.

The mass of the injected air was calculated integrating the estimated flow through the injection valve. The flow, in turn, was calculated using the standard orifice equation, measured pressure ratio across the valve and the experimentally determined relation between the valve position and its effective area.

As the first measure of the response improvement, the acceleration time from 30 to 80 kph in 3^{rd} gear is considered. The results are shown in Figure 4.12. As expected, a higher pressure in the supply allows for increased benefits in engine response. Injecting even a significant mass of air at the pressure of 2.5 bar reduced the acceleration time by only 0.2 seconds. It can be deduced that to achieve significant improvements, it is more effective to inject a given amount of air for a shorter time, but at a higher pressure.

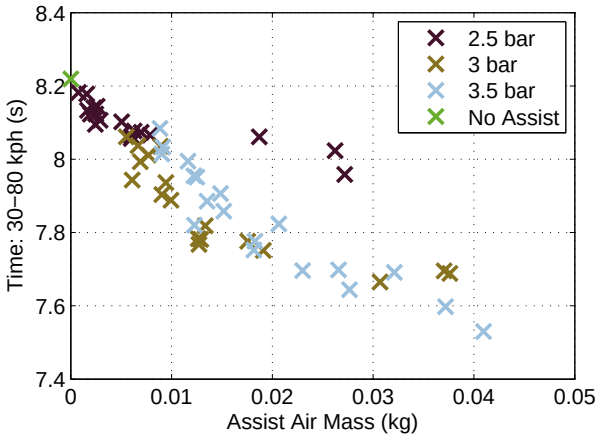

Figure 4.12: Time from 30 to 80 kph as a function of injected quantity of air.

A relative reduction in time-to-torque is a common metric for assessing the transient response. It is defined as:

$$\Delta t_{\%T,i} = \frac{t_{\%T,i} - t_{\%T,conv}}{t_{\%T,conv}} \tag{4.1}$$

with $t_{\%T,i}$ being the time it takes from the initial level of torque up to a given percentage of the final torque for an investigated configuration and $t_{\%T,conv}$ being the similarly defined time for a reference system. In this case, the reference response is that of the engine without boost assistance. Three levels of torque were considered for this study: 50, 70 and 90% of maximum torque. The corresponding plots are shown in Figure 4.13.

The analysis of the presented figures leads to the conclusion that the reduction in time to 50% of maximum torque is not significantly dependent on the pressure of air supply. The dependency is, however, visible in Figures 4.13b and 4.13c, where the improvements achieved with various supply pressures can be distinguished. These experimental results can be explained by the speed, up to which the turbocharger was accelerated in each case. The mass of air injected over a shorter period of time caused the turbocharger to spin up faster than the same amount injected over longer period of time. The turbocharger speed can be linked with the level of fuel injection via the smoke limit. Each of the considered supply pressures was sufficient to accelerate the turbocharger to quickly achieve

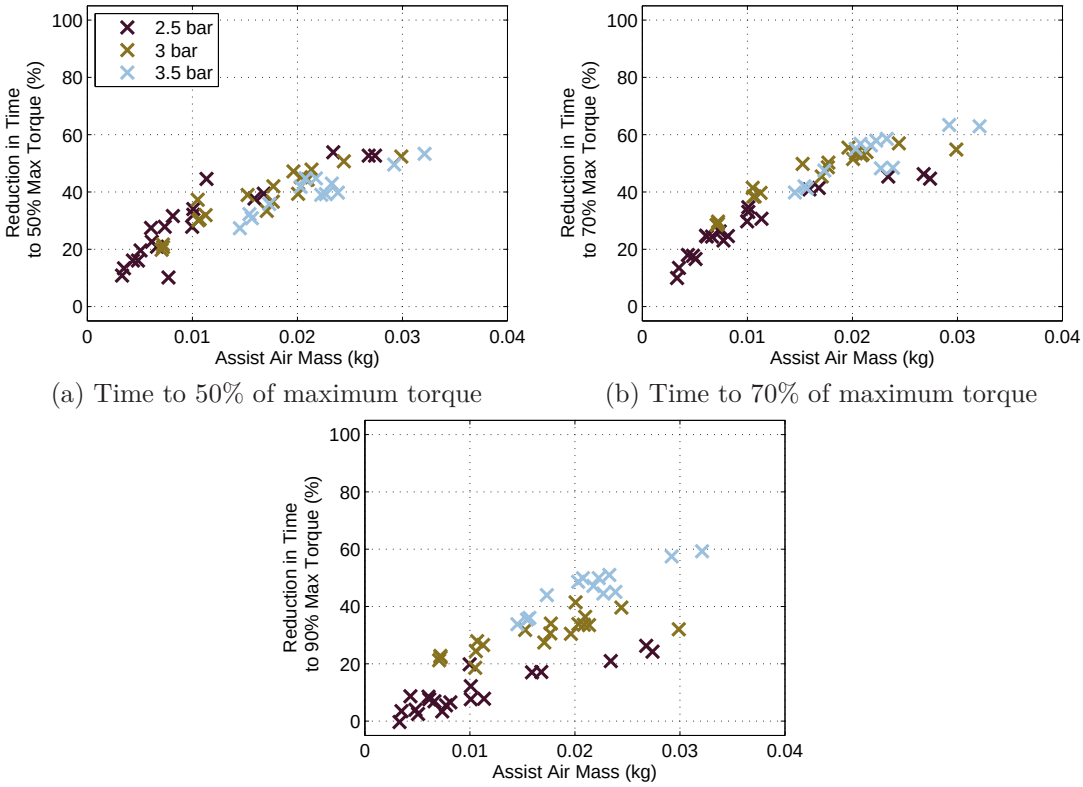

(a) Time to 50% of maximum torque

(b) Time to 70% of maximum torque

(c) Time to 90% of maximum torque

Figure 4.13: Sensitivity of improvements to compressed air supply parameters.

50% of the maximum torque and therefore no distinction is observed in Figure 4.13a. The 2.5 bar supply cannot accelerate the turbocharger sufficiently quickly to achieve the 70% of the maximum torque as fast as the other supply levels. Similarly, one needs 3.5 bar of supply to achieve 60% reduction in time to 90% of maximum torque.

Bearing in mind the differences between the simulation model and the actual engine as well as certain differences in the details of test setups, the simulation results previously shown in Figure 4.5 appear to be consistent with experimental findings. Very comparable levels of transient response improvement were found using the parametric study conducted using the 1D model and during engine testing. The amount of air required to achieve these improvements was considerably lower during experimental verification: 60% improvement was achieved with about 0.06 kg of air in simulations and only 0.03 kg during experiments.

Further simulations revealed that it was a difference in the initial engine speeds that caused the difference in the amount of required air: tip-in with 1D model started at 850 RPM, whereas the initial engine speed used during engine tests was 1100 RPM, below which the Dual Mass Flywheel protection was limiting the response.

In this way, the simulation-based assessment of system capabilities is confirmed to give realistic predictions of expected closed-loop system performance.

4.2.4 Conclusions

In this section, the experimental results confirming the effectiveness of injecting the compressed air into the exhaust manifold were presented. For this purpose the test rig was enhanced with compressed air supply to allow for investigating how various supply pressures affect the achievable benefits. The levels of considered pressures were selected to be within the range of pressures recorded in the exhaust manifold during normal engine operation. To control the engine with the compressed air assistance, Real-Time MPC implemented on the rapid prototyping system was used. The main benefit of this approach lies in the optimisation-based coordination of both available actuators: the VGT and the assist valve.

It was verified that the injection of the compressed air into the exhaust manifold is a very effective method of overcoming the turbo-lag. Such benefit was quantified for 3^{rd} gear tip-in manoeuvres. Improvements up to 60% reduction in time to torque accompanied by significantly and favourably modified torque delivery profile were recorded. The results also provided an insight into the dependency of expected benefits on assistance system parameters: supply pressure and the amount of injected air.

4.3 Realisation of compressed air assistance system

This section describes the implementation of a simple system which achieves both air storage and turbo assist. The concept was developed during internal discussions within the group involving Prof Nick Collings, Prof Keith Glover, Dr

Alex Darlington and Dr Paul Dickinson. In comparison to the concepts previously described in the literature, this system offers significant improvement in transient performance while requiring very limited additional hardware and simple changes in engine control.

The proposed concept is described here along with its implementation and the setup for experimental verification. Test results are then presented. The section finishes with a discussion of challenges facing a practical application of this concept.

4.3.1 BREES concept

The primary function of the proposed concept is to mitigate the turbo-lag effect in highly-boosted internal combustion engines. The desired outcome is to offer enhanced driveability of vehicles equipped with powertrains based on downsized SI or turbocharged Diesel engines. The BRaking Exhaust Energy Storage (BREES) concept is now explained based on a standard Diesel EGR/VGT air-path:

Assistance Phase: Improved transient performance is given by injecting compressed air into the exhaust manifold to accelerate the turbocharger in situations when low gas flow prevents achieving the driver's torque demand. During the injection it takes advantage of the fact that the engine block operates as a non-return valve (with the EGR valve closed). The amount of injected air is adjusted using a control valve. The position demand for the valve is based on the boost pressure tracking error, taking into consideration the prevention of the excessive pumping losses and respecting the upper limit on the exhaust manifold pressure and the compressor surge limit.

Charging Phase: During the engine overrun, when no fuel is injected and the transmission remains engaged, high pressure in the exhaust manifold is achieved by restricting the gas exiting from the manifold (in this application by closing the VGT beyond the standard end point). The composition of the pressurized gas is therefore virtually entirely air. In this phase, the controllable valve used previously for gas injection now permits the storage tank to be recharged.

To implement these functionalities only a compressed gas tank, additional exhaust manifold connection and a single control valve are necessary as shown in Figure 4.14.

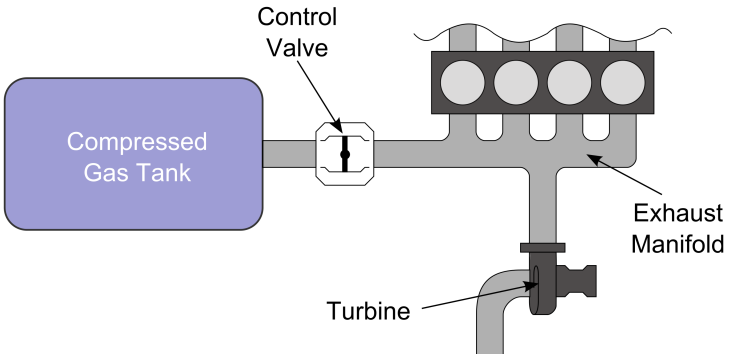

Figure 4.14: Compressed gas tank and control valve allowing for charging and assistance phases.

4.3.2 Implementation

The additional gas fitting (introduced for experiments described in the previous section) is now used to facilitate both the collection of compressed gas and injection to assist the turbocharger.

To generate higher exhaust back pressure during engine overrun, the end-stop of the VGT was moved to allow the vanes to shut somewhat more than in their standard calibrated configuration. A tank for collecting the compressed gas was taken from a portable air compressor with a non-optimised volume of 24 litres. Two solenoid valves (valve A sealing in the direction from the tank to the exhaust manifold and valve B sealing in the opposite direction) were used to control the flow of gas to and from the tank (see Figure 4.15).

The use of solenoid valves limits the actuation of the additional compressed air-valves to ON-OFF control. Basic control logic was used to open valve B for storage of the gas when the exhaust manifold pressure was greater than the tank pressure and no fuel was injected, with the maximum tank pressure for this study set to 3.5 bar. The VGT position demand during tank charging was set

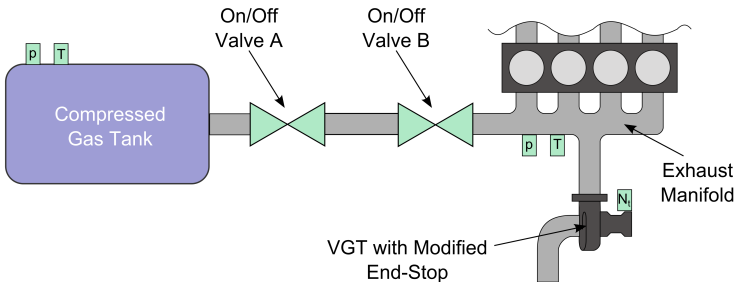

Figure 4.15: Implementation of the BREES concept on VGT equipped engine.

to close fully (subject to $p_x < 3.5$ bar). Similarly, during tip-ins valve A was opened at the start of the acceleration until the boost pressure demand was met or the pressure in the exhaust manifold was equal to that of the tank. During air-assisted operation the VGT position demand was limited to a level equivalent to the original end-stop position. An investigation of the influence of the VGT position during assistance and the maximum tank pressure can be found in the appendix B.

4.3.3 Test manoeuvre

The system collects compressed gas during braking for later use during a tip-in. Since turbo-lag is more pronounced in higher gears, a 3^{rd} gear test profile (defined in terms of the vehicle speed demand) was generated as can been seen in Fig. 4.16. The profile consists of a braking phase with a deceleration of 0.1g from an engine speed of approximately 2750 RPM down to 1150 RPM followed by a tip-in, where the simulated vehicle is accelerated as quickly as possible back to 80 kph ($\sim$ 2750 RPM).

4.3.4 Speed-load profile

To follow the test profile the engine was operated in closed loop, adjusting the position of the accelerator pedal and a simulated braking action based on the vehicle speed error. The resulting simulated vehicle speed profiles showing the engine transient capabilities are shown in Figure 4.16. There is no difference in the

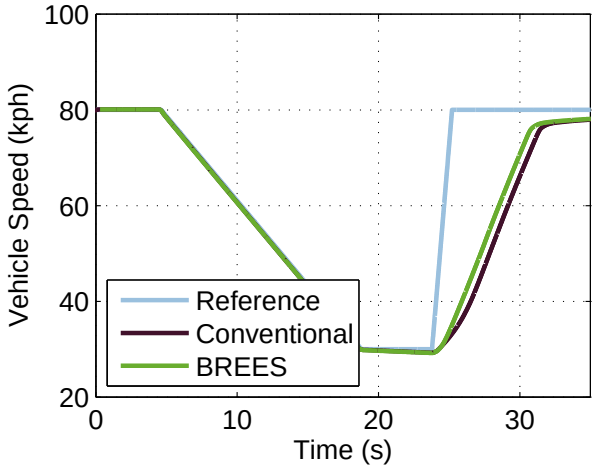

Figure 4.16: Test profile: in-gear braking and tip-in.

behaviour of the vehicle during the braking phase but a considerable improvement in the acceleration time is observed with BREES enabled operation.

The resulting engine speed-load profiles for the manoeuvre are shown in Figure 4.17. Considering the manoeuvre from the start, the engine goes through:

Deceleration: When the BREES system was enabled, an increased negative torque during the braking phase was measured due to the additional back pressure generated by the modified VGT end-stop.

Tip-in: In the case of conventional engine operation, a deficit in maximum torque is observed at engine speeds below 1500 RPM. The BREES system is seen to significantly increase the low-end brake torque, which rises sharply up to about 250 Nm by 1300 RPM. Above 1500 RPM the torque output from both systems is comparable.

4.3.5 Assisted acceleration

Time series data for measured shaft torque during the acceleration phase is displayed in Figure 4.18a. Both the conventional and BREES systems show similar behaviour up to 130 Nm, which corresponds to the smoke limit for the initial

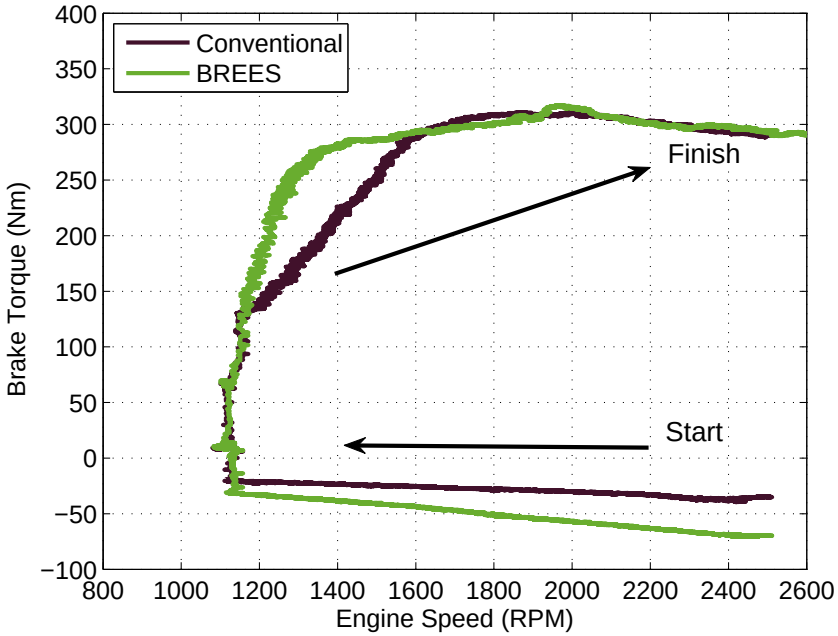

Figure 4.17: Engine speed-load profiles during the manoeuvre.

level of intake manifold pressure. After this point, the plot of the conventional configuration clearly shows the turbo-lag with its characteristic convex profile. In contrast, the BREES system can be seen to have a much sharper rise with a profile closer to that of a naturally aspirated engine, which should result in improved driveability characteristics.

The improvement in transient performance can also be evaluated using a time-to-torque metric. The reduction of time required to reach a certain level of brake torque with the BREES system is shown in Figure 4.19.

The improved acceleration of the turbocharger is the primary reason behind the faster torque delivery in the case of BREES enabled operation. Figure 4.18b shows the turbocharger speed during the transient. The plot confirms the effectiveness of exhaust manifold injection, which was enabled between 24 and 26 seconds. The system was able to rapidly accelerate the turbocharger, particularly over the first second when the pressure ratio of the storage tank to exhaust manifold was greatest. Accordingly, the significantly increased compressor speed

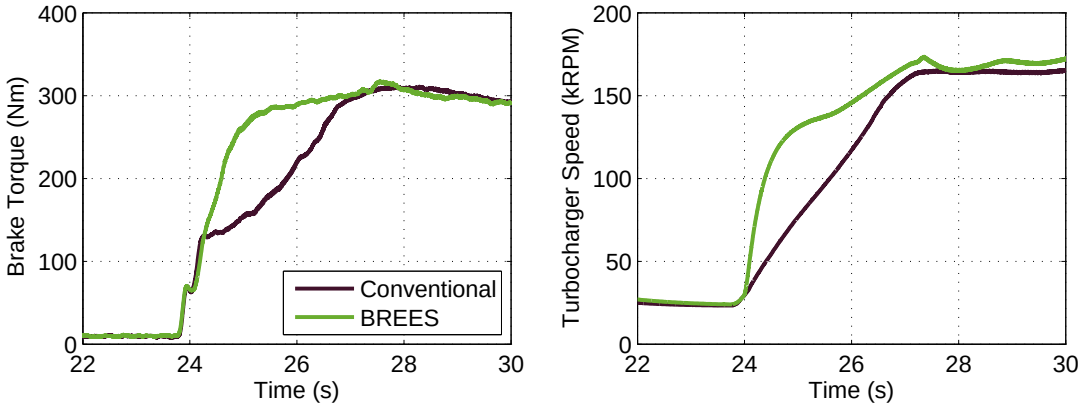

(a) Brake torque

(b) Turbocharger speed

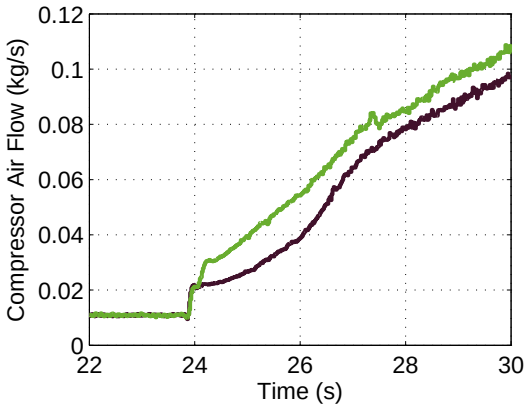

(c) Compressor air-flow

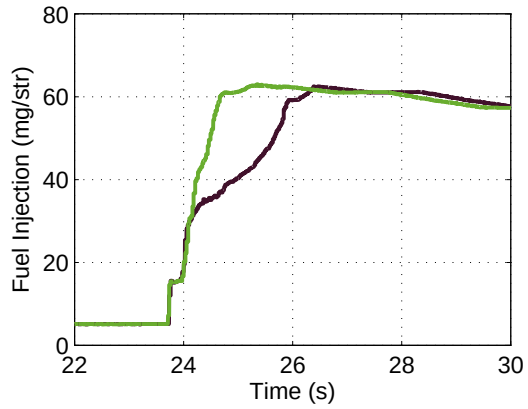

(d) Fuel injection

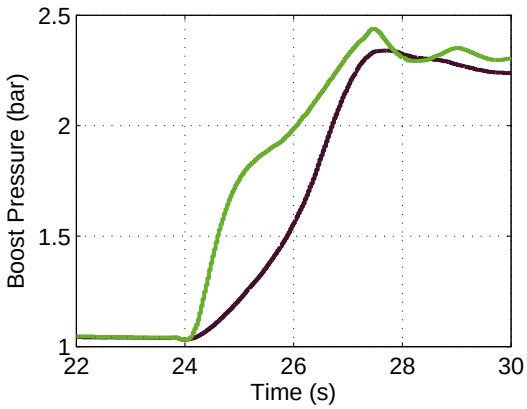

(e) Boost

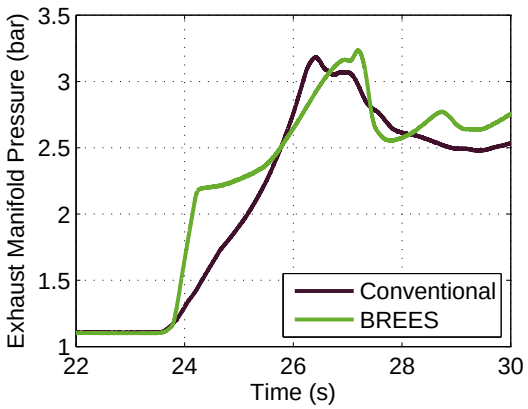

(f) Exhaust manifold pressure

Figure 4.18: Acceleration phase with and without BREES.

results in much higher intake air flow (see Figure 4.18c). This raises the intake manifold pressure and therefore, the mass of air entering the cylinders, thus al-

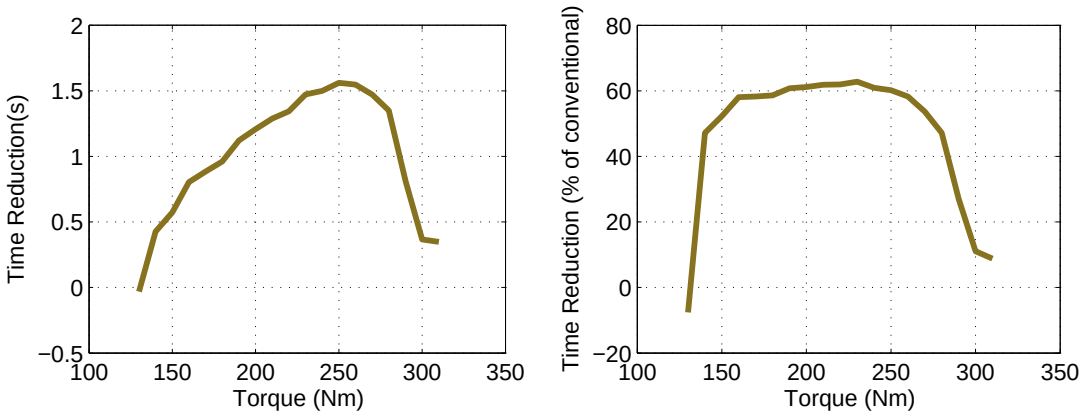

(a) Absolute (b) Relative

Figure 4.19: Reduction in time-to-torque.

lowing increased injection of fuel without violating the smoke limit (as shown in Figure 4.18d). In this way a significant improvement in transient torque is achieved. The effect of injection is clearly visible on the plot of the exhaust manifold pressure (see Figure 4.18f), where a sharp increase at the time of 24 seconds is observed. This contrasts with the plot for the conventional operation. The capability to reduce the time of generating high intake manifold pressures is verified in Figure 4.18e.

4.3.6 Air management

During the test manoeuvre considered, the compressed gas tank is charged during the braking phase and discharged during the tip-in. Figure 4.20 shows the recorded levels of pressure in the storage, intake and exhaust manifolds.

The initial pressure of gas in the tank was below 2.5 bar. During the engine overrun the VGT is controlled to close as far as possible, which results in an increased level of back pressure. The pressure in the exhaust manifold rises to almost 4 bar, which is sufficient to charge the tank up to 3.5 bar within only 2 seconds. The valves are then shut until the injection of air is required to assist the turbocharger. Starting at 24 seconds, the tank is discharged to the exhaust manifold over a 1 second period, dropping to a level below 2.5 bar. As a result the exhaust manifold pressure rises immediately to more than 2 bar, which causes

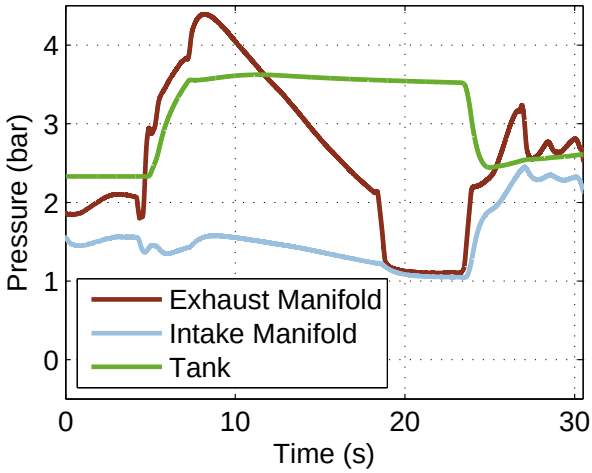

Figure 4.20: Tank, exhaust and intake manifold pressures during the manoeuvre.

the turbocharger speed to increase rapidly and generate higher intake manifold pressures.

Assuming an adiabatic expansion, using the ideal gas law and the measured conditions in the tank pre and post injection, the mass of injected air was calculated to be 0.027 kg. This value and the achieved reduction in time-to-torque are consistent with the experiments conducted using the compressed air supplied from the workshop reservoir (see Figure 4.13).

4.3.7 Practical considerations

The compressed gas stored in the tank consists almost entirely of air because it is collected only during engine overrun. Therefore, injecting this gas into the exhaust manifold during full load acceleration affects the reading from the UEGO sensor, which ceases to be indicative of the in-cylinder air fuel ratio (see Figure 4.21a).

For both the conventional and the BREES-enabled operation, immediately after the tip-in the fuel mass flow was increased up to the smoke limit. During the BREES transient, the reading from the UEGO was affected by the additional oxygen from the air injection. A model-based correction would be necessary to estimate the air-fuel-ratio if it was required during this phase of operation.

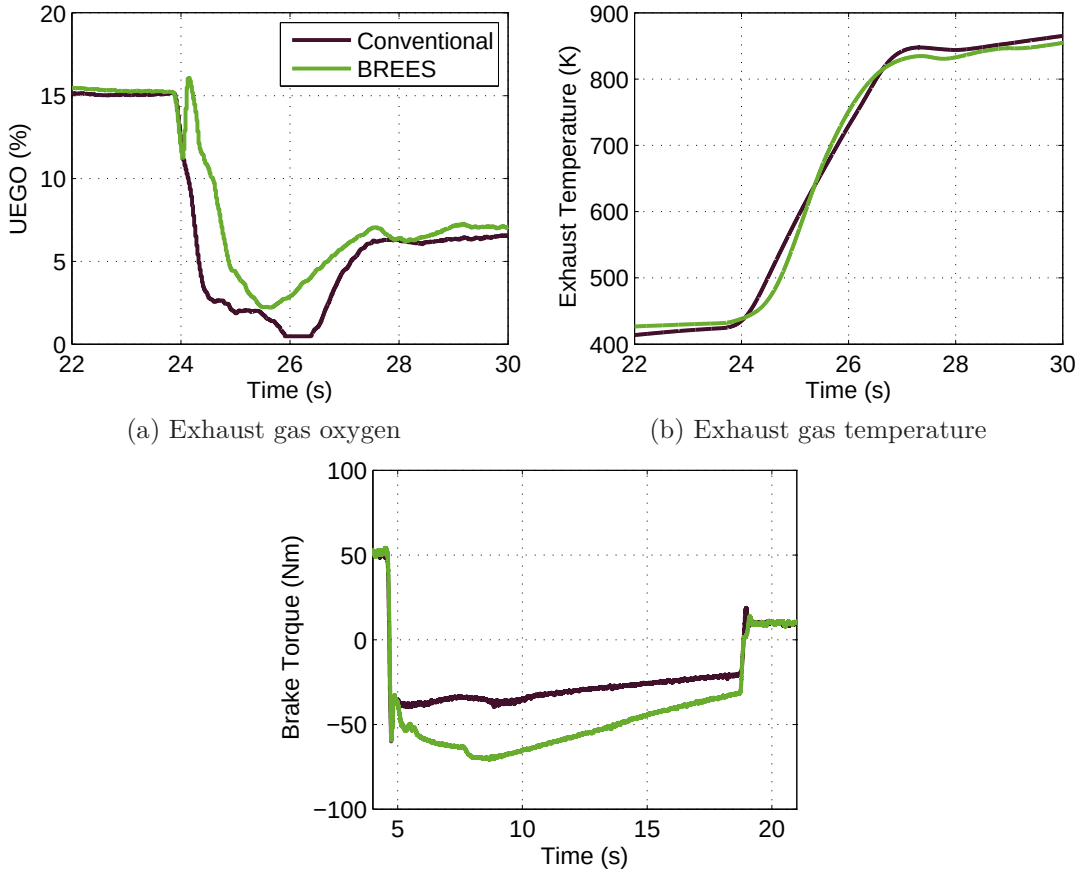

(a) Exhaust gas oxygen

(b) Exhaust gas temperature

(c) Engine braking

Figure 4.21: Secondary effects of the BREES system on engine/vehicle operation.

Data acquired during the tests indicated that the compressed air injection does not significantly affect the exhaust manifold gas temperature (see Figure 4.21b). A certain effect is, however, captured: it is observed that the initial build-up of the exhaust temperature in the case of BREES is slower than in the conventional mode. There are two potential reasons why only a small difference is observed. Firstly, the ratio of mass flow from the block is at least comparable to the air injection. Secondly, the temperature is measured with 1.5 mm K-type thermocouple, which has a poor bandwidth. The simulation environment is more suitable for such an investigation and results presented in the first section of this chapter (see Figure 4.4b) confirm the temperature of the gas flowing through the turbine is reduced from 1000 K to 800 K during the start of the transient

due to the addition of the cooler assist-gas. The increased mass flow through the engine into the exhaust quickly mitigates this effect. Nevertheless, compressed air injection affects the gas temperature for a short time and the impact of BREES on the durability of turbine should be assessed. The fact that the temperature does not actually drop, only its rate of increase is reduced, indicates that it is unlikely the turbine longevity would be significantly affected.

During the BREES-enabled operation, the low-end engine response is significantly improved. This means, however, that at low engine speeds the mechanical components of the engine (in particular the turbine, the dual mass flywheel, the crankshaft and others) are excited with loads of different magnitude and frequency characteristics than in the case of conventional operation. A detailed characterisation of these effects has not been pursued in this study.

An important challenge for the BREES system is the consistency of the engine performance. The presented results were generated with a 24 litre tank and a single braking manoeuvre charged the tank to a level that was sufficient for a single tip-in acceleration. The tank charging took only 2 seconds, but the clutch had to remain engaged during braking, which may be not consistent with individual driving practice. During acceleration the tank was discharged within 1 second. It is, however, observed that the most critical period is the first few hundreds milliseconds, when the mass flow is greatest and the injection time could be reduced.

It is also observed that moving the end-stop of the VGT to facilitate the tank charging changed the overrun characteristics of the engine (see Figure 4.21c). To ensure the consistency of the engine behaviour during overrun, one could adopt the same strategy of closing the VGT also for situations when the compressed air tank is already full. Another option could be to deliver a consistent vehicle behaviour by modulating the demand from the braking system. This approach has been investigated for electric hybrid vehicles with the capability of regenerative braking. Braking systems that are able to compensate for varying powertrain torque are known to be costly.

If the tank was charged only during braking, one could imagine a possible lack of repeatability during manoeuvres involving multiple tip-ins and no braking. However, charging may also be possible during low load operation. This action

would require an increase in fuelling quantity and change in VGT position. The control challenge here would be to make this imperceptible to the driver. One possible drawback of this strategy is that the proportion of combustion products stored in the tank would be significantly increased, which may be particularly important when considering condensation/freezing issues.

Further investigation is required to determine the most effective design of the compressed air tank. An excessive tank volume would lead to a packaging problem. On the other hand having a bigger tank or a tank with multiple chambers would allow for increased assistance capability. A constant pressure tank as considered in [Ma and Ma, 2010] is another design option.

The design of a control valve or valves is another challenge. Ideally the valve could be accurately adjusted independently of the pressure ratio across it, which can be significantly greater or less than 1. Another requirement on the valve design is that it seals in both directions as this is crucial for maintaining the pressurized air in the tank and not allowing combustion products into the tank during high load operation.

4.3.8 Conclusions

The presented experimental results were generated with a simple control algorithm. Continuous control over the injection valve should result in reduced usage of resources, but the scale of performance improvement offered by the application of more sophisticated control is expected to be insignificant.

The BREES system might lend itself to secondary applications not investigated here. For example the use of air injection in the exhaust manifold is established as a means of mitigating emissions in gasoline engines [Lee, 2010], [Sim et al., 2001]. It is also possible that the tank could be used for the temporary storage of noxious emissions at propitious moments.

The experimental results presented here were based on a VGT equipped Diesel engine. The VGT mechanism was key in generating the sufficient backpressure for tank charging. Wastegated turbocharger systems would require an additional valve to generate backpressure or alternatively, the wastegate design could be modified to incorporate this functionality. For air-path systems equipped with

high pressure EGR, it is possible that a single, three-way valve could be used to regulate both the EGR flow and compressed air injection.

The BREES concept could also have application in heavy-duty / off road / generator set / etc. - in fact any situation where load following is an issue. Accommodating a tank of significant volume may not be as challenging in these applications as in passenger vehicles. Some designs of heavy duty Diesel turbochargers already incorporate a mechanism for generating high back pressures to assist with engine braking.

4.4 Summary

In this chapter, improving transient response of engines by means of boost assistance systems was investigated.

All of the approaches considered in simulations showed some improvement in the transient torque response and hence vehicle acceleration. Of the systems considered, pre-compressor assistance offered the best performance by a considerable margin as it avoids any limitations due to compressor surge. However achieving this level of performance required additional hardware (a non-return valve to prevent the air flowing back out of the air-box rather than into the engine and a compressor bypass valve) and also required a prohibitive mass of air. The electric turbo assistance and the exhaust manifold air assistance methods offered relatively similar performance. They both accelerated the turbocharger as fast as possible within the constraint imposed by the surge line. Intake air assistance was also limited by the surge line, but did not spin the turbocharger up as quickly, which resulted in it giving the least improvement over the standard engine.

A dedicated hardware system was developed to provide a convenient method for assessing the operation of engine with compressed air injected into the exhaust manifold. The air was supplied from a workshop reservoir and injected via a controllable valve. In this way, the effectiveness of the technique was verified. The level of recorded improvements was consistent with simulation findings. By modifying the compressed air supply pressure and the calibration of controller, the influence of system parameters on the engine response was evaluated.

Finally, a concept for the air-path arrangement that exploits the exhaust man-

ifold assist while requiring very limited additional hardware and limited engine control modifications was developed.

A 3^{rd} gear braking and tip-in manoeuvre was used as a representative test. The compressed air collected during the braking phase was sufficient to provide assistance during the acceleration phase. The experimental results show that the time to torque during this 3^{rd} gear tip-in acceleration was reduced by approximately 60%.

A number of practical considerations for in-vehicle application were discussed. These include: the influence of the system on engine overrun/braking characteristics, UEGO sensor measurement, gas temperature in the manifold and packaging issues. Opportunities for potential emissions benefits were also highlighted. As with many energy storage systems, challenges associated with resource management and repeatability are also envisaged.

Chapter 5

Summary and outlook

The work described in this thesis focused on investigating the transient response of turbocharged engines. The study was conducted considering this problem from engine control perspective striving to identify how recent advances in control theory and implementation can help in reducing CO_2 emissions from modern passenger cars. Since the beginning of the research work described here, the concept of engine downsizing (and down-speeding) has become a widely accepted method for reducing CO_2 emissions from modern gasoline engines, while modern Diesel engines have been equipped with more sophisticated turbocharging systems.

Engines applied in passenger cars are required to operate over a wide range of speeds and loads. Naturally aspirated engines have to be sized appropriately to provide a required maximum torque and power despite being often used at lower loads over low speed range. Pressure charging introduces an opportunity for ensuring the same dynamic range with reduced engine swept volumes. When coupled with down-speeding, it leads to significantly reduced pumping and friction losses during operation at part-load. The transient response of such engines is, however, affected by the dynamics of the air-path.

As system dynamics is one of the essential topics in the field of control engineering, this thesis pursued the opportunities for improving the transient response of highly turbocharged engines by applying some state-of-art engine simulation and control tools. The study was based on 2.0 litre light-duty Diesel engine. A simulation-based assessment of several air-path enhancement concepts led to the identification of compressed gas injection into the exhaust manifold as an effective

way of overcoming the turbo-lag. This was then verified experimentally on an engine test rig, which was developed to support this investigation.

The main contributions and findings of this work are listed in the following section.

Contributions and further work

Easily reconfigurable close-to-optimal closed-loop controller for 1D simulation models.

When operated within standard range, a modern Diesel VGT-EGR air-path is a highly non-linear open loop stable system. 1D simulation models are the state-of-art tools for simulating complete engines and are particularly suitable for air-path investigations. During significant transients, for example a full-load tip-in, the air-path traverses a wide range of rapidly changing operating points. The main requirement for a controller during these manoeuvres is to ensure that the engine operates within some physical limits. Furthermore, when additional actuators are available (e.g. boost assist systems or second stage of turbocharging), the controller is required to coordinate all the available inputs to ensure a satisfactory level of reference tracking. There often exists a preference with regard to actuator selection, because some of them come with a penalty due to the usage of certain energy resources.

Model predictive control (MPC) is a framework particularly suited to multi-variable problems with constraints. For this reason, it was selected as the base concept for controllers used in this work. Based on the knowledge of past states and inputs, MPC optimises the future behaviour of a system model (prediction model) over a finite time horizon. If the system model is linear, constraints are linear and the cost function is quadratic, the resulting optimisations can be converted to quadratic programming problems, which can be solved efficiently. To ensure this desired feature and easy reconfiguration of the controller to various air-path designs, it is proposed here to simplify the 1D simulation model to a Mean Value Engine Model. The full-state feedback for the MVEM can be read-

ily obtained from virtual 1D model measurements. At each controller execution instant, the MVEM is linearised and discretised around the instantaneous operating point and, in this way, the desired form of prediction models is obtained. The operating points around which the system is linearised are not necessarily its equilibria and non-zero state derivatives appear in the prediction model equations. Simplifications of the MVEM lead to a mismatch with the 1D model, because of which the state-derivatives of both models are not identical. Estimating the state-derivatives of the 1D model from virtual measurements and treating them as the instantaneous state-derivatives in the prediction model was shown to result in closed-loop step responses characterised with negligible overshoot and steady-state reference tracking error. Moreover, when the MPC controller was applied to the MVEM itself, it was shown that such a system results in the performance close to the solution of a related optimal control problem. Further simulations of the 1D model with the MPC controller showed that it is possible to ensure that the engine operates within required constraints.

It has been shown that MPC can be effectively used to avoid the compressor surge limit, when 1D models are used for engine simulation. This encouraging result has been demonstrated by simulating a tip-in transient at high altitude conditions. The surge limit is a particularly interesting constraint, because (when defined as in this thesis) it is a state-dependent constraint. Due to a close coupling between the VGT actuation and the flow through the compressor, avoiding the surge limit by an aggressive opening of the VGT may be counter-productive. To achieve the successful surge avoidance control, the surge limit has been defined as an output of the model, which could be then used in the prediction model. More systematic treatment of this problem and developing certain design recommendations for addressing such constraints would be an interesting theoretical question.

An interesting enhancement of the optimisation setup would be to include additional constraints, which have been shown in the literature to give stability guarantees for similarly formulated controllers. The MPC setup used in this work assumed constant system matrices and constant engine speed and fuelling over the entire prediction horizon. In spite of these simplifications, the closed-loop performance was satisfactory. Nevertheless, it would be interesting to apply

more sophisticated MPC formulations to the considered problem to better understand the effect of the above stated assumptions on the resulting performance. One could also consider linearising the system along nominal state trajectories, which would remove the state-derivative offset from the prediction model equations. This could, however, not be necessarily beneficial as one would loose the opportunity of feeding additional information (in the form of estimated state derivatives) to reduce the mismatch between the prediction model and the system being controlled.

The proposed controller, probably after some modifications, could be also applied to different systems/control problems. For example, dual-loop EGR systems and multiple stages of turbocharging are currently considered for new Diesel air-path systems. Coordinating all the actuators to follow multiple reference signals occurring during drive-cycles is not trivial. A MPC-based controller would be a very well suited tool for optimising such transients using 1D simulation models. Pressure pulses in the air-path are critical for a successful operation of low pressure EGR and, therefore, it is envisaged that some bespoke enhancements in the prediction model would be required for such an investigation. In principle, a similar approach could also be applied to turbocharged SI engines. In this case, the treatment of engine block characteristics would need to be enhanced to account for a more varying volumetric efficiency, variable valve timing systems and the effect of spark timing.

Systematic procedure for assessing air-path concepts

With an easily reconfigurable and systematically formulated closed-loop controller capable of delivering close-to-optimal performance, a rigorous procedure for assessing the transient capabilities of various air-path concepts can be developed. Such a procedure was applied to investigate the transient performance of the air-path with boost assistance systems. These included a turbocharger electric assist and various methods based on injecting compressed air into the air-path. The simulation tool developed made it possible to perform parametric studies to determine the influence of the TEA characteristics on expected benefits and compare the effectiveness of the concepts based on compressed air injection. Of

the three air-path injection points considered, the exhaust manifold was identified as the most attractive with respect to the offered improvements and the usage of resources.

The procedure that has been developed can support decisions at an early design stage, when the air-path system is selected. At this product development stage the engine block may not yet exist, in which case creating a fully parameterised 1D simulation model may not be possible. To reduce the development effort with limited impact on the accuracy of analysis, instead of 1D model a 'template' MVEM parameterised with some typical values can be used for engine simulations in the presented procedure.

Experimental verification of boost assistance by injecting compressed air into the exhaust manifold

To verify the findings of simulations, the experimental facility was equipped with a system for controlled injection of compressed air. An additional fitting was also made in the exhaust manifold of the engine. The MPC controller used in simulations was converted into a code, that could be executed on the rapid prototyping system. An ECU by-pass was used to override the internal VGT position demand with the MPC calculation results. In this way, the VGT and the assist valve were simultaneously coordinated to ensure boost reference tracking during engine experiments. The experimental results confirmed the extent to which the transient response can be improved by exhaust manifold assist. The tests also provided an insight into how these improvements depend on compressed air supply pressure.

There are several difficulties in applying the previously developed MPC formulation to the Real-Time control of the engine. Firstly, the controller has to account for the dynamics of sensors and actuators. The MVEM used for predictions included states for masses of gas stored in particular air-path sections. These can be determined from the measurements of pressures and temperatures in the volumes. The challenging conditions in the exhaust manifold necessitate the use of thermocouples of significant diameter, which affect steady-state measurements and introduce significant smoothing. Difficult actuator characteristics

were only partially mitigated by low-level position controllers, which had an effect on the achieved results. Therefore, there exists significant scope for improvement.

Estimating the state and state derivatives, which are essential for satisfactory predictions of future system behaviour, is challenging. Even in the simulation setup with 1D model, state derivatives calculated using MVEM for a measured state led to a poor closed-loop performance. During engine tests, some simple approaches were used to give sufficiently good estimates for the desired quantities, but it is envisaged that the controller would benefit from more systematic approach to this problem. Applying a state (and a state derivative) observer would be a natural starting point, but it would not address the question of accuracy of the prediction models. Deriving a more appropriate metric for model accuracy (which would most likely be different to $\mathcal{H}_\infty$-type model inaccuracy treatment) and relating such metric to the achievable controller performance would be an important contribution not only to the considered application, but also of a wider relevance.

BREES concept - a low component count, compressed air based system for reducing turbo-lag

The effectiveness of the exhaust manifold compressed air assist led to the development of the BREES concept. When applied to a VGT/EGR Diesel air-path, the concept in its minimum configuration includes a tank attached to the exhaust manifold via a controllable valve. The tank is recharged during braking (when no fuel is injected) thanks to a high exhaust manifold pressure generated with a fully closed VGT. The air is then available for injection into the manifold during a tip-in acceleration leading to $\sim$60% reduction in time-to-torque. The concept was implemented on the test rig with a 24 litre tank and two ON/OFF valves. The conducted experiments confirmed its effectiveness. The air was stored in the tank at the pressure of 3.5 bar, which was sufficient to deliver the expected benefits. The window of exhaust manifold pressures enabling the BREES system varied between slightly above 1 bar during the low load operation to about 4 bar during engine braking and tank recharging.

Ensuring consistency in engine performance may be the biggest challenge for

the BREES system. This reduces to maintaining the tank pressurised sufficiently for boost assistance at any instance. Charging the tank during a low load operation ('fire-to-fill' functionality) is one approach that could potentially address this issue. This could be an interesting future work item. Other investigations include adapting the BREES concept to SI engines with wastegated turbochargers.

Appendix A: Calibration of RT-MPC

In this appendix, the influence of the RT-MPC calibration on the resulting boost control performance is discussed. The investigation is based on the experimental results of testing the engine operation during a 3^{rd} gear tip-in manoeuvre (exactly the same as discussed in section 3.4.4). The control system is SISO, because only the standard VGT/EGR air-path configuration is considered: boost pressure is controlled by adjusting the VGT valve position and the EGR valve is fully closed.

Before the effect of calibration can be investigated, a set of controller performance measures is required. Time-to-boost is a measure often used for tip-in manoeuvres (see Figure 1a). It is defined here as the time at which 98% of the demanded step in pressure is achieved. Time-to-boost is, however, only marginally affected by the MPC calibration - to achieve a short time-to-boost the VGT simply has to be fully closed and this was the case for all of the applied calibrations.

Three more appropriate measures for the boost pressure control performance are introduced in Figure 1b. The standard definitions of maximum overshoot and maximum undershoot are used. The third measure, called *average regulation error*, is the time average of the difference of the demanded and the measured boost pressure. It is essentially the green shaded area shown in Figure 1b) divided by the time from when 98% of boost was achieved to the end of the test.

The fourth measure evaluates how smooth is the resulting actuator trace. The raw VGT position feedback signal was filtered with a non-causal moving window filter of the width of 4 engine cycles. The result of applying such a filter is shown

in Figure 1c. The filtered signal is then subtracted from the raw signal and the 2-norm of such a difference (shown in Figure 1d) is used as the input smoothness measure, called the *Actuation Index*.

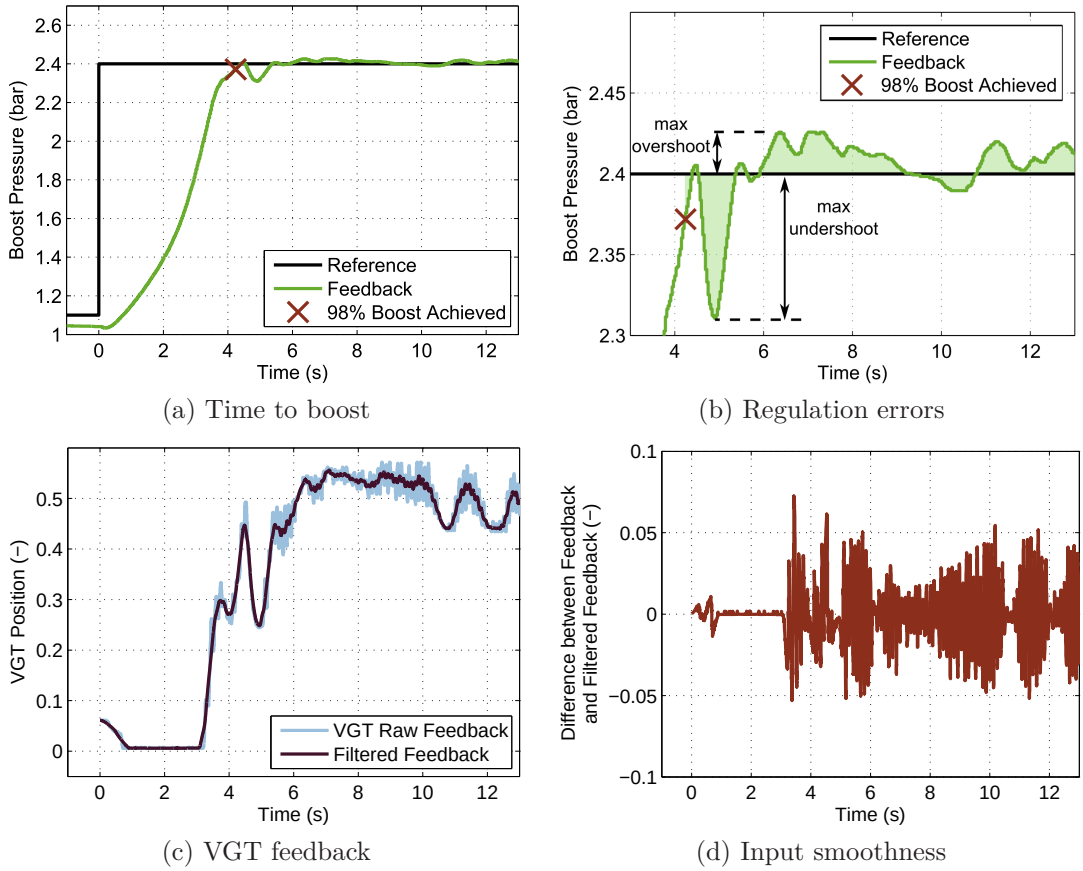

(a) Time to boost

(b) Regulation errors

(c) VGT feedback

(d) Input smoothness

Figure 1: Controller performance measures.

The cost function used in the MPC formulation penalises the boost tracking error and the rate of change of the input. The weighting of the boost tracking Q (in this appendix, Q will be used instead of $Q(i_{p_i}, i_{p_i})$ defined in section 3.4.4) was set to 10 for each of the tests. The terminal cost P was equal to Q at all times. In the first part of the analysis, determining a suitable weight R (similarly, R is used meaning $R(i_{\Delta u_{vgt}}, i_{\Delta u_{vgt}})$ from section 3.4.4) on VGT actuation is considered. Several values for the R parameter were selected, resulting in a range of R-to-Q ratios as shown in Figure 2. For each value of R, three repetitions of the test were conducted.

In this formulation boost tracking error was expressed in bar and VGT position was normalised (i.e. its range was from 0 to 1).

To provide a reference for the analysis of controller performance with various calibrations, the engine was also tested with the standard ECU controller. The performance measures calculated for results of such tests are shown as dark crosses in Figure 2. At each of the plots in this figure, the dependency of a performance measure on R-to-Q ratio could be approximated by a smooth non-linear curve. The average regulation error and the actuation index are treated as the most important metrics. The presented figures indicate that R-to-Q ratios in the range between 2 and 4 result in a good trade-off between these two indices. Maximum overshoot and undershoot for this range are also close to the minimum values of these measures.

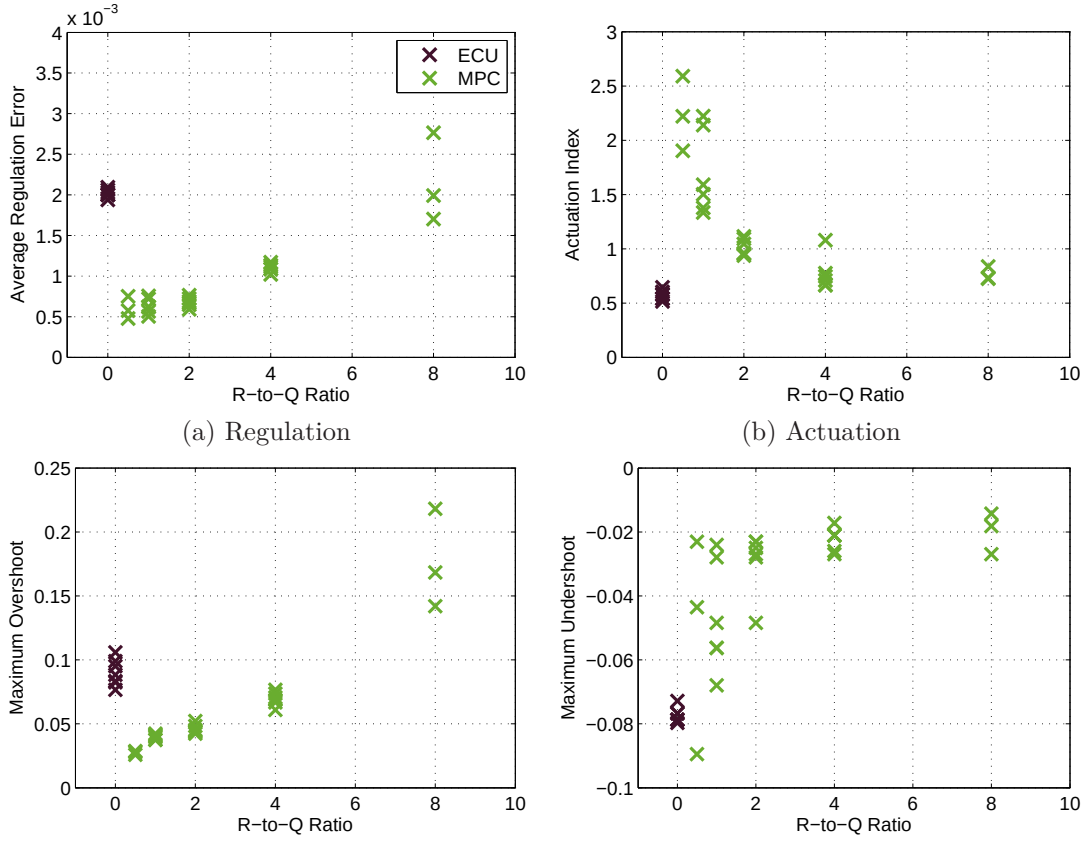

(a) Regulation

(b) Actuation

(c) Maximum overshoot

(d) Maximum undershoot

Figure 2: Calibration of penalty on the rate of change of the VGT.

It is worth noticing that the variance of the results obtained with the standard ECU strategy is considerably lower than that of some MPC tests. For example, the MPC results with the R-to-Q ratio of 8 showed a significant variance in the average regulation error and the maximum overshoot, whereas with the R-to-Q ratio of 0.5 or 1, a significant spread in the actuation index and the maximum undershoot was observed. This behaviour can be explained by the method of estimating the instantaneous state derivatives. They are calculated taking the difference between the last two measurements and are therefore significantly affected by measurement noise. Implementing a state observer could be one of possible ways to reduce this effect.

A similar approach was undertaken to investigate the influence of the control horizon on the system performance. For these tests the prediction horizon was set to 15 and the same range of R-to-Q ratios was investigated. Each combination was repeated twice. The results are shown in Figure 3. To improve readability the mean of two runs was determined for each combination of parameters and a line fitted to these mean values for each considered length of the control horizon. The results indicate that the control horizon has only a minor effect on the achievable performance. Furthermore, the two runs for each of the combinations of parameters often resulted in significantly different performance measures.

Similar set of experiments was performed to evaluate the influence of the prediction horizon on the engine response. For these tests the control horizon was set to 6. The observed differences were marginal as shown in Figure 4.

The engine tests presented in 3.4.4 were conducted with the R-to-Q ratio of 2, the control horizon of 10 and the prediction horizon of 15.

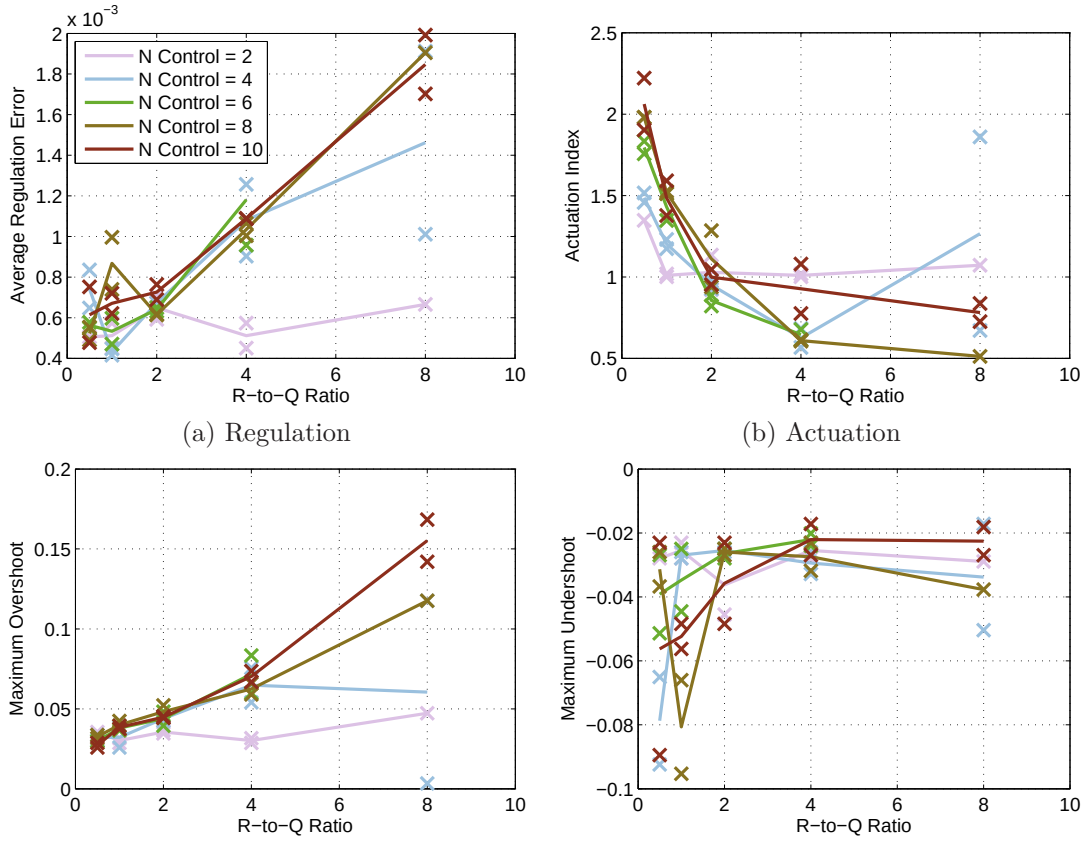

(a) Regulation

(b) Actuation

(c) Maximum overshoot

(d) Maximum undershoot

Figure 3: Calibration of MPC control horizon.

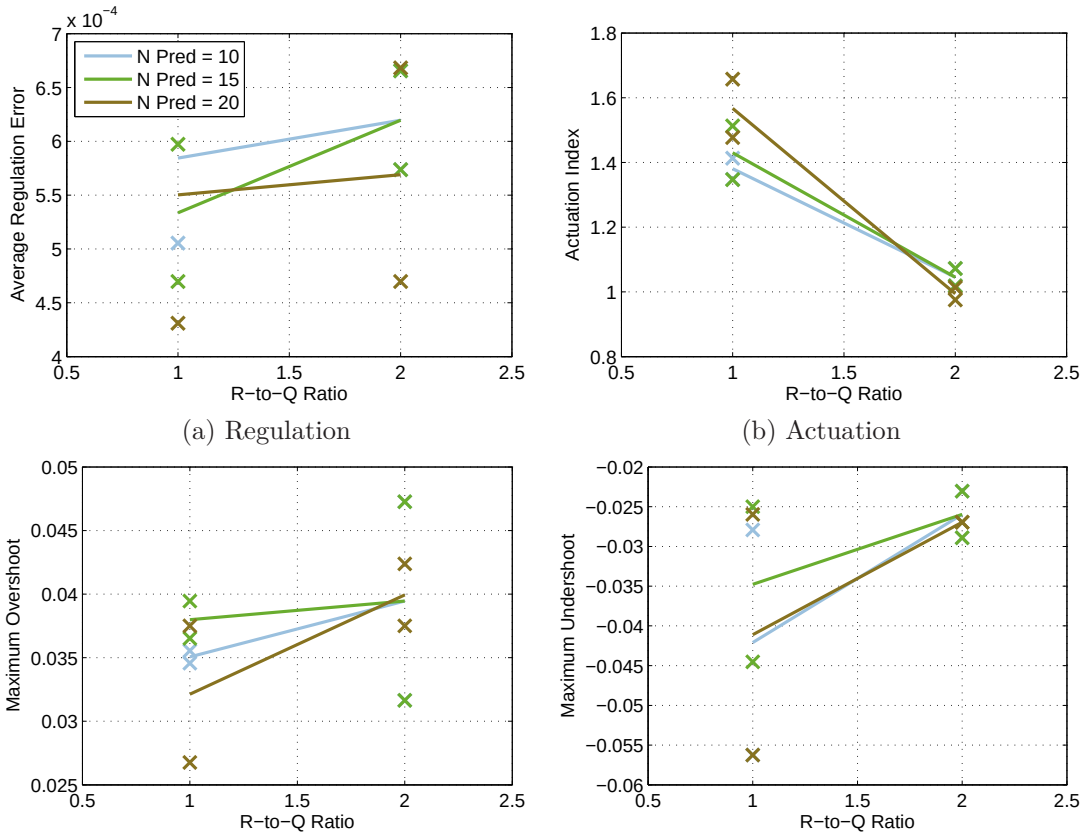

(a) Regulation

(b) Actuation

(c) Maximum overshoot

(d) Maximum undershoot

Figure 4: Calibration of MPC prediction horizon.

Appendix B: Calibration of controller for BREES experiments

The implementation of the BREES concept described in section 4.3 required a number of system design choices, which may have an effect on the overall system performance. These include both the control logic used during experiments and some particular parameters/thresholds with which the controller was calibrated. In this appendix a more detailed description of the controller is given along with the evaluation of the influence of some calibration parameters on engine response.

During the testing of the BREES concept, the engine control was based on the original ECU strategy. The original code was, however, customised in two ways:

driver torque demand was recalibrated to enable increased fuel injection at low engine speeds. This process involved removing certain engine torque limitations and increasing the driver demand for a given accelerator pedal position at low engine speeds. An example of resulting operation is shown in Figure 5a, where the *Final Torque Demand* is the signal, based on which the level of fuel injection is determined. After a tip-in the driver torque demand increases to the full-load level subject to the smoke limit, which gives BREES the opportunity to perform better (see Figure 5b). The original ECU code was used for the calculation of the smoke limit. Furthermore,

the engine protection limit and the DMF protection limits were kept intact.

VGT control by-pass was used selectively, i.e. the VGT position was forced to close fully during the braking phase of the BREES test manoeuvre. During the acceleration, a certain lower bound was imposed on the VGT position to compensate for moving the end-stop. At all remaining instances the VGT position was determined by the original ECU strategy according to its boost control algorithm.

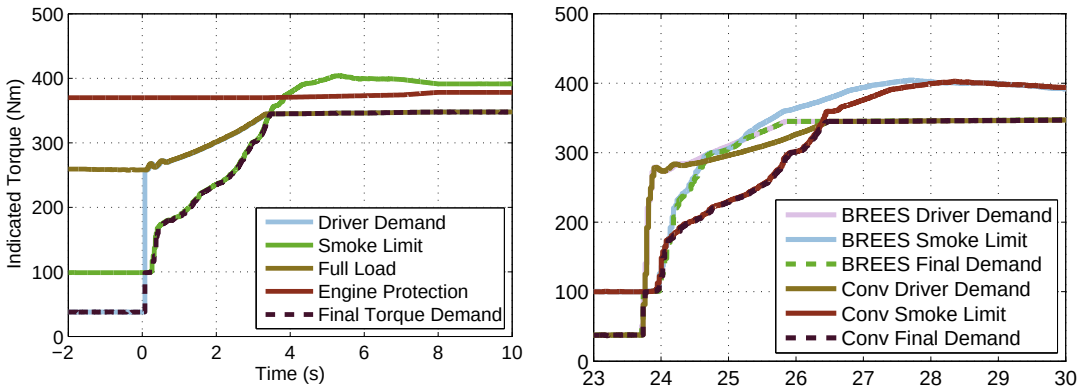

(a) Recalibrated torque demand

(b) Torque demand for BREES

Figure 5: Recalibrated torque demand and smoke limit during conventional and BREES-enabled operation.

The control logic for experiments with the BREES system was the following. The ON/OFF valves were controlled for tank recharging if:

- Accelerator pedal position was below a threshold
- Measured shaft torque was below 0
- Pressure in the tank was below the exhaust manifold pressure
- Pressure in the tank was below a threshold
- Safety limits were satisfied

The valves were controlled for boost assistance if:

- The difference between the tank pressure and the exhaust manifold was above a threshold
- The difference between the demanded intake manifold pressure and the actual manifold pressure was above a threshold
- Accelerator pedal position was above a threshold
- The difference between the surge limit and the post-compressor pressure was above a threshold
- Safety limits were satisfied

In this control algorithm two parameters could potentially affect the overall system performance, i.e. the limitation of VGT position during the acceleration and the limit on maximum tank pressure. The BREES system was tested with a set of different values for these parameters and the results are shown in Figure 6. The maximum closing of VGT during the acceleration may not be optimal, because the VGT end-stop was moved to enable the capability of tank charging. The fully closed VGT may result in significantly increased pumping losses and thus have a negative effect on the transient response. The VGT position of 0.2 was previously verified to give a similar back pressure to the fully-closed VGT with the original end-stop position. As it is observed in Figure 6a this is also the position, which ensures the maximum achievable torque response. Similar investigation for the limitation on the maximum tank pressure reveals that the value of 3.5 bar is sufficient to ensure a very fast response. Lower pressure values, however, also deliver significant improvement over the conventional operation. For the plots presented in chapter 4 the maximum tank pressure was set to 3.5 and during the acceleration the lower bound on the VGT position was 0.2.

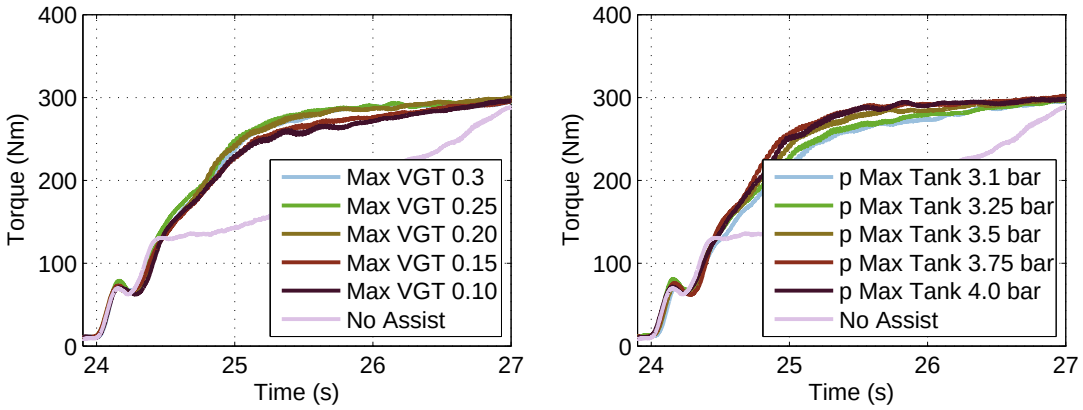

(a) Effect of VGT limit

(b) Effect of tank pressure limit

Figure 6: Influence of controller calibration on the performance of BREES system.

Appendix C: Investigation of MPC calculations

In this appendix, the MPC calculations which led to the result showed in Figure 3.11 are investigated. The controller was executed every 50ms and used the prediction horizon of 10 steps and the control horizon of 5 steps.

A snapshot of the simulation at the time of 4.30 seconds is presented in Figure 7a. The plot for intake manifold pressure is given in the top left corner (referred to as *Controlled Variable* or CV), the plot for VGT position is showed in top right corner (*Manipulated Variable* or MV) and the value of optimised cost function at each prediction step is presented at the bottom plot. The final results of simulation are shown in black solid lines. The operating points at which the MVEM was linearised is denoted with red circles. To support this analysis, the solid red line shows the result of forward simulation of a linear system with VGT frozen at the initial position and the solid bright blue line shows the result of a linear system simulation with VGT fully closed. Finally, the blue crosses denote the optimised evolution of the controlled and the manipulated variables.

The analysis for the time of 4.30 seconds shows the level the inaccuracy in predictions introduced by setup simplifications: linearisation of the MVEM, the assumption of fixed matrices, and the assumption of constant speed and fuelling during the entire prediction horizon. Because the optimiser resulted in the VGT remaining fully closed for the entire horizon, the total cost function consists of only the penalty on the error of boost tracking (the constant reference of 2.4 bar is shown as green line).

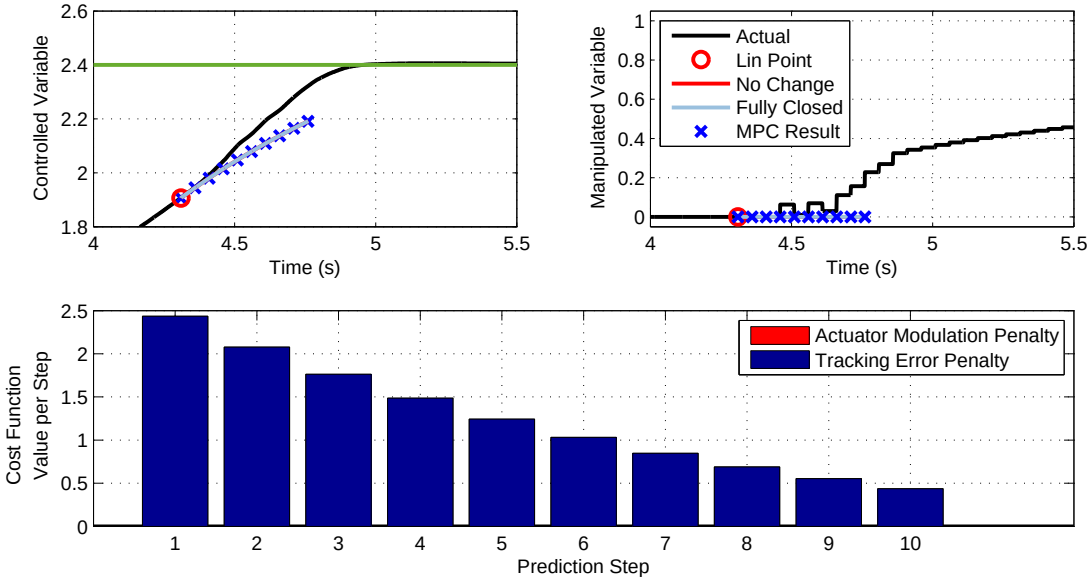

(a) t = 4.30s

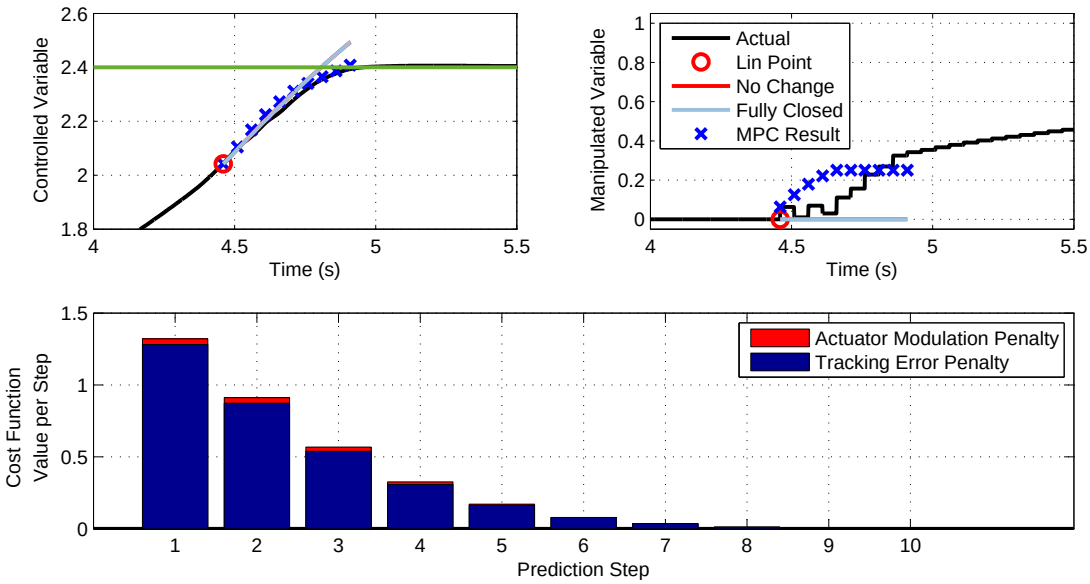

(b) t = 4.45s

The most significant difference between the solution of OCP and the simulation with MPC appeared around the knee region at the plot for the *Controlled Variable*, i.e. between the time of 4.35 and 4.55 seconds (please refer to Figure 3.11). The VGT plot for MPC showed two ripples, whereas the solution of OCP

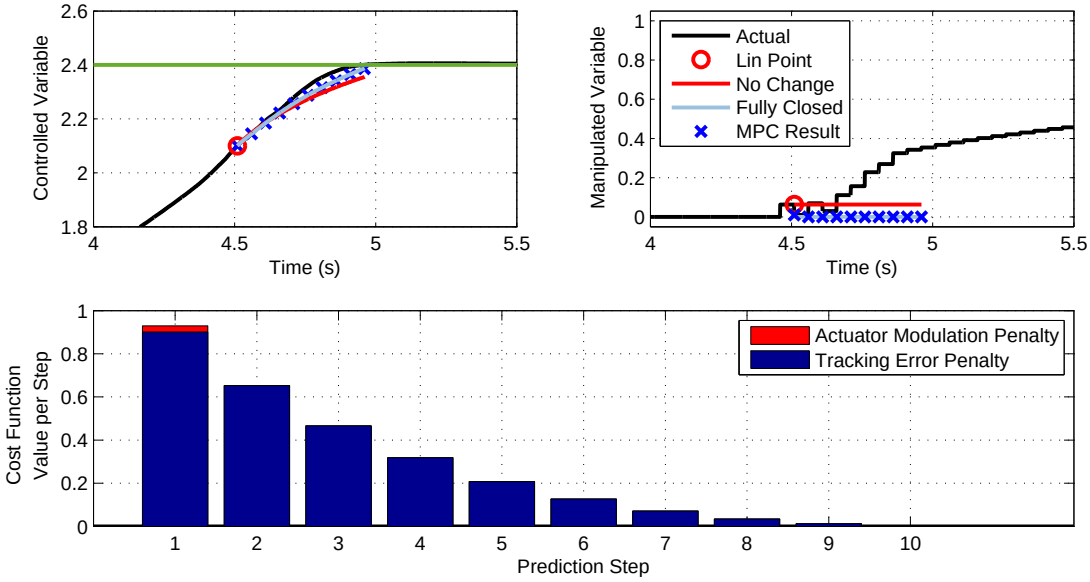

(c) t = 4.50s

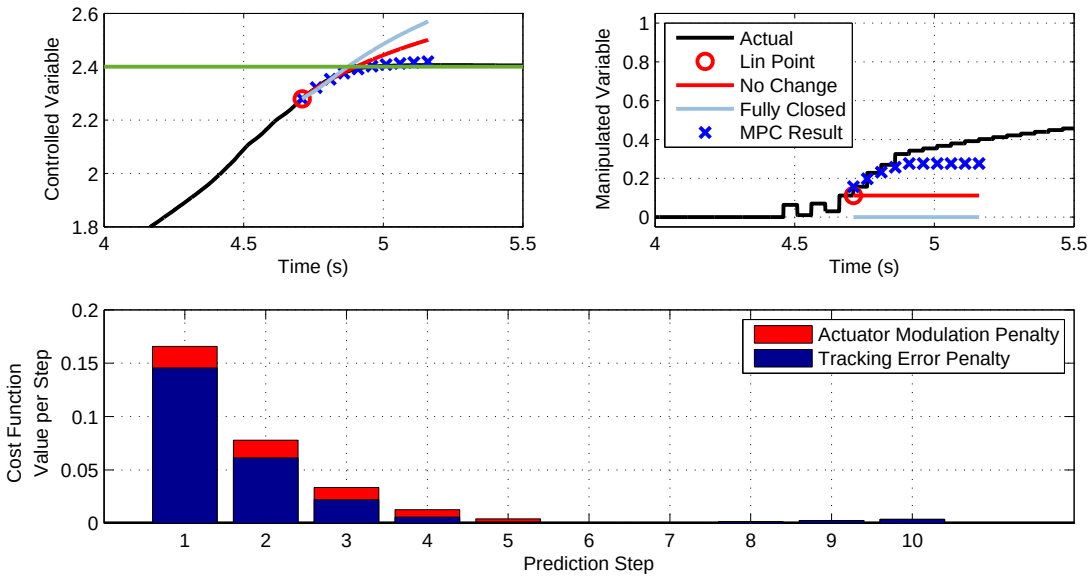

(d) t = 4.70s

returned a fully closed VGT for this short period. This behaviour is explained in Figure 7b. The forward linear simulation of the system with VGT fully closed resulted in the *CV* overshooting the reference. Because at this stage the tracking error dominates the cost function (see the bottom plot), the optimiser chose to actuate the MV to ensure the *CV* remains below the reference. At the next

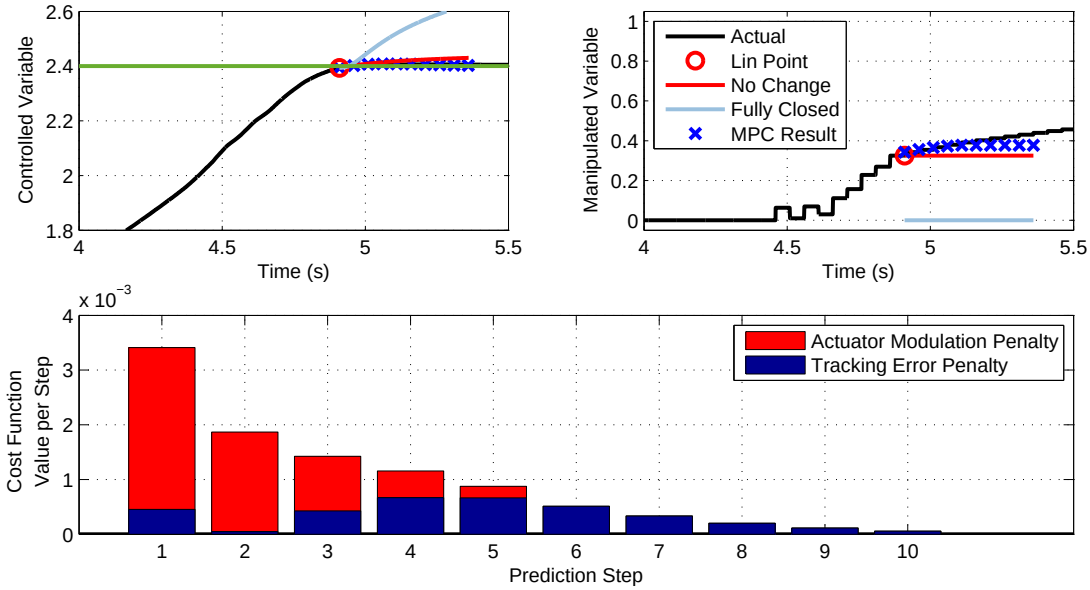

(e) t = 4.90s

Figure 7: MPC calculations during a third gear tip-in manoeuvre.

instance shown in Figure 7c, the system was linearised with the VGT slightly opened. With the resulting linear model it was predicted that with even fully closed VGT, the reference will not be exceeded. If the VGT stayed fixed at the initial position, a bigger tracking error would occur. This behaviour highlights how the simplifications used in the MPC setup affect the boost control performance.

At the time of 4.70 seconds (see Figure 7d), a much more desirable operation of the controller is observed. The system is linearised in the vicinity of the reference CV with a non-saturated MV. The optimiser selects the future inputs to facilitate a smooth transition in boost pressure. The optimised MV and the predicted CV are very close to the actual simulation model behaviour. The modulation of the actuator amounts now for a significant part of the cost function and is traded-off with reference tracking.

Finally, the regulation of boost pressure around a set-point is shown in Figure 7e. At this point in time, the engine speed is still increasing and introduces a varying measured disturbance to the system. The plots confirm that the influ-

ence of disturbance is effectively attenuated by progressive opening of the VGT. Because the system operates very near the CV set-point, the cost function is dominated by the modulation of the actuator.

References

Accurate Technologies. NoHooks rapid prototyping software. online, March 2013. URL `http://www.accuratetechnologies.com`.

European Automobile Manufacturers' Association ACEA, 2012. URL `http://www.acea.be/collection/statistics`.

R. Amari, F. Chabrier, P. Tona, and P. Moulin. A nonlinear MPC strategy for wastegate-actuated turbocharged engines: Early investigations. *Advances in Automotive Control*, 2010.

F. An and J. DeCicco. Trends in technical efficiency trade-offs for the U.S. light vehicle fleet. *SAE Technical Paper*, (2007-01-1325), 2007.

S. Arnold, C. Balis, P. Barthelet, E. Poix, T. Samad, G. Hampson, and S. Shahed. Garrett electric boosting systems (EBS) program federal grant DE-FC05-00OR22809. Technical report, Honeywell Turbo Technologies, 2005.

ASAM. ASAM2 Meta Language (AML or ASAM MCD 2MC). URL `http://www.asam.net/`.

C. Balis, Ch. Middlemass, and S. M. Shahed. Design and development of e-turbo for suv and light truck applications. In *Diesel Engine Emissions Reduction Conference*, 2003.

S. Behrendt, P. Dunow, and B. P. Lampe. An application of model predictive control to a gasoline engine. In *18th International Conference on Process Control*, 2011.

A. Bemporad, M. Morari, V. Dua, and E. N. Pistikopoulos. The explicit linear quadratic regulator for constrained systems. *Automatica*, 38:3–20, 2002.

K. Bhatt. *Potential for Meeting the EU New Passenger Car CO_2 Emissions Targets*. PhD thesis, Massachusetts Institute of Technology, 2010.

J. Black, P. G. Eastwood, K. Tufail, T. Winstanley, Y. Hardalupas, and A. M. K. P. Taylor. The effect of VGT vane control on pumping losses during full-load transient operation of a common-rail Diesel engine. *SAE Technical Paper*, (2007-24-0063), 2007.

F. Borrelli, M. Baotic, J. Pekar, and G. Stewart. On the computation of linear model predictive control laws. *Automatica*, 46, 2010.

Bosch. *Automotive Handbook*. Robert Bosch GmbH, 2011.

L. Cheah, A. Bandivadekar, K. Bodek, E. Kasseris, and J. B. Heywood. The trade-off between automobile acceleration performance, weight, and fuel consumption. *SAE Int. J. Fuels Lubr.*, 2009.

U. Christen and R. Busch. The art of control engineering: Science meets industrial reality. In *Proc. IFAC E-COSM*, 2012.

U. Christen, K. Vantine, and N. Collings. Event-based mean-value modeling of DI Diesel engines for controller design. *SAE Technical Paper*, (2001-01-1242), 2001.

D. Cieslar, P. Dickinson, A. Darlington, K. Hegarty, N. Collings, and K. Glover. Mean-value oxygen concentration modelling and experimental validation using fast UEGO sensors. paper presented at Powertrain Modelling and Control Conference in Bradford, September, 2012.

J. A. Cook, J. Sun, J. H. Buckland, I. Kolmanovsky, H. Peng, and J. W. Grizzle. Automotive powertrain control: A survey. *Asian Journal of Control*, 8, 2006.

G. E. Daniels. Measurement of gas temperature and the radiation compensating thermocouple. *Journal of Applied Meteorology*, 7, 1968.

A. Darlington, K. Glover, and N. Collings. A simple Diesel engine air-path model to predict the cylinder charge during transients: Strategies for reducing transient emissions spikes. *SAE Technical Paper*, (2006-01-3373), 2006.

L. del Re, P. Ortner, and D. Alberer. *Automotive Model Predictive Control: Models, Methods and Applications*, chapter Chances and Challenges in Automotive Predictive Control, pages 1–22. Springer, 2010.

M. Densing, H. Turton, and G. Bäuml. Conditions for the successful deployment of electric vehicles - a global energy system perspective. *Energy*, 47:137 –149, 2012.

DfT. Cars registered for the first time by CO_2 emission band, Great Britain, annually from 2001, April 2012a. URL `http://assets.dft.gov.uk/statistics/tables/veh0256.xls`.

DfT. Factors considered important when buying a car - full license holders only: 2010-2011, January 2012b. URL `http://assets.dft.gov.uk/statistics/tables/att0229.xls`.

G. Dixon and J. Hill. Car buyer attitude survey, May 2009. URL `www.lowcvp.org.uk/assets/reports/LowCVP.pdf`.

C. Donitz, I. Vasile, C. Onder, and L. Guzzella. Realizing a concept for high efficiency and excellent driveability: The downsized and supercharged hybrid pneumatic engine. *SAE Technical Paper*, (2009-01-1326), 2009. doi: 10.4271/2009-01-1326.

EEA. Monitoring CO_2 emissions from new passenger cars in the EU: summary of data for 2011. Technical report, European Environment Agency, 2012.

EPA. Light-duty automotive technology, carbon dioxide emissions, and fuel economy trends: 1975 through 2011. Technical Report EPA-420-R-12-001a, U.S. Environmental Protection Agency, 2012.

EU. Regulation (EC) no 443/2009 of the European Parliament and of the Council of 23 April 2009 setting emission performance standards for new passenger cars

as part of the community's integrated approach to reduce CO2 emissions from light-duty vehicles. Technical report, Official Journal of the European Union, L 140/1.

P. Falcone, F. Borrelli, J. Asgari, H. E. Tseng, and D. Hrovat. Predictive active steering control for autonomous vehicle systems. *IEEE Transactions on Control Systems Technology*, 15, 2007.

P. Falcone, F. Borrelli, H. E. Tseng, J. Asgari, and D. Hrovat. Linear time-varying model predictive control and its application to active steering systems: Stability analysis and experimental validation. *International Journal of Robust and Nonlinear Control*, 18, 2008.

H. J. Ferreau, P. Ortner, P. Langthaler, L. del Re, and M. Diehl. Predictive control of a real-world Diesel engine using an extended online active set strategy. *Annual Reviews in Control*, 31:293–301, 2007.

O. Flärdh. *Modeling, Control and Optimization of the Transient Torque Response in Downsized Turbocharged Spark Ignited Engines*. PhD thesis, KTH Stockholm, 2012.

N. Fraser, H. Blaxhill, G. Lumsden, and M. Bassett. Challenges for increased efficiency through gasoline engine downsizing. *SAE Technical Paper*, (2009-01-1053), 2009.

FURORE. *R&D Technology Roadmap: A contribution to the identification of key technologies for a sustainable development of European road transport*. European Automotive Research Partners Association (EARPA).

A. U. Genc. *Linear Parameter-Varying Modelling and Robust Control of Variable Cam Timing Engines*. PhD thesis, University of Cambridge, 2002.

S. George, G. Morris, Pearce D. Dixon, J., and G. Heslop. Optimal boost control for an electrical supercharging application. *SAE Technical Paper*, (2004-01-0523), 2004.

D. Goldfarb and A. Idnani. A numerically stable dual method for solving strictly convex quadratic programs. *Mathematical Programming*, 27, 1983.

L. Guzzella and A. Amstutz. Control of Diesel engines. *IEEE Control Systems*, 1998.

L. Guzzella and C.H. Onder. *Introduction to Modeling and Control of Internal Combustion Engine Systems*. Springer, 2004.

L. Guzzella and A. Sciarretta. *Vehicle Propulsion Systems: Introduction to Modeling and Optimization*. Springer, 2005.

D. Hancock, N. Fraser, M. Jeremy, R. Sykes, and H. Blaxhill. A new 3 cylinder 1.2l advanced downsizing technology demonstrator engine. *SAE Technical Paper*, (2008-01-0611), 2008.

E. Hendricks. Engine modelling for control applications: A critical survey. *Meccanica*, 32:387–396, 1997.

M. Herceg, T. Raff, R. Findeisen, and F. Allgöwer. Nonlinear model predictive control of a turbocharged Diesel engine. In *Proc. of the IEEE International Conference on Control Applications*, 2006.

C. A. Herrera. *Hybrid Internal Combustion Engine: Driving a Vehicle Using Air Compressed in Braking*. PhD thesis, Massachusetts Institute of Technology, June 1998.

J. B. Heywood. *Internal Combustion Engine Fundamentals*. McGraw-Hill, 1988.

B. Houska and H.J. Ferreau. ACADO Toolkit User's Manual. http://www.acadotoolkit.org, 2009–2011.

B. Houska, H.J. Ferreau, and M. Diehl. ACADO Toolkit – An Open Source Framework for Automatic Control and Dynamic Optimization. *Optimal Control Applications and Methods*, 32(3):298–312, 2011.

S. Ibaraki, Y. Yamashita, K. Sumida, H. Ogita, and Y. Jinnai. Development of the "hybrid turbo", an electrically assisted turbocharger. Technical report, Mitsubishi Heavy Industries, 2006.

S. Ibaraki, I. Tomita, M. Ebisu, and T. Shiraishi. Development of a wide-range centrifugal compressor for automotive turbochargers. Technical report, Mitsubishi Heavy Industries, 2012.

M. Iwadare, M. Ueno, and S. Adachi. Multi-variable air-path management for a clean Diesel engine using model predictive control. *SAE Int. J. Engines*, 2: 764–773, 2009.

M. Jung. *Mean-Value Modelling and Robust Control of the Airpath of a Turbocharged Diesel Engine*. PhD thesis, University of Cambridge, February 2003.

M. Jung, R. G. Ford, K. Glover, N. Collings, U. Christen, and J.M. Watts. Parameterization and transient validation of a variable geometry turbocharger for mean-value modeling at low and medium speed-load points. *SAE Technical Paper*, (2002-01-2729), 2002.

H. Kang, C. Tai, E. Smith, X. Wang, T.-C. Tsao, J. Stewart, and P.N. Blumberg. Demonstration of air-power-assist (APA) engine technology for clean combustion and direct energy recovery in heavy duty application. *SAE Technical Paper*, (2008-01-1197), 2008.

K. Kar, S. Roberts, R. Stone, M. Oldfield, and B. French. Instantaneous exhaust temperature measurements using thermocouple compensation techniques. *SAE Technical Paper*, (2004-01-1418), 2004.

M. Karlsson, K. Ekholm, P. Strandh, R. Johansson, and P. Tunestal. Multiple-input multiple-output model predictive control of a Diesel engine. In *Proc. 6th IFAC Symposium on Advances in Automotive Control*, 2010.

T. Katrasnik, F. Trenc, Medica V., and S. Markic. An analysis of turbocharged Diesel engine dynamic response improvement by electric assisting systems. *Transactions of the ASME*, 127, 2005.

T. Keviczky and G. J. Balas. Flight test of a receding horizon controller for autonomous UAV guidance. *American Control Conference*, 2005.

J. King, M. Heaney, E. Bower, N. Jackson, J. Saward, A. Fraser, G. Morris, P. Bloore, T. Cheng, J. Borges-Alejo, and M. Criddle. HyBoost - an intelligently electrified optimised downsized gasoline engine concept. In *10th International Conference on Turbochargers and Turbocharging, (IMechE)*, 2012.

I. Kolmanovsky, P. Moraal, M. van Nieuwstadt, and A. Stefanopoulou. Issues in modelling and control of intake flow in variable geometry turbocharged engines. In *Proceedings of the 18th IFIP conference on system modeling and optimization*, 1997.

I. Kristoffersson. *Model Predictive Control of a Turbocharged Engine*. PhD thesis, KTH Stockholm, 2006.

P. Langthaler and L. del Re. Fast predictive oxygen charge control of a Diesel engine. In *Proc. American Control Conference*, 2007.

P. Langthaler and L. del Re. Robust model predictive control of a Diesel engine airpath. In *Proceedings of the 17th World Congress The International Federation of Automatic Control*, 2008.

B. Lecointe and G. Monnier. Downsizing a gasoline engine using turbocharging with direct injection. *SAE Technical Paper*, (2003-01-0542), 2003.

C. Y. Lee, H. Zhao, and T. Ma. A low cost air hybrid concept. *Oil & Gas Science and Technology*, 65, 2010.

D. Lee. *Effects of Secondary Air Injection During Cold Start of S.I. Engines*. PhD thesis, MIT Department of Mechanical Engineering, 2010.

T. K. Lee. *Optimal Calibration and Transient Control of High Degree of Freedom Internal Combustion Engines*. PhD thesis, University of Michigan, 2009.

O. Leufvén. *Compressor Modeling for Control of Automotive Two Stage Turbochargers*. PhD thesis, Linköpings Universitet, 2010.

J. M. Lujan, H. Climent, C. Guardiola, and J. V. Garcia-Ortiz. A comparison of different algorithms for boost pressure control in a heavy-duty turbocharged Diesel engine. *Proc. IMechE, Part D: J. Automobile Engineering*, 2007.

T. Ma and J. Ma. Supercharger air hybrid vehicle. *SAE Technical Paper*, (2010-01-0822), 2010.

J. M. Maciejowski. *Predictive Control with Constraints*. Prentice Hall, 2002.

D. W. MacKenzie. *Trends and Drivers of the Performance - Fuel Economy Trade-off in New Automobiles*. PhD thesis, Massachusetts Institute of Technology, 2009.

H. L. MacLean and L. B. Lave. Evaluating automobile fuel/propulsion system technologies. *Progress in Energy and Combustion Science*, 29:1–69, 2003.

T. Maruyama, T. Shimura, A. Ejiri, Y. Ikai, and K. Shimotani. Model predictive control applied to a Diesel engine air-path system with dead time. In *Proc. SICE Annual Conference*, 2011.

A. Mehmood, S. Laghrouche, and M. El Bagdouri. Control of the electro-pneumatic VGT actuator with friction compensators. In *Proc. of the 18th World Congress IFAC*, 2011.

P. Moraal and I. Kolmanovsky. Turbocharger modeling for automotive control applications. *SAE Technical Paper*, (1999-01-0908), 1999.

P. Moulin and J. Chauvin. Modeling and control of the air system of a turbocharged gasoline engine. *Control Engineering Practice*, 2009.

V. Mueller, R. Christmann, S. Muenz, and V. Gheorghiu. System structure and controller concept for an advanced turbo-charger/EGR system for a turbocharged passenger car Diesel engine. *SAE Technical Paper*, (2005-01-3888), 2005.

A. Murilo, M. Alamir, and P. Ortner. Experimental validation of a parameterized NMPC for a Diesel engine. In *Proc. of IFAC Workshop on Engine and Powertrain Control, Simulation and Modeling*, pages 175–182, 2009. doi: 10.3182/20091130-3-FR-4008.00024.

NAIGT. An independent report on the future of the automotive industry in the UK. Technical report, New Automotive Innovation and Growth Team (NAIGT), 2009.

T. Noguchi, Y. Takata, Y. Yamashita, Y. Komatsu, and S. Ibaraki. 220,000-r/min, 2-kw permanent magnet motor drive for turbocharger. *Electrical Engineering in Japan*, 161, 2007.

NRC. Assessment of fuel economy technologies for light-duty vehicles. Technical report, National Research Council, 2011.

G.J. Offer, D. Howeyb, M. Contestabile, R. Clague, and N.P. Brandon. Comparative analysis of battery electric, hydrogen fuel cell and hybrid vehicles in a future sustainable road transport system. *Energy Policy*, 38:24–29, 2010.

P. Ortner and L. del Re. Predictive control of a Diesel engine air path. *IEEE Transactions on Control Systems Technology*, Vol. 15:449–456, 2007.

P. Ortner, P. Langthaler, J. Garcia-Ortiz, and L. del Re. MPC for a Diesel engine air path using an explicit approach for constraint systems. In *Proceedings of the 2006 IEEE International Conference on Control Applications*, 2006.

P. Ortner, R. Bergmann, H. Ferreau, and L. del Re. Nonlinear model predictive control of a Diesel engine airpath. In *Proc. of the IFAC Workshop on Control Applications of Optimisation (CAO)*, 2009.

G. Palmieri, O. Barbarisi, S. Scala, and L. Glielmo. *Automotive Model Predictive Control: Models, Methods and Applications*, chapter An Integrated LTV-MPC Lateral Vehicle Dynamics Control: Simulation Results, pages 231–255. Springer, 2010.

G. Papalambrou and N.P. Kyrtatos. Controlled injection of compressed air in marine Diesel engine intake for improved load acceptance. In *Proc. IFAC ECOSM*, 2009.

G. Pasaoglu, N. Honselaar, and Ch. Thiel. Potential vehicle fleet CO_2 reductions and cost implications for various vehicle technology deployment scenarios in Europe. *Energy Policy*, 40:404–421, 2012.

P. D. Pfister and Y. Perriard. Very-high-speed slotless permanent-magnet motors: Analytical modeling, optimization, design, and torque measurement methods. *IEEE Transactions on Industrial Electronics*, 57, 2010.

C. D. Rakopoulos. *Diesel Engine Transient Operation*. Springer-Verlag, 2009.

R. D. Reitz. Directions in internal combustion engine research. *Combustion and Flame*, 160:1–8, 2013.

Ricardo Inc. A study of potential effectiveness of carbon dioxide reducing vehicle technologies. Technical Report EPA420-R-08-004a, United States Environmental Protection Agency, 2008.

Ricardo Software. WAVE help. WAVE Version 8.3, 2011.

J.-J. Rueger. Powertrain trends and future potential. In *DEER Conference*. Robert Bosch, 2009.

M. Sassano, T. E. Passenbrunner, M. Hirsch, L. del Re, and A. Astolfi. Approximate optimal control of the air path of a Diesel engine. In *American Control Conference*, 2012.

S. Saulnier and S. Guilain. Computational study of Diesel engine downsizing using two-stage turbocharging. *SAE Technical Paper*, (2004-01-0929), 2004.

S.M. Shahed and K.-H. Bauer. Parametric studies of the impact of turbocharging on gasoline engine downsizing. *SAE Technical Paper*, (2009-01-1472), 2009.

H. S. Sim, K. Min, and S. H. Chung. Effect of synchronized secondary air injection on exhaust hydrocarbon emission in a spark ignition engine. *Proc. of the IMechE, Part D: Journal of Automobile Engineering*, 215, 2001.

G. Stewart and F. Borrelli. A model predictive control framework for industrial turbodiesel engine control. In *Proceedings of the 47th IEEE Conference on Decision and Control*, 2008.

J. M. Sullivan and M. Sivak. Carbon capture in vehicles: A review of general support, available mechanisms, and consumer-acceptance issues. Technical Report UMTRI-2012-12, The University of Michigan, Transportation Research Institute, 2012.

G. Tavcar, F. Bizjan, and T. Katrasnik. Methods for improving transient response of Diesel engines - influences of different electrically assisted turbocharging topologies. *Proc. of the IMechE, Part D: Journal of Automobile Engineering*, 2011.

Ch. Thiel, A. Perujo, and A. Mercier. Cost and CO_2 aspects of future vehicle options in europe under new energy policy scenarios. *Energy Policy*, 38:7142 – 7151, 2010.

M. van Nieuwstadt, I. Kolmanovsky, P. Moraal, A. Stefanopoulou, and M Jankovic. Experimental comparison of EGR - VGT control schemes for a high speed Diesel engine. *IEEE Control Systems*, 20, 2000.

O. Varnier. *Trends and Limits of Two-Stage Boosting Systems for Automotive Diesel Engines*. PhD thesis, Universidad Politecnica de Valencia, 2012.

J. Wahlström and L. Eriksson. Modelling Diesel engines with a variable-geometry turbocharger and exhaust gas recirculation by optimization of model parameters for capturing non-linear system dynamics. *Proc. of the IMechE, Part D: Journal of Automobile Engineering*, 225, 2011.

N. Watson and M. S. Janota. *Turbocharging the Internal Combustion Engine*. The Macmillan Press Ltd, 1982.

X. Wei and L. del Re. Gain scheduled $\mathcal{H}_\infty$ control for engine air path systems of diesel engines using LPV techniques. *IEEE Transaction on Control Systems Technology*, 15, 2007.

F. Westin. *Simulation of Turbocharged SI-Engines - with Focus on the Turbine*. PhD thesis, KTH Stockholm, 2005.

Y. Yamashita, S. Ibaraki, K. Sumida, M. Ebisu, B. An, and H. Ogita. Development of electric supercharger to facilitate the downsizing of automobile engines. Technical report, Mitsubishi Heavy Industries, 2010.

S. M. Zoepf. *Automotive Features: Mass Impact and Deployment Characterization.* PhD thesis, Massachusetts Institute of Technology, 2011.